DUAL FREQUENCY RECONFIGURABLE REFLECTARRAY ANTENNA OF SPLIT RING ELEMENTS WITH RF MEMS SWITCHES

A THESIS SUBMITTED TO
THE GRADUATE SCHOOL OF NATURAL AND APPLIED SCIENCES
OF
MIDDLE EAST TECHNICAL UNIVERSITY

BY

CANER GÜÇLÜ

IN PARTIAL FULFILLMENT OF THE REQUIREMENTS
FOR
THE DEGREE OF MASTER OF SCIENCE
IN
ELECTRICAL AND ELECTRONICS ENGINEERING

SEPTEMBER 2010

Approval of the Thesis:

DUAL FREQUENCY RECONFIGURABLE REFLECTARRAY ANTENNA OF SPLIT RING ELEMENTS WITH RF MEMS SWITCHES

submitted by **CANER GÜÇLÜ** in partial fulfillment of the requirements for the degree of **Master of Science in Electrical and Electronics Engineering Department, Middle East Technical University** by,

Prof. Dr. Canan Özgen
Dean, Graduate School of **Natural and Applied Sciences** _____

Prof. Dr. İsmet Erkmen
Head of Department, **Electrical and Electronics Engineering** _____

Assoc. Prof. Dr. Özlem Aydın Çivi
Supervisor, **Electrical and Electronics Engineering Dept., METU** _____

Prof. Dr. Tayfun Akın
Co-Supervisor, **Electrical and Electronics Engineering Dept., METU** _____

Examining Committee Members:

Assoc. Prof. Dr. S. Sencer Koç
Electrical and Electronics Engineering Dept., METU _____

Assoc. Prof. Dr. Özlem Aydın Çivi
Electrical and Electronics Engineering Dept., METU _____

Assist. Prof. Dr. Lale Alatan
Electrical and Electronics Engineering Dept., METU _____

Dr. Julien Perruisseau-Carrier
Centre Tecnològic de Telecomunicacions de Catalunya _____

Engineer, MSc. Erim İnal
Aselsan A.Ş. _____

Date: September 2, 2010

I hereby declare that all information in this document has been obtained and presented in accordance with academic rules and ethical conduct. I also declare that, as required by these rules and conduct, I have fully cited and referenced all material and results that are not original to this work.

Name, Last name: Caner Güçlü

Signature:

ABSTRACT

DUAL FREQUENCY RECONFIGURABLE REFLECTARRAY ANTENNA OF SPLIT RING ELEMENTS WITH RF MEMS SWITCHES

Güçlü, Caner

MSc., Department of Electrical and Electronics Engineering

Supervisor : Assoc. Prof. Dr. Özlem Aydın Çivi

Co-Supervisor : Prof. Dr. Tayfun Akın

September 2010, 106 pages

Dual band (K and Ka) electronically scanning reflectarray with RF MEMS switches is designed, implemented and measured. Unit cell of the reflect array is composed of conductor backed split-ring elements. In order to steer the beam, the phase of the incident circularly polarized wave is controlled by RF MEMS switches that modify the angular orientation of split-rings individually. Reflectarray is designed using unit cell approach with periodic boundary conditions. The antenna is fabricated by using surface micromachining process developed in METU MEMS Center. Radiation patterns of the antenna are measured and compared with the simulations. It has been shown that the reflectarray is capable of beam switching to 35° in Ka band, 24° in K band.

Keywords: Reflectarray, RF MEMS switches, Reconfigurable antennas, Split-ring, Dual band antennas.

ÖZ

ÇİFT FREKANSTA ÇALIŞAN YENİDEN YAPILANDIRILABİLİR RF MEMS ANAHTARLI AYRIK HALKA YANSITICI DİZİ ANTENİ

Güçlü, Caner

Yüksek Lisans, Elektrik ve Elektronik Mühendisliği Bölümü

Tez Yöneticisi : Doç. Dr. Özlem Aydın Çivi

Ortak Tez Yöneticisi : Prof. Dr. Tayfun Akın

Eylül 2010, 106 sayfa

Çift bantlı (K ve Ka) elektronik tarama yeteneğine sahip RF MEMS anahtarlı yansıtıcı dizi anten tasarlandı, üretildi ve ölçüldü. Yansıtıcı dizi antenin birim hücresi iletken katmanla sonlandırılmış ayrık halkalardan oluşmaktadır. Hüzme döndürme amacıyla her bir ayrık halkanın açısal konumunu RF MEMS anahtarlarla ayarlayarak, dairesel polarizasyonlu dalgaların fazları kontrol edilmektedir. Yansıtıcı dizi anten, periyodik sınır koşulları yaklaşımından yararlanarak birim hücreler şeklinde tasarlanmıştır. Anten ODTÜ MEMS merkezinde geliştirilen yüzey mikro-işleme süreciyle üretilmiştir. Işıma örüntüleri ölçülmüş ve benzetim sonuçlarıyla karşılaştırılmıştır. Ana hüzmenin Ka bandında 35°'ye K bandında 24°'ye döndürülebildiği gösterilmiştir.

Anahtar Kelimeler: Yansıtıcı dizi anteni, RF MEMS anahtarlar, Yeniden yapılandırılabilir antenler, Ayrık halka, Çift bantlı antenler.

“A taste for truth at any cost is a passion which spares nothing.”

Albert Camus

ACKNOWLEDGMENTS

I would like to thank Assoc. Prof. Dr. Özlem Aydın Çivi for her endless guidance, encouragement, and support. Her advices and the research opportunities that she created helped me gain a vision as a young scientist and paved my road to the future as a better researcher. I would like to present my deepest gratitude to Dr. Julien Perruisseau-Carrier for his continuous support, care and the ideas and approaches which made this study successful in such a short term. Also the important contributions of Prof. Dr. Tayfun Akın are a great chance for a new researcher and the research opportunities that he provided are of great importance for me. I would like to thank him for all his guidance.

I would like to thank to Prof. Dr. Altunkan Hızal, Assoc. Prof. Dr. Şimşek Demir, and Assoc. Prof. Dr. Seyit Sencer Koç for being close and helpful to me whenever I need their valuable ideas.

I would like to express my dearest appreciations to Dr. Kağan Topallı and Dr. Mehmet Ünlü. Their patience and mentoring skills, that I always admired, provided me a perfect environment to start as a new researcher. I would not have developed my skills and aspects as a real engineer without their supervision. I thank them very much for not only being perfect technical mentors, but standing always next to me as older brothers, sharing their experiences.

I declare my gratitutes to METU RF MEMS Group members. I would like to thank Ömer Bayraklı for sharing his technical background and helping me as an antenna engineer. Ozan Doğan Gürbüz, Özgehan (Şahin) Kılıç, Çağrı Çetintepe, İlker

Comart, Ramazan Çetin, and Korkut Kaan Tokgöz are not just colleagues to me, they are my friends. Their endless help and support always made me feel secure and confident while dealing with difficulties. They have always kept our office as a friendly ambience and a safe haven.

I appreciate the efforts of METU MEMS Facility personnel, especially Orhan Akar for his kind support and Evrim Özçakır for her contributions in fabrication. Also I wish to acknowledge that this thesis is partially supported by the Scientific and Technical Research Council of Turkey (TUBITAK-EEEAG-107E090) and COST IC0603 ASSIST.

I always think that man in life can have three families: the one he is born into, the one that is born to his hands and the one he acquires throughout his life- friends. I would like to thank my friends Emre Yılmaz, Emre Tatlı, Çiğdem Okuyucu, and Dilara Çalık, Gürkan Yılmaz who have always been close and supportive. Their continuous company has always made me a stronger person against the hardships.

I would like to express my deepest thanks to my girl friend Ayça Çavcı who has been family to me, the best friend and the owner of the warmest embrace in which I found the strength and the joy of living. The whole course of this study would not be as easy without her presence.

I particularly kept the last words for my family: my father Bülent Hilmi Güçlü, my mother Ayhan Güçlü, and my brother Tansel Güçlü. I cannot even think of how life would turn out without their unconditional love and selfless care.

To my family and friends, I dedicate this thesis.

TABLE OF CONTENTS

LIST OF TABLES

TABLES

LIST OF FIGURES

FIGURES

CHAPTER 1

INTRODUCTION

Recently smart antenna applications, electronic beam shaping technologies are emerging research topics. Their area of application varies from telecommunication technologies to radar applications, from data links to automated systems in daily use. Reconfigurable reflectarray antennas constitute a highly advantageous type for these applications. The advantages of the simple reflector type antennas and the phased arrays are combined in reflectarray antennas. In this study RF MEMS technology is integrated with the reflectarray antenna type to provide reconfigurability.

In this thesis a circularly polarized reconfigurable dual frequency reflectarray antenna element with RF MEMS switches operating at 22.65 GHz and 34 GHz is designed. The reflectarray element is composed of split rings in two different sizes integrated with RF MEMS switches to obtain dual frequency operation. The phase shift principle is applied with the rotation of split-rings that the location of splits are controlled by turning on and off the RF MEMS switches that are placed with 60° spacing. The rotational phase shift principle is applied, by switching properly and rotating the 'split' of the ring. In Figure 1.1, the element and the antenna are illustrated. A prototype on which the on and off-state switches are modeled by perfect shorts and opens is designed and fabricated. The reflectarray antenna is capable of 35°and 24° beam steering in Ka and K bands respectively. There are a total of 109 Ka band and 124 K band split-rings employed. This reflectarray antenna is the first reconfigurable reflectarray antenna capable of phase control in dual bands in literature to the author's knowledge.

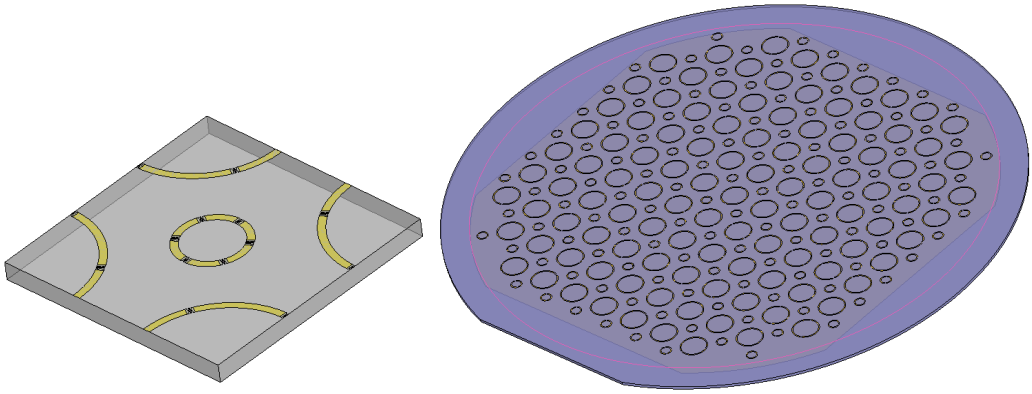

Figure 1.1 Overview of the reflectarray element and the antenna.

This introductory chapter gives the principles of reflectarray design with an overview of various reflectarray antenna applications. Then the objectives of the thesis are explained, and the organization of the thesis is presented to the reader.

1.1 Reflectarray Antennas

In this section the reflectarray antenna concept is explained and various important works in the literature are mentioned.

1.1.1 Definition and Historical Development

The reflectarray antenna is a well known antenna type whose history can be traced back to '70s [1]. The reflectarray antenna combines the advantages of the simple reflector type antennas and the phased arrays. While designing reflector type antennas, the phase front tailoring is done by making use of the different path lengths over the reflector surface. They are mostly preferred since there is no need for complex feed systems. As another common type, the phased arrays are well known and highly utilized antennas that make use of phase shifter technologies to create the desired phasing of the elements to shape the beam according to the requirements. Since their direction of radiation is determined by proper phasing, they provide freedom of physical positioning and can be mounted as desired. Reflectarray

antennas are composed of reflective elements that are especially designed to achieve phase control. Thus they are the synthesis of the phased array concept in 2D and the space feeding systems from reflector antennas. They transform the incident wave's phase front upon reflection to achieve the formation of the desired beam. It solves the complex feed-network problems of phased arrays via space-feed and volume occupation problem of reflector antennas via its planar shape.

In Figure 1.2, the reflectarray principle is depicted. The incident field on the reflectarray elements is tuned accurately to provide the phase shift upon reflection. The reflected wave front is formed by the reflected waves with the desired phase distribution, so that the phase front is adjusted to obtain the desired beam.

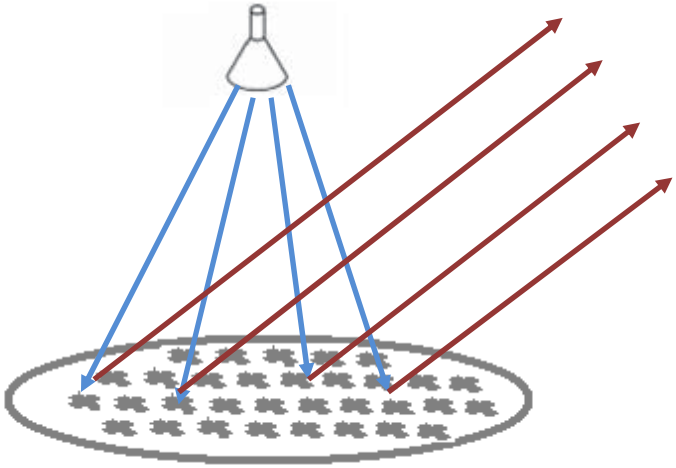

Figure 1.2 The reflectarray antenna, formation of the desired beam upon reflection.

The reflectarray antenna design is based on element design. The element design is done in various states corresponding to various reflection angles, according to the phase control principles. The phase design curve is the graph where the reflection phase is plotted against the element states. This curve is a convenient graph that shows the phase coverage, resolution and the linearity of a reflectarray element. Also the reflection magnitude versus element states can be another helpful plot.

The reflectarrays can be configured to provide pencil-beam radiation patterns, as well as multi-contoured beams. Reconfigurability can be brought in reflectarray concept to achieve electronic beam scanning.

The reflectarray antenna capabilities depend on the element properties. Reflection phase and reflection magnitude on a single element should be characterized to better analyze the behavior. Most important property of an element is the phase coverage, i.e. the phase shift contributed upon reflection. It is a fact that the magnitude of the reflected field from an element is primarily dependent on the free-space propagation loss from feed to reflectarray surface. In addition, the dielectric losses occurring in the reflective element; as well, the integrated phase shifting circuitry contributes to the losses.

The first reflectarray was proposed by Berry, Malech and Kennedy in [2]. The design was composed of short ended waveguides with variable lengths. The required phasing was formed by the delays in the waveguides where the incident field is coupled, traveled, reflected at the short end and radiated back into the sky.

In 1977 the spiraphase reflectarray was developed by Phelan [1]. This structure was implementing the rotational phase-shift principle which constitutes the basic principle in this thesis. This design employed switching diodes in a 4-arm spiral antenna. Also in '70s the microstrip antennas were developing, however the application of microstrip antennas in reflectarray concept was first done by Malagisi in 1978, [3]. Unfortunately the combination of reflectarrays with microstrip technology was no further studied until the late '80s when the necessity of low profile and low mass antennas emerged.

1.1.2 Notable Reflectarray Antennas in Literature

In reflectarrays, phase control is achieved by using several methods. One of the most favorable methods is to use variable-size patches [4], rings [5], and dipoles [6]. Also the bandwidth problem in the variable-size patch applications are solved by stacking double and triple layers of patches of different sizes, [7, 8]. The idea of loading the rectangular patches with stubs is another way of phase control. The incident field coupled to the rectangular patch travels along the stubs of different lengths reflects back and re-radiates. This method is demonstrated in [9].

The aperture coupled microstrip patch antenna is very suitable for designing a reflectarray element. The line coupled to the patch can be altered to control the phase. This type of element is suitable for single or dual polarization or circular polarization. The variable length transmission line coupled through the slot to the patch is implemented in [10]. Achieving wide phase range to solve the bandwidth problem by loading stubs is demonstrated in [11]. In addition, this element can be integrated with switches and active structures to introduce reconfigurability. A sample with Metal Semiconductor Field Effect Transistor to amplify and adjust the phase is shown in [12]. Also the linearly polarized ACMP (Aperture Coupled Microstrip Patch) antenna using RF MEMS switches to provide reconfigurability is studied [13-15].

The rotational phase shift principle which was first put forward by Phelan [1], is used in various applications to design circularly polarized reflectarrays. This principle states that the phase of the co-polarized wave upon circularly polarized wave incidence is linearly dependent on the elements rotation angle. Rotating patches are designed to utilize this principle in [16]; as well, multiple dipoles are employed with the same principle [17]. The most important applications of this phase control method in the context of this thesis are the ones using split-ring elements in single and dual frequency reflectarrays [18-21]. The work presented in this thesis also is a

dual frequency reflectarray with split-rings. In addition, this reflectarray unit cell element is the capable of phase control in two frequencies independently; at this aspect it is the only reconfigurable dual frequency ever presented to the author's knowledge.

The reconfigurable reflectarray configurations employ several techniques as tunable dielectrics, varactor diodes, PIN diodes and MEMS implementations including micro-motors and RF MEMS.

Varactor diodes affect on the radiation susceptance of antennas by capacitive loading. In [22] , the 2D rectangular patches are biased at their centers with vias through the substrate and ground plane. Then each patch is connected to the neighboring patches with varactors. By properly adjusting the voltage distribution, the surface turns in to a tunable impedance surface making it possible to steer beams. In [23], PIN and varactor diodes are put into a cross-shaped microstrip loop for a dual polarized, polarization flexible reflective cell whose phase can be dynamically controlled.

The tunable dielectrics may be used as substrates, or to fill cavities. Then the frequency/phase response of the reflective element is controlled by biasing these structures electrically. The examples for these applications are ferroelectric thin film, liquid crystals (LC) [24-28].

1.1.3 MEMS in Reflectarray Antennas

MEMS (Micro Electro-Mechanical Systems) is an enabling technology in microwave and antenna engineering field, for being suitable for monolithic fabrication, enabling miniaturization of the transceivers.

In [29], a pseudo-ring structure as the reflectarray element loaded with 5 pairs of switches is shown. The element has 360° phase coverage. The design is experimentally validated by testing in rectangular waveguide simulator. In another study [30], a suspended patch is designed and fabricated by micromachining. As the suspending patch is pulled down by electrostatic actuation, the phase is tuned. But the reflection phase characteristic is poor and limited to 200° coverage. In [31], a patch-slot element is utilized as the reflectarray cell. The slot of the element is loaded with RF MEMS shunt switches; approximately 120° phase coverage is demonstrated.

Most of the reflectarrays with MEMS are implemented only in unit cells and characterized by waveguide simulators. There a few examples of full reflectarrays with MEMS [13, 30, 32-34] and only one with measurement results, [13]. The reflectarray presented in this thesis also provides full reflectarray design.

1.2 Thesis Objective and Organization

The goal of this thesis is to design a reconfigurable circularly polarized dual band reflectarray antenna composing of split-ring elements integrated with RF MEMS switches. Rotational phase shift principle is implemented as the phase control principle. The RF MEMS fabrication process developed in Middle East Technical University is utilized in design. The objectives are stated as follows:

- Rotational phase shift principle,
    - is studied to reach a mathematical expression and a better comprehension of the phenomenon.
    - is implemented using a split-ring element.

- A reflectarray element,
    - capable of controlling the phase of the co-polarized reflected wave

upon a circularly polarized incident wave
    - having a linear phase design curve and 360° phase coverage in two frequency bands
    - achieving phase control in two frequency bands simultaneously, i.e. independent operation in both bands
    - integrated with RF MEMS switches, to provide 120° phase resolution in both bands

  is designed.

- A reflectarray antenna prototype,
    - composed of the aforementioned element
    - capable of beam switching between broad side and 24° at 24.4 GHz and 35° at 35.5 GHz.
    - that is aimed to verify the dual frequency split-ring element operation
    - composed of split-rings with short/open modeling of the MEMS switches instead of fully operational RF MEMS implementation.

  is designed, fabricated and measured.

This thesis constitutes a collection of the studies in the frame of the mentioned objectives. The studies and accomplishments up to date are bundled together in the course of five chapters. Beyond this introductory Chapter 1, which gives a summary of the reflectarray concept with historical background and provides the reader with organizational details of this thesis, the contents of the chapters are explained as follows:

Chapter 2: The rotational phase shift principle is defined. The mathematical expressions are derived to have an insight view to the phenomenon. The conditions on the reflective element and the illumination of the reflectarray antenna for the realization of the principle are given.

Chapter 3: The split-ring element is studied by means of simulation tools.

The element is subject to a parametric analysis. The essential information to tune the reflective characteristics is investigated in order to implement the rotational phase shift principle. In addition the characteristics of a reflectarray element operating at a single frequency composed of a split-ring is designed and characterized.

Chapter 4: A dual band reflectarray element of split-rings is designed and characterized. RF MEMS switch topology is given and the dual band reflectarray element with integrated switches is presented. A prototype reflectarray antenna design with radiation pattern simulation results is provided. Then these results are compared with the measurement results of the fabricated prototype.

Chapter 5: The conclusions and future works are explained. The discussion of the goals and achievements are made.

CHAPTER 2

THEORY OF THE ROTATIONAL PHASE SHIFT PRINCIPLE

2.1 Introduction

The reflectarray antenna design is basically dependent on the capabilities and characteristics of the reflective element. Along many techniques concerning the linearly polarized waves, some of which can be also applied to circularly polarized waves, there is the rotational phase shift principle special to circularly polarized waves. This chapter presents the theoretical derivations, and meanings of the final form of the reflection equation.

2.2 The Rotational Phase Shift Principle

In case of the circularly polarized wave incident on a reflective element, when the element is rotated the phase of the reflected wave is linearly dependent on the relative angular position of the reflective topology. This type of dependence requires some conditions on the incident and reflected waves, and derivation is hence important for the design process of the reflective element. The same principle was previously demonstrated in [1], [35] and a mathematical derivation is briefly given in [16] with a specific application.

Throughout this thesis, the electromagnetic waves of interest are circularly polarized. This is the reason for denoting a common convention. Since the circularly polarized waves with opposite senses constitute an independent orthogonal basis set for the

electromagnetic plane waves, any plane wave can be expressed as a sum of two circularly polarized plane waves with opposite senses. The co- and cross-polarization terms in the context of circularly polarized waves refer to the sense of interest and the latter sense respectively.

The rotational phase shift principle is explained as follows. Upon incidence of a circularly polarized wave onto a reflective surface, the phase of the reflected co-polarized circularly wave is linearly proportional to the angular position of the reflective element. That is, the phase of reflection may be controlled by the relative angular orientation of the reflective element. The phase shift is totally dependent on the geometry, and it is independent of the frequency of operation as well as the reflection coefficient of co-polarized wave.

2.3 Derivation of the Linear Proportionality

In this section the mathematical derivation of the rotational phase shift principle is given. The derivation provides an in-depth view for the design.

The aim is mathematically to reach an expression relating the reflection characteristics of an element and the reflection characteristics of its physically rotated version. The starting point of the derivation is deducing the reflection parameters of the rotated version by mathematical elaboration using coordinate transformations. In Figure 2.1, the reflective element (which is backed by a ground plane) and the physical rotation angle is demonstrated. Although the figure depicts a split-ring element on the plane, the derivation is valid for any arbitrary reflective surface.

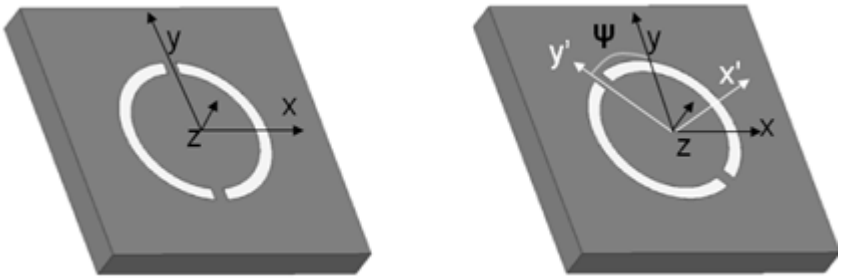

Figure 2.1 The illustration of a reflective element and rotation about z-axis.

Regarding Figure 2.1, there are two distinct coordinate systems. The primed coordinate system and the basic coordinate system have the common z/z' axes. The primed coordinate system is defined to have rotated about the common z axis, by an arbitrary angle ψ. In other words the primed and basic coordinate systems share the common XY plane, and the origin, but there is a rotational offset about z axis. For the initial state of the reflective element, say ψ=0°, the two coordinate systems are the same. It is assumed that the reflection coefficients for the element are known. From this point on, for the primed coordinate systems, the reflection coefficients for the reflective element is always the same and known, but the reflection coefficients with regard to the basic coordinate system is easy to derive applying rotational transformation matrices forth and back.

For conventional purposes, the incident and reflected fields in general are expressed as follows:

$$E^{inc} = (E_{x'}^{inc}\hat{a}_{x'} + E_{y'}^{inc}\hat{a}_{y'})e^{jz'} = (E_x^{inc}\hat{a}_x + E_y^{inc}\hat{a}_y)e^{jz} \tag{2.1}$$

$$E^{ref} = (E_{x'}^{ref}\hat{a}_{x'} + E_{y'}^{ref}\hat{a}_{y'})e^{-jz'} = (E_x^{ref}\hat{a}_x + E_y^{ref}\hat{a}_y)e^{-jz} \tag{2.2}$$

Note that e^{jz} and e^{-jz} are used for the incident and reflected field expressions respectively. From this point on, the derivations are assumed to be carried on at z=z'=0, on the surface where the reflection takes place. That is why the exponential terms are not represented.

The reflection characteristics are handled as an S-matrix, relating the reflection and cross-coupling of the x and y components of the incident and reflected fields. For example, the reflection characteristics for primed coordinate system correspond to:

$$\begin{pmatrix} E_{x'}^{ref} \\ E_{y'}^{ref} \end{pmatrix} = [S'] \begin{pmatrix} E_{x'}^{inc} \\ E_{y'}^{inc} \end{pmatrix} = \begin{pmatrix} s'_{11} & s'_{12} \\ s'_{21} & s'_{22} \end{pmatrix} \begin{pmatrix} E_{x'}^{inc} \\ E_{y'}^{inc} \end{pmatrix} \tag{2.3}$$

The Equation (2.3) shows the reflected and incident electric field quantities, the reflections and the cross-coupling between x and y components. The assumption is that this matrix is at hand. The goal is to achieve a similar matrix equation for the non-primed coordinate system:

$$\begin{pmatrix} E_{x}^{ref} \\ E_{y}^{ref} \end{pmatrix} = [S] \begin{pmatrix} E_{x}^{inc} \\ E_{y}^{inc} \end{pmatrix} = \begin{pmatrix} s_{11} & s_{12} \\ s_{21} & s_{22} \end{pmatrix} \begin{pmatrix} E_{x}^{inc} \\ E_{y}^{inc} \end{pmatrix} \tag{2.4}$$

To reach the s-matrix, the transformations between basic and the primed coordinate system is to be applied. These transformation matrices are as follows:

$$\begin{pmatrix} x \\ y \end{pmatrix} = \begin{pmatrix} \cos(\Psi) & -\sin(\Psi) \\ \sin(\Psi) & \cos(\Psi) \end{pmatrix} \begin{pmatrix} x' \\ y' \end{pmatrix} \tag{2.5}$$

$$\begin{pmatrix} x' \\ y' \end{pmatrix} = \begin{pmatrix} \cos(\Psi) & \sin(\Psi) \\ -\sin(\Psi) & \cos(\Psi) \end{pmatrix} \begin{pmatrix} x \\ y \end{pmatrix} \tag{2.6}$$

When the primed incident field is expressed with respect to the basic coordinate system:

$$\begin{pmatrix} E_{x'}^{inc} \\ E_{y'}^{inc} \end{pmatrix} = \begin{pmatrix} \cos(\Psi) & \sin(\Psi) \\ -\sin(\Psi) & \cos(\Psi) \end{pmatrix} \begin{pmatrix} E_{x}^{inc} \\ E_{y}^{inc} \end{pmatrix} \tag{2.7}$$

Then the reflected field expression in primed coordinate system is reached by combining Equations (2.3) and (2.7):

$$\begin{pmatrix} E_{x'}^{ref} \\ E_{y'}^{ref} \end{pmatrix} = \begin{pmatrix} s'_{11} & s'_{12} \\ s'_{21} & s'_{22} \end{pmatrix} \begin{pmatrix} \cos(\Psi) & \sin(\Psi) \\ -\sin(\Psi) & \cos(\Psi) \end{pmatrix} \begin{pmatrix} E_{x}^{inc} \\ E_{y}^{inc} \end{pmatrix} \tag{2.8}$$

The reflected field components in the basic coordinate system in terms of the primed coordinate system component are as follows:

$$\begin{pmatrix} E_x^{ref} \\ E_y^{ref} \end{pmatrix} = \begin{pmatrix} \cos(\Psi) & -\sin(\Psi) \\ \sin(\Psi) & \cos(\Psi) \end{pmatrix} \begin{pmatrix} E_{x'}^{ref} \\ E_{y'}^{ref} \end{pmatrix} \tag{2.9}$$

Combining the Equations (2.8) and (2.9):

$$\begin{pmatrix} E_x^{ref} \\ E_y^{ref} \end{pmatrix} = \begin{pmatrix} \cos(\Psi) & -\sin(\Psi) \\ \sin(\Psi) & \cos(\Psi) \end{pmatrix} \begin{pmatrix} s'_{11} & s'_{12} \\ s'_{21} & s'_{22} \end{pmatrix} \begin{pmatrix} \cos(\Psi) & \sin(\Psi) \\ -\sin(\Psi) & \cos(\Psi) \end{pmatrix} \begin{pmatrix} E_x^{inc} \\ E_y^{inc} \end{pmatrix} \tag{2.10}$$

The Equation (2.10) is a very important step because:

1. This is the first fundamental result, since it gives the reflected wave properties for any normally incident wave as a function of:
    a. A single characteristic S-matrix which is pertaining to a specific angular orientation of the reflective element,
    b. The angle of rotation of the reflective element.
2. This is a big advantage over characterizing the different angular orientations of the element to be regarded as simple angular rotations.

The reflective element is assumed to be composing of reciprocal materials, this makes the off-diagonal terms equal; $s'_{12} = s'_{21}$. With this contribution, after the necessary matrix multiplication operations the incident and reflected field relations in terms of physical rotation angle and the reflection characteristics at hand (which pertain to the primed coordinate system) the final form is:

$$\begin{aligned} \begin{pmatrix} E_x^{ref} \\ E_y^{ref} \end{pmatrix} &= [S] \begin{pmatrix} E_x^{inc} \\ E_y^{inc} \end{pmatrix} \\ &= \begin{pmatrix} [s'_{11}\cos^2(\Psi) + s'_{22}\sin^2(\Psi) & [(s'_{11} - s'_{22})\sin(\Psi)\cos(\Psi) \\ -2s'_{12}\sin(\Psi)\cos(\Psi)] & +s'_{12}(\cos^2(\Psi) - \sin^2(\Psi))] \\ [(s'_{11} - s'_{22})\sin(\Psi)\cos(\Psi) & [s'_{11}\sin^2(\Psi) + s'_{22}\cos^2(\Psi) \\ +s'_{12}(\cos^2(\Psi) - \sin^2(\Psi))] & +2s'_{12}\sin(\Psi)\cos(\Psi)] \end{pmatrix} \begin{pmatrix} E_x^{inc} \\ E_y^{inc} \end{pmatrix} \end{aligned} \tag{2.11}$$

To better analyze the matrix relation in (2.11), decomposing [S'] is a very helpful

method. [S'] can be expressed as a sum as shown:

$$[S'] = [S']_A + [S']_B + [S']_C \tag{2.12}$$

$$\begin{pmatrix} s'_{11} & s'_{12} \\ s'_{21} & s'_{22} \end{pmatrix} = \begin{pmatrix} A & 0 \\ 0 & A \end{pmatrix} + \begin{pmatrix} B & 0 \\ 0 & -B \end{pmatrix} + \begin{pmatrix} 0 & -jC \\ -jC & 0 \end{pmatrix} \tag{2.13}$$

Where:

$$A = \frac{1}{2}(s'_{11} + s'_{22}) \tag{2.14}$$

$$B = \frac{1}{2}(s'_{11} - s'_{22}) \tag{2.15}$$

$$C = js'_{12} \tag{2.16}$$

Simply using the distribution of multiplication over summation, the final expression can be meaningfully derived. It can be seen that any matrix [S'] can be decomposed into the three matrices in Equation (2.13). Moreover, as previously mentioned any incident wave can be expressed in terms of two circularly polarized waves of opposite senses. This is the reason that the reflected field will be examined upon incident circularly polarized fields. The reflected field expressions for the circularly polarized incident field are examined for each part (namely: $[S']_A$, $[S']_B$ and $[S']_C$) of the matrix [S'] to build up the final expression of the reflected field.

$$\text{Let } \begin{pmatrix} E_x^{inc} \\ E_y^{inc} \end{pmatrix} = \begin{pmatrix} 1 \\ \pm j \end{pmatrix} E_0^{inc} \tag{2.17}$$

- For the partial solution of $\begin{pmatrix} s'_{11} & s'_{12} \\ s'_{21} & s'_{22} \end{pmatrix}_A = \begin{pmatrix} A & 0 \\ 0 & A \end{pmatrix}$, the Equation (2.11) turns into:

$$\begin{pmatrix} E_x^{ref} \\ E_y^{ref} \end{pmatrix}_A = \begin{pmatrix} [A\cos^2(\Psi) + A\sin^2(\Psi) & [(A-A)\sin(\Psi)\cos(\Psi) \\ -2\cdot 0\cdot\sin(\Psi)\cos(\Psi)] & +0\cdot(\cos^2(\Psi) - \sin^2(\Psi))] \\ [(A-A)\sin(\Psi)\cos(\Psi) & [A\sin^2(\Psi) + A\cos^2(\Psi) \\ +0\cdot(\cos^2(\Psi) - \sin^2(\Psi))] & +2\cdot 0\cdot\sin(\Psi)\cos(\Psi)] \end{pmatrix} \begin{pmatrix} E_x^{inc} \\ E_y^{inc} \end{pmatrix} \tag{2.18}$$

$$= \begin{pmatrix} A & 0 \\ 0 & A \end{pmatrix} \begin{pmatrix} E_x^{inc} \\ E_y^{inc} \end{pmatrix} \tag{2.19}$$

After taking into account the incident field expressed as in Equation (2.17):

$$\begin{pmatrix} E_x^{ref} \\ E_y^{ref} \end{pmatrix}_A = \begin{pmatrix} A & 0 \\ 0 & A \end{pmatrix} \begin{pmatrix} 1 \\ \pm j \end{pmatrix} E_0^{inc} \tag{2.20}$$

$$\begin{pmatrix} E_x^{ref} \\ E_y^{ref} \end{pmatrix}_A = A \begin{pmatrix} 1 \\ \pm j \end{pmatrix} E_0^{inc} \tag{2.21}$$

The reflected field in Equation (2.21) is the cross polarized wave upon reflection. One should note that the direction of propagation reversed while the electric field vector is scaled by A.

- For the partial solution of $\begin{pmatrix} s'_{11} & s'_{12} \\ s'_{21} & s'_{22} \end{pmatrix}_B = \begin{pmatrix} B & 0 \\ 0 & -B \end{pmatrix}$, the Equation (2.11) turns into:

$$\begin{pmatrix} E_x^{ref} \\ E_y^{ref} \end{pmatrix}_B = \begin{pmatrix} [B\cos^2(\Psi) - B\sin^2(\Psi) & [(B+B)\sin(\Psi)\cos(\Psi) \\ -2\cdot 0\cdot\sin(\Psi)\cos(\Psi)] & +0\cdot(\cos^2(\Psi)-\sin^2(\Psi))] \\ [(B+B)\sin(\Psi)\cos(\Psi) & [B\sin^2(\Psi) - B\cos^2(\Psi) \\ +0\cdot(\cos^2(\Psi)-\sin^2(\Psi))] & +2\cdot 0\cdot\sin(\Psi)\cos(\Psi)] \end{pmatrix} \begin{pmatrix} E_x^{inc} \\ E_y^{inc} \end{pmatrix} \tag{2.22}$$

$$= \begin{pmatrix} B(\cos^2(\Psi)-\sin^2(\Psi)) & 2B\sin(\Psi)\cos(\Psi) \\ 2B\sin(\Psi)\cos(\Psi) & -B(\cos^2(\Psi)-\sin^2(\Psi)) \end{pmatrix} \begin{pmatrix} E_x^{inc} \\ E_y^{inc} \end{pmatrix} \tag{2.23}$$

$$= B \begin{pmatrix} \cos(2\Psi) & \sin(2\Psi) \\ \sin(2\Psi) & -\cos(2\Psi) \end{pmatrix} \begin{pmatrix} E_x^{inc} \\ E_y^{inc} \end{pmatrix} \tag{2.24}$$

After taking into account the incident field expressed as in Equation (2.17):

$$\begin{pmatrix} E_x^{ref} \\ E_y^{ref} \end{pmatrix}_B = B \begin{pmatrix} \cos(2\Psi) & \sin(2\Psi) \\ \sin(2\Psi) & -\cos(2\Psi) \end{pmatrix} \begin{pmatrix} 1 \\ \pm j \end{pmatrix} E_0^{inc} \tag{2.25}$$

$$= B\begin{pmatrix} \cos(2\Psi) \pm j\sin(2\Psi) \\ \sin(2\Psi) \pm j\cos(2\Psi) \end{pmatrix} E_0^{inc} \tag{2.26}$$

$$= B\begin{pmatrix} \cos(2\Psi) \pm j\sin(2\Psi) \\ \mp j(\cos(2\Psi) \pm j\sin(2\Psi)) \end{pmatrix} E_0^{inc} \tag{2.27}$$

$$= B\begin{pmatrix} e^{\pm j2\Psi} \\ \mp j e^{\pm j2\Psi} \end{pmatrix} E_0^{inc} \tag{2.28}$$

$$\begin{pmatrix} E_x^{ref} \\ E_y^{ref} \end{pmatrix}_B = Be^{\pm j2\Psi} \begin{pmatrix} 1 \\ \mp j \end{pmatrix} E_0^{inc} \tag{2.29}$$

The reflected field in Equation (2.29) is co-polarized with the incident wave. Note the y-component is reversed as the x-component is the same and the direction of propagation is reversed upon reflection. It is easily seen that a phase multiplication is present while the vector is scaled by B. This is a reflected co-polarized wave whose phase is in advance or delayed - depending on the circular polarization sense- twice the physical rotation angle of the reflective element.

- For the partial solution of $\begin{pmatrix} s'_{11} & s'_{12} \\ s'_{21} & s'_{22} \end{pmatrix}_C = \begin{pmatrix} 0 & -jC \\ -jC & 0 \end{pmatrix}$, the Equation (2.11) turns into:

$$\begin{pmatrix} E_x^{ref} \\ E_y^{ref} \end{pmatrix}_C = \begin{pmatrix} [0\cdot\cos^2(\Psi) + 0\cdot\sin^2(\Psi) & [(0-0)\sin(\Psi)\cos(\Psi) \\ -2\cdot(-jC)\cdot\sin(\Psi)\cos(\Psi)] & +(-jC)\cdot(\cos^2(\Psi) - \sin^2(\Psi))] \\ [(0-0)\sin(\Psi)\cos(\Psi) & [0\cdot\sin^2(\Psi) + 0\cdot\cos^2(\Psi) \\ +(-jC)\cdot(\cos^2(\Psi) - \sin^2(\Psi))] & +2\cdot(-jC)\cdot\sin(\Psi)\cos(\Psi)] \end{pmatrix} \begin{pmatrix} E_x^{inc} \\ E_y^{inc} \end{pmatrix} \tag{2.30}$$

$$= \begin{pmatrix} j2C\sin(\Psi)\cos(\Psi) & -jC(\cos^2(\Psi) - \sin^2(\Psi)) \\ -jC(\cos^2(\Psi) - \sin^2(\Psi)) & -j2C\sin(\Psi)\cos(\Psi) \end{pmatrix} \begin{pmatrix} E_x^{inc} \\ E_y^{inc} \end{pmatrix} \tag{2.31}$$

$$= -jC\begin{pmatrix} -\sin(2\Psi) & \cos(2\Psi) \\ \cos(2\Psi) & \sin(2\Psi) \end{pmatrix} \begin{pmatrix} E_x^{inc} \\ E_y^{inc} \end{pmatrix} \tag{2.32}$$

After taking into account the incident field expressed as in Equation (2.17):

$$\begin{pmatrix} E_x^{ref} \\ E_y^{ref} \end{pmatrix}_C = -jC \begin{pmatrix} -\sin(2\Psi) & \cos(2\Psi) \\ \cos(2\Psi) & \sin(2\Psi) \end{pmatrix} \begin{pmatrix} 1 \\ \pm j \end{pmatrix} E_0^{inc} \tag{2.33}$$

$$= C \begin{pmatrix} -\sin(2\Psi) & \cos(2\Psi) \\ \cos(2\Psi) & \sin(2\Psi) \end{pmatrix} \begin{pmatrix} -j \\ \pm 1 \end{pmatrix} E_0^{inc} \tag{2.34}$$

$$= C \begin{pmatrix} j\sin(2\Psi) \pm \cos(2\Psi) \\ -j\cos(2\Psi) \pm \sin(2\Psi) \end{pmatrix} E_0^{inc} \tag{2.35}$$

$$= C \begin{pmatrix} \pm(\cos(2\Psi) \pm j\sin(2\Psi)) \\ -j(\cos(2\Psi) \pm j\sin(2\Psi)) \end{pmatrix} E_0^{inc} \tag{2.36}$$

$$= C \begin{pmatrix} \pm e^{\pm j2\Psi} \\ -je^{\pm j2\Psi} \end{pmatrix} E_0^{inc} \tag{2.37}$$

$$= \pm C \begin{pmatrix} e^{\pm j2\Psi} \\ \mp je^{\pm j2\Psi} \end{pmatrix} E_0^{inc} \tag{2.38}$$

$$\begin{pmatrix} E_x^{ref} \\ E_y^{ref} \end{pmatrix}_C = \pm Ce^{\pm j2\Psi} \begin{pmatrix} 1 \\ \mp j \end{pmatrix} E_0^{inc} \tag{2.39}$$

The reflected field in Equation (2.39) is co-polarized with the incident wave. Note the y-component is reversed as the x-component is the same and the direction of propagation is reversed upon reflection. It is easily seen that a phase multiplication is present while the vector is scaled by C. This is also a reflected co-polarized wave whose phase is in advance or delayed -depending on the circular polarization sense- twice the physical rotation angle of the reflective element.

Then the total resultant reflected field expression for the reflective element having the reflection matrix [S'] with a ψ° angular offset is upon incident field mentioned in (2.17) can be found as:

$$\begin{pmatrix} E_x^{ref} \\ E_y^{ref} \end{pmatrix} = \begin{pmatrix} E_x^{ref} \\ E_y^{ref} \end{pmatrix}_A + \begin{pmatrix} E_x^{ref} \\ E_y^{ref} \end{pmatrix}_B + \begin{pmatrix} E_x^{ref} \\ E_y^{ref} \end{pmatrix}_C \tag{2.40}$$

$$\begin{pmatrix} E_x^{ref} \\ E_y^{ref} \end{pmatrix} = (B \pm C) e^{\pm j2\Psi} \begin{pmatrix} 1 \\ \mp j \end{pmatrix} E_0^{inc} + A \begin{pmatrix} 1 \\ \pm j \end{pmatrix} E_0^{inc} \tag{2.41}$$

Finally the phasor expressions of the incident and reflected fields in terms of the entries of [S'] and physical rotation angle ψ° are stated as follows:

$$E^{inc} = E_0^{inc} (\hat{a}_x \pm j\hat{a}_y) e^{jz} \tag{2.42}$$

$$\begin{aligned} E^{ref} = & \\ & E_0^{inc} [\frac{1}{2}(s'_{11} - s'_{22}) \pm j s'_{12}] (\hat{a}_x \mp j\hat{a}_y) e^{\pm j2\Psi} e^{-jz} \\ & + E_0^{inc} [\frac{1}{2}(s'_{11} + s'_{22})] (\hat{a}_x \pm j\hat{a}_y) e^{-jz} \end{aligned} \tag{2.43}$$

The interpretation of the reflected field expression is the key points of the reflective element design:

- Since the initial state, i.e. the matrix [S'] may be arbitrarily chosen; the simulation results for any angular position of the reflective element can provide the reflection levels of co- and cross-polarized reflected field levels. Referring to Equations (2.11) and (2.43) :

$$\Gamma_{co-pol.} = \frac{1}{2}(s'_{11} - s'_{22}) \pm j s'_{12} \tag{2.44}$$

$$\left| \frac{1}{2}(s'_{11} - s'_{22}) \pm j s'_{12} \right| = \left| \frac{1}{2}(s_{11} - s_{22}) \pm j s_{12} \right| \tag{2.45}$$

$$\Gamma_{cross-pol.} = \frac{1}{2}(s'_{11} + s'_{22}) \tag{2.46}$$

$$\frac{1}{2}(s'_{11} + s'_{22}) = \frac{1}{2}(s_{11} + s_{22}) \tag{2.47}$$

The magnitude of the reflected co-polarization level is constant with ψ -as expected the phase is not-, while the reflection magnitude and phase of the cross-

polarized component are constant, i.e. $\Gamma_{cross-pol.}$ is constant.

- The linear dependence of the phase of the reflected co-polarized wave on the rotation angle is independent of the reflection level.

- The sign of phase contribution by the rotational phase control principle depends on the sense of circular polarization.

- When the incident field is not a perfect circularly polarized wave (Regarding (2.48), $N \neq 0$), i.e. includes a cross-polarized wave; the element will not be capable of totally controlling the phase of the reflected co-polarized wave (Equation (2.49)).

  Moreover if the reflected field is required to be a perfect circularly polarized wave whose phase can be controlled by rotation, the cross-polarization should be suppressed by the reflective element ($\Gamma_{cross-pol.} = 0$) along with a perfect circularly polarized incident wave (N=0).

$$E^{inc} = M(\hat{a}_x + j\hat{a}_y)e^{jz} + N(\hat{a}_x - j\hat{a}_y)e^{jz} \tag{2.48}$$

$$\begin{aligned} E^{ref} = & \\ & [\Gamma_{co-pol.}Me^{+j2\Psi} + \Gamma_{cross-pol.}N](\hat{a}_x - j\hat{a}_y)e^{-jz} \\ & +[\Gamma_{co-pol.}Ne^{-j2\Psi} + \Gamma_{cross-pol.}M](\hat{a}_x + j\hat{a}_y)e^{-jz} \end{aligned} \tag{2.49}$$

2.4 Conclusion

Explanation of rotational phase control principle has been the main concern of this chapter. An in-depth aspect is acquired through the mathematical basis. The conditions to guarantee successful implementation of the principle are examined and well derived. It is evident that the most important factor is to provide an almost perfect circularly polarized incident wave. Also to increase the gain the reflective

element should well suppress the cross-polarized reflected component. Under these conditions the normally incident wave can be reflected as a totally phase-controllable co-polarized wave. As the incidence angle varies from normal, the characteristics are due investigations and these are strongly prone to the element type.

To utilize this principle in the reflectarray design, extensive comprehension of the principle should be figured out. In the beginning of the derivation, the coordinate systems are relatively rotated. This means that the whole plane is rotated actually, not the element. In reflectarray implementation, all the elements can independently rotate on the plane locally, that is, the principle is applied locally to each element. The assumption is that the unit cell of the reflectarray antenna exhibits the similar behavior over its own course, which is the each individual cell can control the phase by rotation independently.

CHAPTER 3

DESIGN OF SINGLE BAND REFLECTARRAY ELEMENT

3.1 Introduction

In this chapter, the element design of a reflectarray is explained. There are various methods used for the design such as designing the reflectarray elements as a unit cell in a periodic environment, or an element-based design using phase-shifters. The preference of these methods depends on the phase control principle employed as well as the design tools at hand. In this chapter, the reflectarray element designed as a unit cell of a periodic structure is studied, the necessary simulation tools, parametrical analysis of the reflective element and the phase design curves achieved by a single frequency split-ring reflectarray element are demonstrated.

The mathematical derivations for canonical structures and application of a theoretical principle to realizable structure to obtain an initial design should always be verified. The design procedure necessarily includes cycles of tests and re-designs. Even if there are available strong mathematical tools; each proposed structure cannot have analytical models, and these analytical models do not lack the requirement of tests. To quicken this design and verification cycle, fast and accurate simulation tools are of great importance.

Upon developing various efficient numerical methods and the capacitance of today's computers; full wave electromagnetic simulation software package programs are in

common use and provide a reliable design environment for the antenna engineers. These package software utilize various numerical methods to solve the integro-differential equations governing the electromagnetic phenomena. Among various numerical methods followings are the most used ones: method of moments (MoM), finite difference-time domain method (FDTD), and finite element method (FEM), fast multipole method (FMM). These methods are compared in [36]. Moreover, commercial software based on these numerical methods are also capable of implementation of various analytical techniques integrated with the numerical methods such as various boundary conditions, periodic arrays.

3.2 Characterization of a Reflectarray Element

The expectations from a reflect array element depend on mainly the system requirements aimed at the beginning of the study. The most general condition is a linear phase curve capable of minimum 360° phase range. Another one is the reflection levels of co- and cross-polarization as well as loss contributed by the unit cell upon reflection. The array theory implies that the beam steering properties of an array is sensitive to proper phasing than the magnitude, the magnitude distribution is effective on side-lobe levels and the beam-width. Thus it can be said that the aforementioned two quantities are to maintain the phase distribution and magnitude levels as desired. Also the frequency response of the reflectarray element is effective both on magnitude and phase. Moreover there may be additional requirements for the unit cell depending on the phase control mechanism. The Chapter 2 is on the requirements of reflectarray and the acquirements from the rotational phase shift principle. For example to use this principle with high gain the cross polarization should be suppressed in the operation frequency. That is why the frequency characteristics should also be set first. Then the rest will be to verify the rotational phase shift principle in a periodic planar array by rotating the element individually.

The reflectarray antennas intrinsically have the elements under illumination with different incident angles that span a solid angle. Figure 3.1 depicts the angle between the surface normal and the incident waves from the illumination horn. It is important

that the designer should consider the phase design curve and magnitude curve should also be examined for various incidence angles. The various incidence angles form the illumination solid angle span and the numerous element states constitute a great number of cases to simulate, and time needed for simulations can also rise drastically. That is why the simulations are also to be carried out for meaningfully sampled states from which the characteristics of the element can be well extracted.

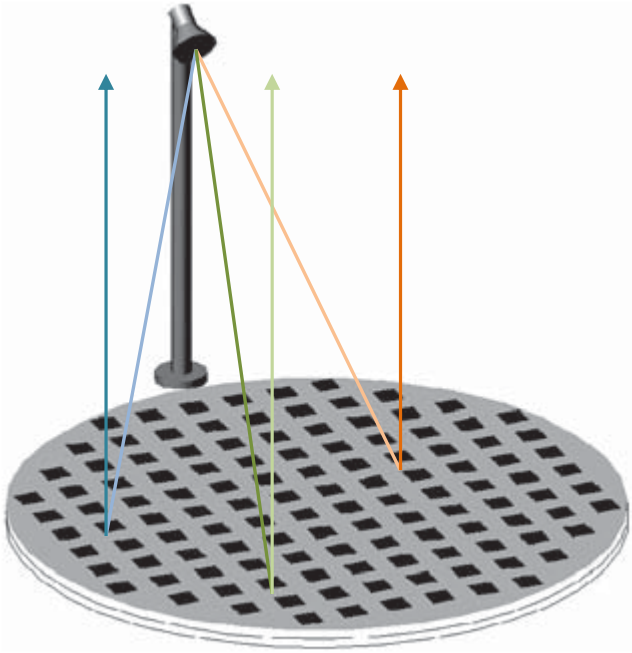

Figure 3.1 The illustration of incidence angle variation on the surface of the reflectarray antenna.

The elements of the reflectarray antenna lie on a surface surrounded by numerous similar elements. The element design procedure should integrate the coupling effects of the surrounding numerous elements. It is obvious that in fact most elements of a reflectarray are surrounded by slightly modified structures to maintain the phase distribution. The reflectarray element is thus designed and characterized in an

infinite planar array while designing in a simulation environment. The unit cell of the infinite array is simulated as a part of an infinite planar array composing of identical elements, as shown in Figure 3.2. The assumption of periodicity is widely accepted in reflectarray element design, although the results are not strictly valid for the elements placed close to the boundary of the array. This is the inevitable result of use of the software environments and the requirement of fast computation, since the cost of computational requirements for characterizing a finite array -if possible- is very high. The infinite array assumption enables the designer to use periodic boundary conditions in FEM, which in turn reduce the computational time.

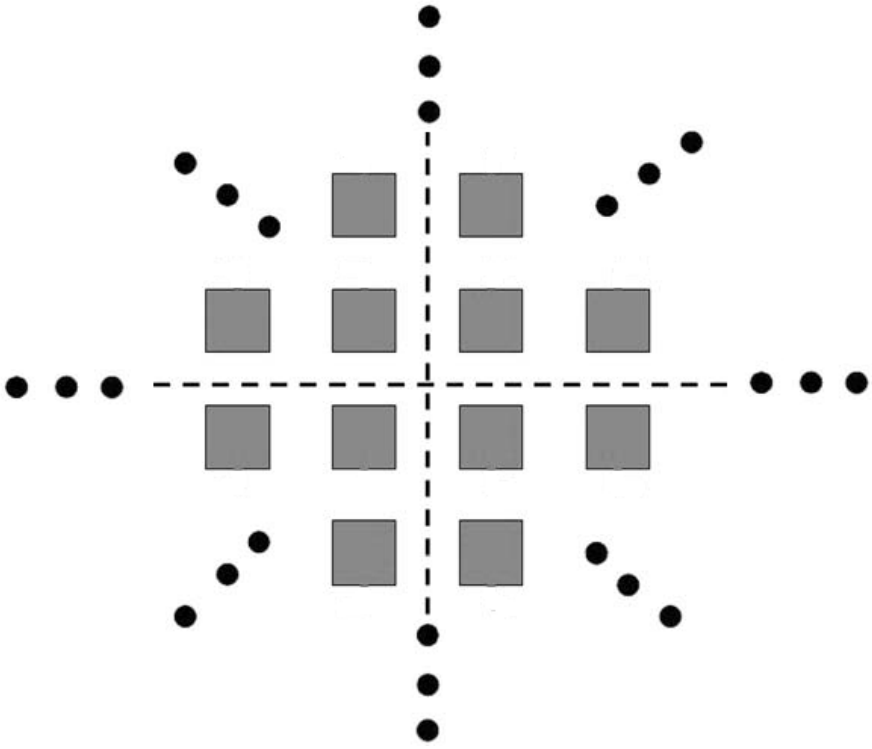

Figure 3.2 Infinite planar array.

To sum up the simulation requirements, the software should handle the following:

- ✓ Simulation of infinite periodic arrays.
- ✓ Ease of use to deduce the incident and reflected field characteristics.
- ✓ The incident wave can be applied at angles other than normal.

3.3 Simulation Environment

HFSS is a commercial full wave electromagnetic field solver. It is implemented based on the finite element method. HFSS solver provides the solutions of E- and H-fields, currents, S-parameters, near and far fields. The 3D structures are meshed automatically, and meshes are refined adaptively. This software is chosen for it includes the tools implemented for simulation of periodic structures, the Floquet port to easily calculate the reflection characteristics for the unit cell. The important parameters for simulations to be reliable are the implemented boundary conditions to the FEM and the meshing quality. First of all meshing is very important; it is no surprise that as the number of meshes increase the simulation results will converge to reality. This has a high cost of memory space and computational capacity of a computer. In this manner the implemented meshing algorithm of HFSS applies an adaptive meshing to increase the mesh number. However, the designer is also able to determine the meshing of any arbitrary element on the design.

HFSS can simulate unit cells and allow various types of periodic structures. This tool can be used to analyze planar or linear infinite arrays. The fields on the periodic boundaries are forced to have the same magnitude and direction with different phases depending on the required incidence angle and/or progressive phasing. The implementation of the periodic array is done by imposing periodic boundary conditions on the couples of surfaces named master and slave attributions. The master and slave boundaries are aligned using vector $\vec{v}$ and $\vec{u}$ in Figure 3.3. The unit cell simulation of a reflectarray cell is carried out by imposing the boundary condition in both dimensions to realize the planar infinite array conditions of the simulation. The implementation of these software tools are shown, because they also make it easier to comprehend the unit cell approach.

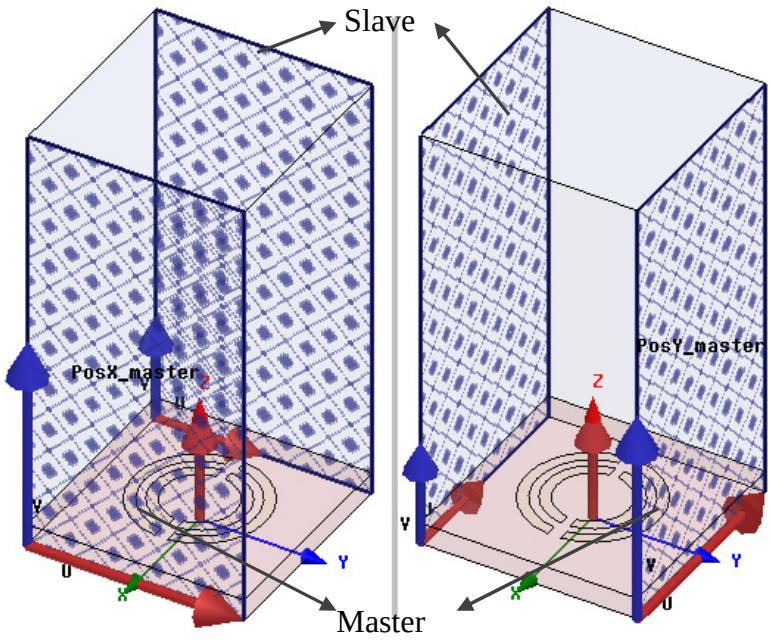

Figure 3.3 Implementation of the master and slave boundaries for periodicity

.

After imposing the periodicity, it is necessary the set-up of the simulation accordingly with proper excitation. Simulations of the unit cell require an incident and reflected plane wave relation. The most suitable tool for this purpose is the Floquet port available in HFSS. The Floquet port implements the Floquet mode spectrum. Floquet mode spectrum expansion is the Fourier domain expansion of the periodic solutions to a wave equation. That is the reason why the Floquet modes can be applied to planar periodic infinite arrays. This approach is valuable since the infinite array assumption is also advantageous in computational costs enabling the use of the Floquet expansion method. The Floquet modes needed to represent the plane wave incidence are automatically calculated by the calculator implemented in HFSS. The number of modes and the propagation and attenuation constants depend on the periodicity in two dimensions and the incidence angle of the wave. When the periodicity of the array is around half a wavelength there is one propagating Floquet mode that can be decomposed as two orthogonal components, and these are sufficient to characterize the plane wave incidence. These modes are named according to the grid system defined by the user and applied at the Floquet port

which are shown in Figure 3.4 as **a** and **b**. For the square unit cell structures like the one investigated in this thesis, the assignment is applied to coincide the **a** vector with x-axis, and **b** vector with y-axis, so that these correspond to the waves propagating in the same direction but having E-fields orthogonal to each other.

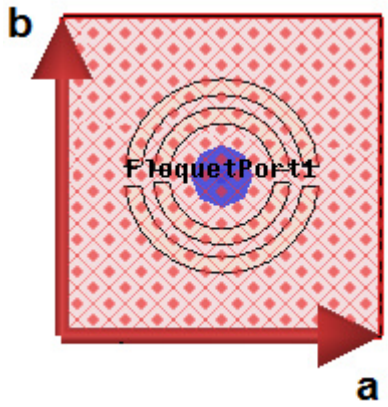

Figure 3.4 Imposing the Floquet port grid guide lines.

The results are easily de-embedded, that is the reference plane of the solutions is transferred to the surface of the reflective element as needed. The screen capture of the 3D modeler of HFSS is shown in Figure 3.5, the de-embedding vector points to the point on the reference plane.

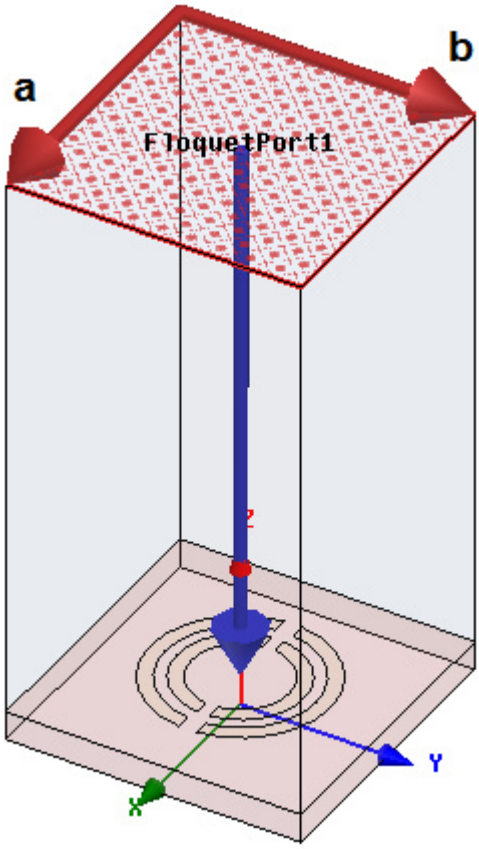

Figure 3.5 De-embedding vector shown, the result is referred to the end point of the blue de-embedding vector.

The simulation results of a Floquet port simulation of a unit cell in infinite planar array yields a 2-port network S-matrix, where the 1st and 2nd ports are aligned with the x- and y-axes respectively. By this means, as indicated in the Chapter 2, the unit cell can be characterized. Then this two-port network can be illustrated as in Figure 3.6.

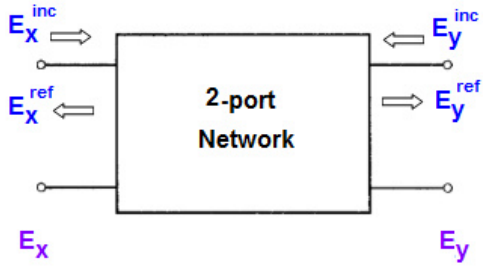

Figure 3.6 2-port representation of the Floquet port.

Recalling the incident and reflected field relation expression which was used in Chapter 2:

$$\begin{pmatrix} E_x^{ref} \\ E_y^{ref} \end{pmatrix} = [S] \begin{pmatrix} E_x^{inc} \\ E_y^{inc} \end{pmatrix} = \begin{pmatrix} s_{11} & s_{12} \\ s_{21} & s_{22} \end{pmatrix} \begin{pmatrix} E_x^{inc} \\ E_y^{inc} \end{pmatrix} \tag{3.1}$$

The simulation result of the Floquet port with two orthogonal modes is the [S] matrix in Equation (3.1). When the incident field is assumed to be the perfect circularly polarized wave:

$$\begin{pmatrix} E_x^{inc} \\ E_y^{inc} \end{pmatrix} = \begin{pmatrix} 1 \\ \pm j \end{pmatrix} E_0^{inc} \tag{3.2}$$

The total reflected field is:

$$E^{ref} = \{(s_{11} \pm j s_{12})\hat{a}_x + (s_{21} \pm j s_{22})\hat{a}_y\} E_0^{inc} \tag{3.3}$$

The reflected co- and cross-polarized waves are:

$$E_{co-pol.}^{ref} = (\hat{a}_x \mp j\hat{a}_y) E_0^{ref,co} \tag{3.4}$$

$$E_{cross-pol.}^{ref} = (\hat{a}_x \pm j\hat{a}_y) E_0^{ref,cross} \tag{3.5}$$

$$E^{ref} = E_{co-pol.}^{ref} + E_{cross-pol.}^{ref} \tag{3.6}$$

Then to find the reflected co- and cross-polarization coefficients, the solution of Equations (3.3) and (3.6) should be calculated.

$$\{(s_{11} \pm js_{12})\hat{a}_x + (s_{21} \pm js_{22})\hat{a}_y\}E_0^{inc} = (\hat{a}_x \mp j\hat{a}_y)E_0^{ref,co} + (\hat{a}_x \pm j\hat{a}_y)E_0^{ref,cross}$$
$$(s_{11} \pm js_{12})\hat{a}_x E_0^{inc} + (s_{21} \pm js_{22})\hat{a}_y E_0^{inc} = \hat{a}_x(E_0^{ref,co} + E_0^{ref,cross}) \mp j\hat{a}_y(E_0^{ref,co} - E_0^{ref,cross}) \quad (3.7)$$

Equalizing the x- and y-components independently:

$$(E_0^{ref,co} + E_0^{ref,cross}) = (s_{11} \pm js_{12})E_0^{inc} \quad (3.8)$$

$$(E_0^{ref,co} - E_0^{ref,cross}) = -(s_{22} \mp js_{21})E_0^{inc} \quad (3.9)$$

The reflection coefficients of the co- and cross-polarized waves upon incidence of a circularly polarized wave:

$$\Gamma_{co} = \frac{E_0^{ref,co}}{E_0^{inc}} = \frac{1}{2}[(s_{11} \pm js_{12}) - (s_{22} \mp js_{21})] = \frac{1}{2}[(s_{11} - s_{22}) \pm j(s_{12} + s_{21})] \quad (3.10)$$

$$\Gamma_{cross} = \frac{E_0^{ref,cross}}{E_0^{inc}} = \frac{1}{2}[(s_{11} \pm js_{12}) + (s_{22} \mp js_{21})] = \frac{1}{2}[(s_{11} + s_{22}) \pm j(s_{12} - s_{21})] \quad (3.11)$$

The Equations (3.10) and (3.11) are important because they constitute the basis to extract the characteristics of the unit cell upon circularly polarized incident wave. The co- and cross-polarized reflection levels are easily extracted from the simulation results via simple algebra.

In this section, the simulation configurations and the utilization of the simulation results is explained. The characterization of the split-ring structure as a phase control element in the unit cell of a reflectarray can be carried out using these methods in the following sections.

3.4 The Split-Ring as a Reflectarray Element

The split-ring element is advantageous for it is capable of reflecting an incident circularly polarized wave as a wave conserving the sense of polarization. Moreover its symmetrical form allows easy implementation of the rotation effect by integrating with RF MEMS switches. The split-ring does not have analytical formulas governing its operation bands. It is important to investigate the effects of parameters on the operation frequencies of a split-ring. Thus, the parametric analysis of the split-ring geometry and the unit cell have been performed and presented in the following sections.

3.4.1. Parametric Study

The unit-cell composing of a single split-ring on a ground backed substrate is studied parametrically to extract valuable information relating these parameters with the frequency and the bandwidth of co-pol. reflection. Then, it is shown that the split-ring can control the phase of the reflected co-pol. wave using the rotational phase shift principle. The response of unit cell is also studied for the oblique incidence cases. The parameters of the split-ring geometry that are changed in the parametric analysis are shown in Figure 3.7.

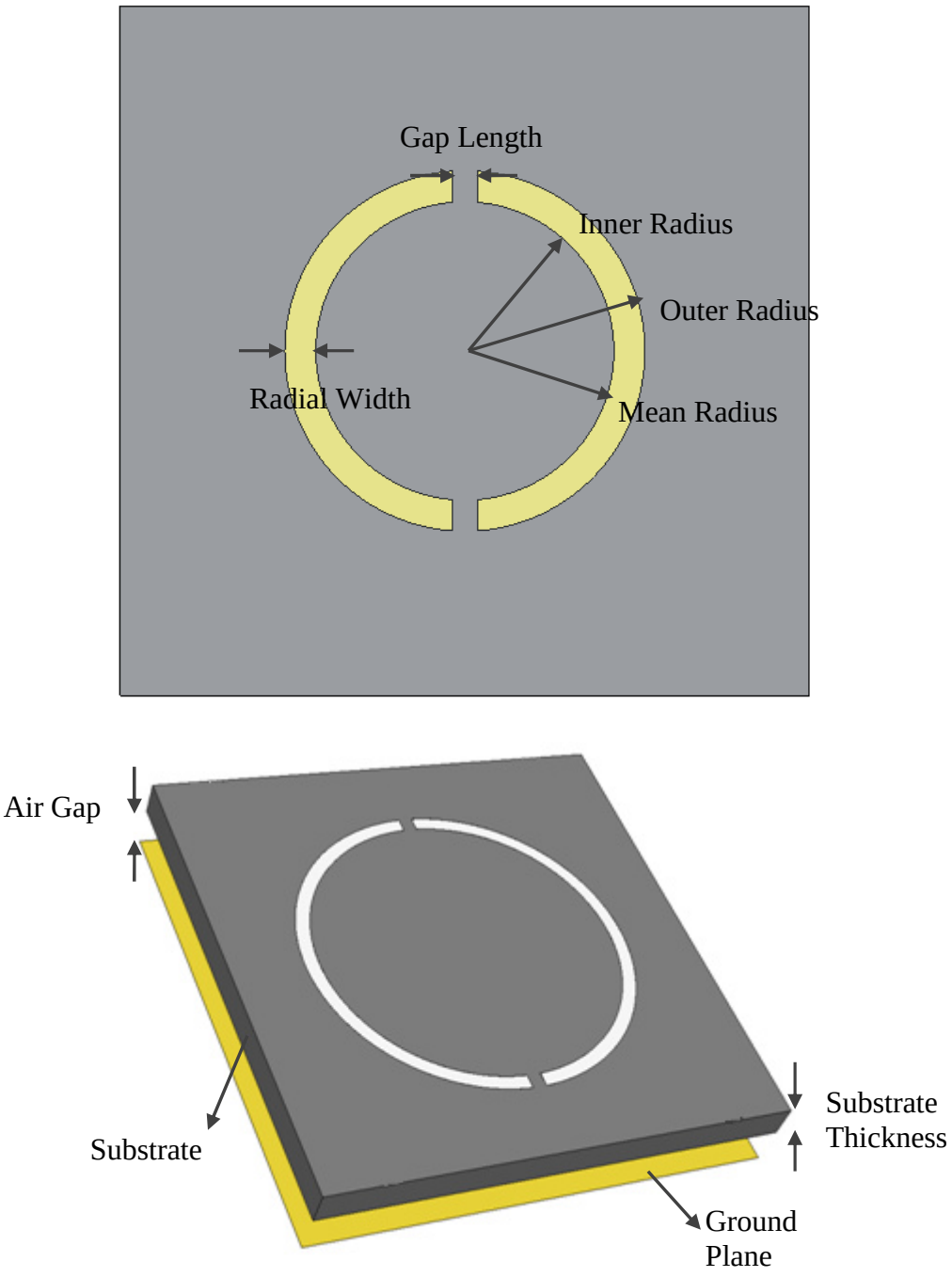

Figure 3.7 The parameters of the split-ring geometry.

Table 3.1 The unit cell and reflective element dimensions.

Initial Design Parameters Used as a Reference	
Inner Radius	0.98mm
Outer Radius	1.18mm
Radial Width	0.20mm
Gap Length	0.20mm
Substrate Thickness	0.50mm
Relative Substrate Permittivity	3.78 (Quartz)
Air Gap	0mm
Unit Cell Dimensions	5.55mm x 5.55mm (0.5λ @ 27 GHz)

In Table 3.1, all the parameter values are given. These values are a basis for the parametrical analysis. The following sections are including simulation results to obtain the effect of these parameters. The variations are carried out around the initial design values given in Table 3.1, this is an easing way of examining the effects. Note that in the initial design air gap thickness is 0mm, i.e. there is no air layer. Air gap thickness parameter is given, since it is used further in this section.

In the following sections this design is examined in terms of frequency response of the cross-pol. reflection coefficient. Recall that the aim was to suppress the cross-pol. reflected component, since the phase control principle employed is only applicable for the co-pol. reflected component. In this context, the operation frequency of a unit cell is defined as the frequency at which the cross-pol. reflection is at minimum. For example in Figure 3.8, the operation frequency is 27.15 GHz. Also the bandwidth is defined as the frequency interval including the operation frequency, in which the cross-pol. reflection coefficient is below -20dB. The bandwidth of the reference design of Table 3.1 as plotted in Figure 3.8 is 0.1 GHz between 27.1 GHz and 27.2 GHz. In the parametric study, these definitions constitute a basis in characterizing the unit cell.

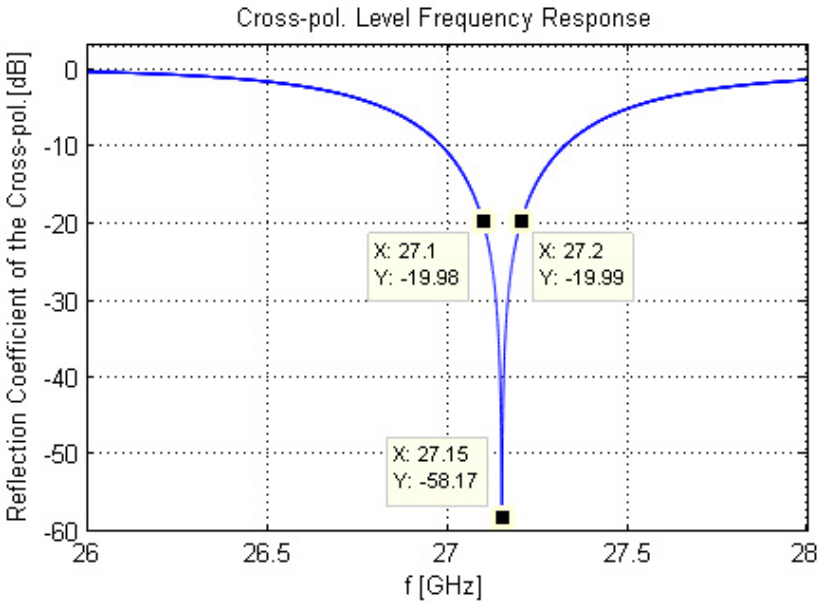

Figure 3.8 The frequency response of the reflection coefficient of the cross-pol.

3.4.1.1 Effect of the Mean Radius

The size of any microwave structure is surely governing its frequency response. Note that in the unit cell design, the size of the split-ring metallization cannot scale the

frequency response since the unit cell dimensions and the substrate height are kept constant. But the metallization is strictly related to the resonant characteristics due to the currents flowing on the split-ring. The simulations with the mean radius values listed in Table 3.2 show that the result is shown in Figure 3.9. As the mean radius increases, the operation frequency is shifted to lower frequencies. This is the expected result of the electrical length relationship. The bandwidth of co-polarized reflection is not affected obviously.

Table 3.2 Mean radius values used in parametrical sweep.

Swept Parameter	
Arithmetic Mean of The Radii	1.075mm 1.080mm 1.085mm 1.090mm 1.095mm 1.100mm
Other parameters set constant	

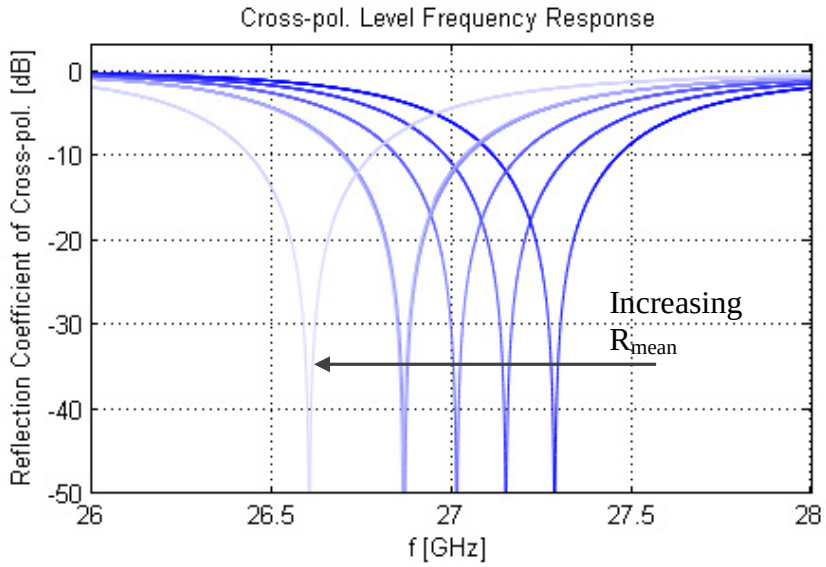

Figure 3.9 Cross-pol. Reflection Coefficient vs. Frequency for varying mean radius.

3.4.1.2 Effect of the Radial Width

The inner and outer radii of the split-ring are subject to testing. The frequency response may not be related to the radii with a mathematical dependence. To investigate the effect of width variance to the frequency response at least the constant parameters should be declared. There should be some initial point such as keeping the arithmetic mean or geometric mean of the inner and outer radii constant. Lacking the analytical expression for the frequency response, any of these assumptions are arbitrary. The results are the comparisons of the constant arithmetic mean radius. In Table 3.3, one can find the radial width values used in parametric sweep. The effect is obviously ineffective on the bandwidth; however the operation frequency is shifted to lower bands, as shown in Figure 3.10. The interpretation is that, the outer radius is more effective in defining the operation frequency.

Table 3.3 Radial width values used in parametrical sweep.

Swept Parameter	
Radial Width	0.180mm 0.190mm 0.200mm 0.210mm 0.220mm
Other parameters set constant *(Arithmetic mean of the radii is kept constant)*	

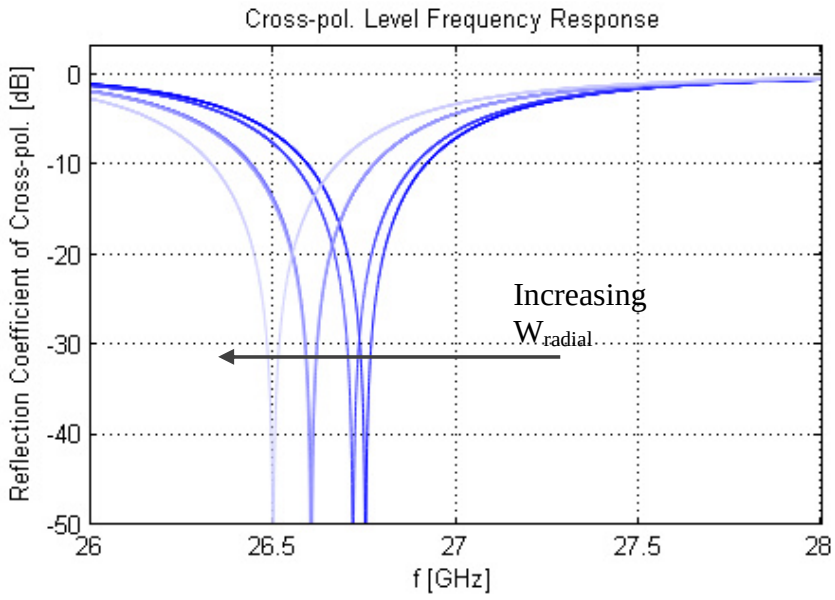

Figure 3.10 Cross-pol. Reflection Coefficient vs. Frequency for varying radial width.

3.4.1.3 Effect of the Gap Length

For the gap length values shown in Table 3.4, the results are illustrated in Figure 3.11. As the gap length is increased; the operation frequency shift to higher frequencies. However, no clear effect on the bandwidth is observed. It should be noted that the gap modifications were carried out in small dimensions that the ring geometry is preserved. This modification shows that the capacitive interaction through the gap is also a very important parameter in determining the operation frequency. The switches are to be implemented on the gaps for the further integration steps. This is an early estimation of the RF MEMS switches' effects on the gap.

Table 3.4 Gap length values used in parametrical sweep.

Swept Parameter	
Gap Length	0.200mm 0.250mm 0.300mm
Other parameters set constant	

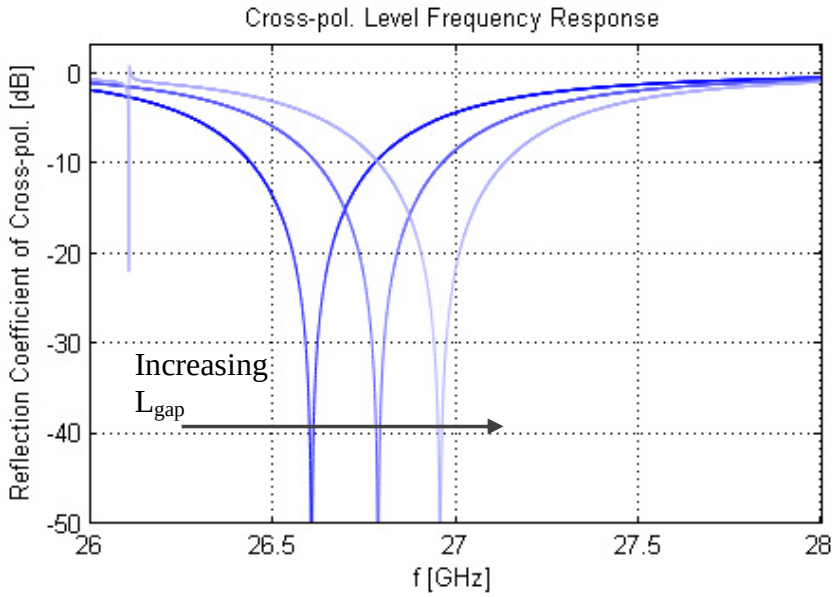

Figure 3.11 Cross-pol. Reflection Coefficient vs. Frequency for varying gap length.

3.4.1.4 Effect of the Unit Cell Dimension

The proposition that the unit cell dimension should affect the frequency response is logical; because the coupling of the elements depends on their separation from each other. In this section the following simulations demonstrates this phenomenon. Table 3.5 shows the unit cell dimensions for which the simulations have been performed, and the corresponding results are given in Figure 3.12. It is evident that the unit cell dimension affects the operation frequency. However, no rule that defines the relation between frequency and unit cell size can be obtained from these simulations. Thus, the unit cell dimension should be optimized with thorough trials.

Table 3.5 Unit cell dimensions used in parametrical sweep.

Swept Parameter	
Unit Cell Dimensions	0.40λ 0.50λ 0.55λ @27 GHz
Other parameters set constant	

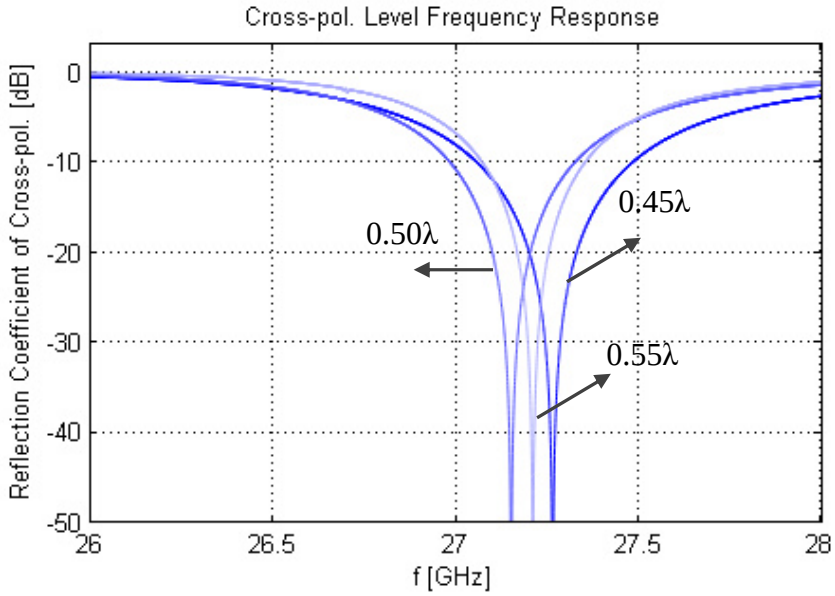

Figure 3.12 Cross-pol. Reflection Coefficient vs. Frequency for varying unit cell dimension.

3.4.1.5 Effect of the Substrate Thickness and Permittivity

Although the substrate selection is mainly dependent on the fabrication process, technology and material availability; it is valuable information to know the effect

osubstrate permittivity and thickness.

Table 3.6 Substrate thickness values used in parametrical sweep.

Swept Parameter	
Substrate Thickness	0.450mm 0.500mm 0.550mm
Other parameters set constant	

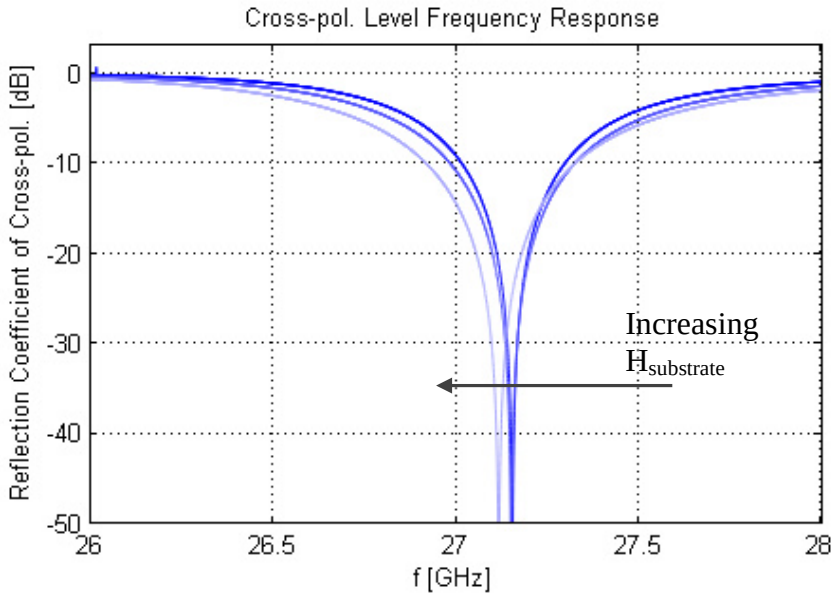

Figure 3.13 Cross-pol. Reflection Coefficient vs. Frequency for varying substrate thickness value.

In Table 3.6, the thickness values of the substrate used in the simulations presented

in Figure 3.13 are listed. It is observed that, the substrate thickness has a slight effect on the bandwidth of the suppression of cross polarized component. The operation frequency is slightly shifted and the bandwidth is slightly increased with the increasing substrate height

Table 3.7 Relative permittivity of substrate values used in parametrical sweep.

Swept Parameter	
Relative Permittivity of the Substrate	3.68 3.78 3.88
Other parameters set constant	

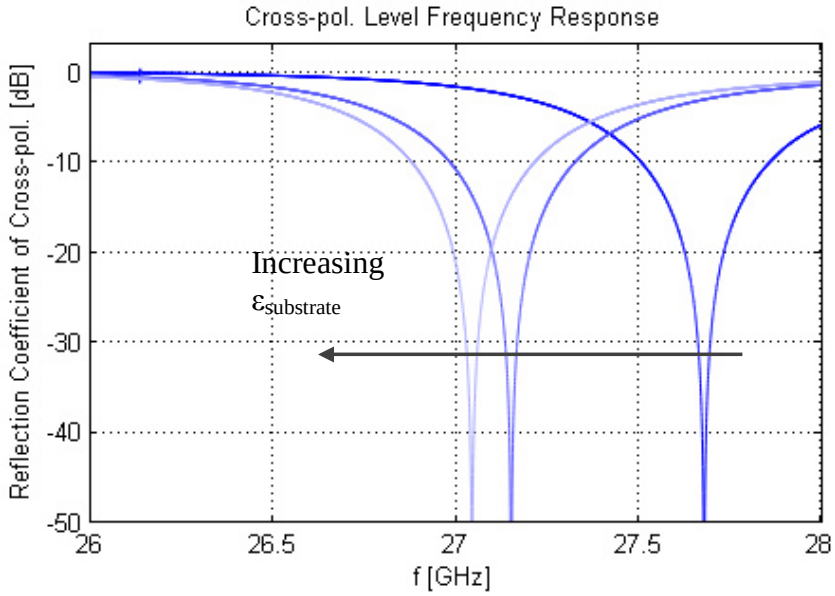

Figure 3.14 Cross-pol. Reflection Coefficient vs. Frequency for varying relative permittivity of the substrate.

The substrate material properties are certainly effective. Therefore permittivity values of the substrate are slightly varied to see the outcome. For the relative permittivity values stated in Table 3.7, the results given in Figure 3.14 show that the operation frequency is highly dependent on the permittivity. The bandwidth is not seriously changed, while the operation frequency is shifted to lower frequencies with increasing substrate permittivity as plotted in Figure 3.14.

The substrate thicknesses of the available materials are standardized, i.e. an arbitrary thickness for custom design is not always available and may cost more time and money. However the positive effect of the substrate thickness in increasing the bandwidth of cross-pol. suppression has to be utilized. On the other hand, it should be also taken into account that the permittivity affects the operation frequency. In Figure 3.14, it is seen that decreasing substrate permittivity is more effective than increasing it. Then it can be understood that adding an intermediate air layer between the ground plane and the bottom of the substrate can be used to increase the bandwidth. Since air has the lowest relative permittivity, the frequency of the operation will be shifted dominantly by its contribution, which can be compensated by adjusting the split-ring dimensions properly and the freedom to modify the air gap height is an advantage.

In Table 3.8, the air gap values are listed. The simulation results with the aforementioned air gap height values are plotted in Figure 3.15. Not that the air gap thickness is indeed very small, but this is only to show the effect with respect to no air gap case. The comparison in Figure 3.15, shows that the bandwidth is increased with increasing air gap height; as well, the frequency is shifted. This is an easy way to adjust the bandwidth.

Table 3.8 Air gap height values used in parametrical sweep.

Swept Parameter	
Air Gap	0.000mm 0.010mm 0.020mm 0.030mm 0.040mm
Other parameters set constant	

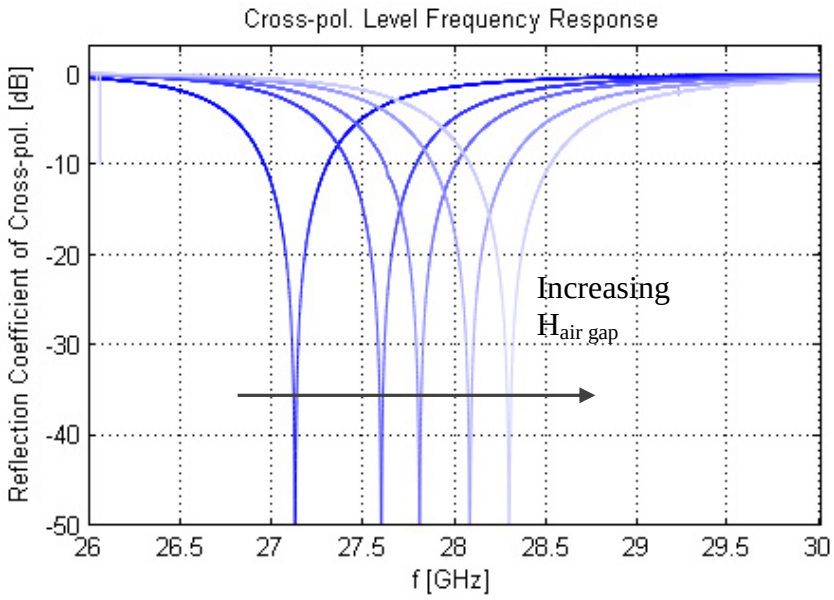

Figure 3.15 Cross-pol. Reflection Coefficient vs. Frequency for varying air gap height between ground plane and the bottom of the substrate.

.

3.4.2 The Reflectarray Unit Cell with Split-ring

The split-ring element is simulated and characterized with its frequency response in an infinite array. The parametric study presented in the previous section shows the important dimensions and how to tune the split-ring. In this section, the phase design curve is obtained by rotating the split ring.

To understand the application of the rotational phase shift principle in an array, it is logical that locally each element will be controlling phase independently over its own course. While using this characteristic in an array configuration, some of the conditions on the application of the phase control principle may be overridden. The most important statement was that only phase control of the reflected co-polarized wave is possible. Then the cross-pol. suppression should be guaranteed at the desired operation frequency for any state of the element.

Comparing the Figure 3.16 and Figure 3.17, these two arrays may have different frequency responses with regard to cross-pol. suppression. While determining the frequency interval in which the cross-pol. suppression is achieved; the approach should also include the comparison of the frequency responses of the infinite arrays for various cases that split-rings are rotated. None of the simulated unit cells can provide the exact frequency response for a reflectarray element, since this response is dependent on interaction with the neighboring elements.

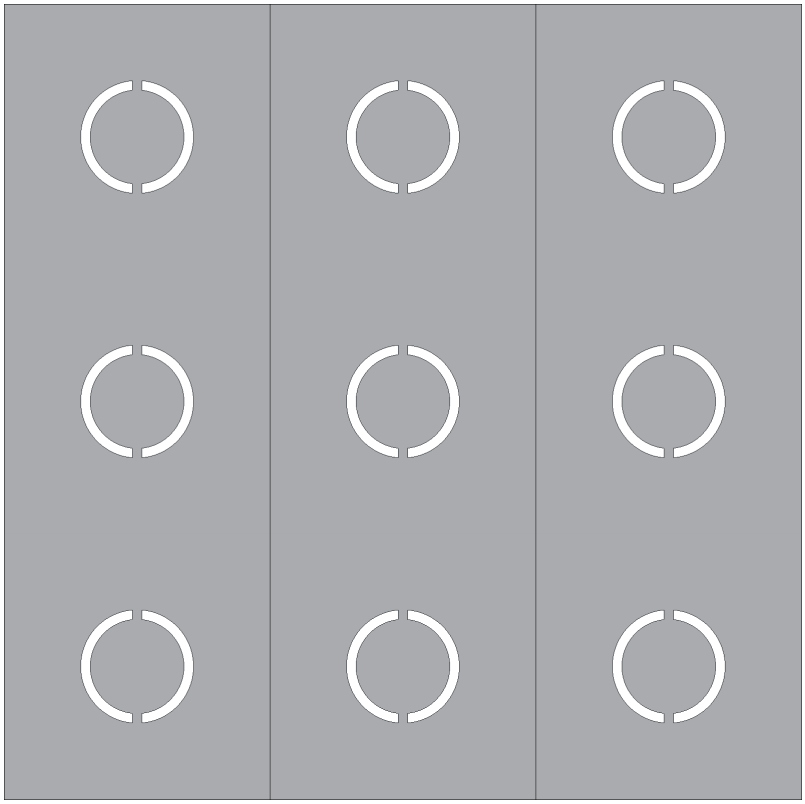

Figure 3.16 A part of an infinite array of unit cells with split-rings in initial state.

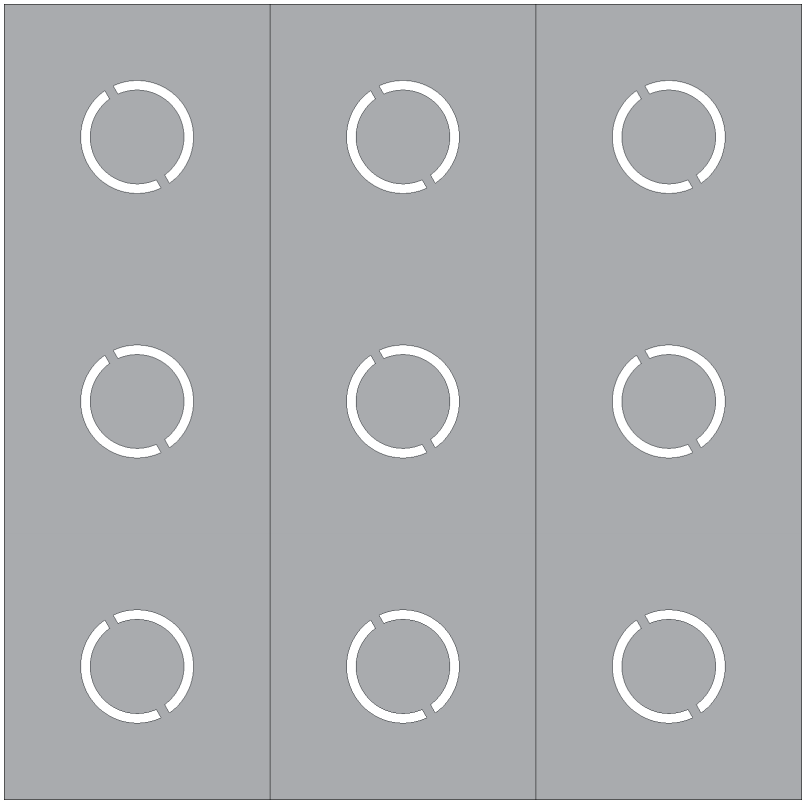

Figure 3.17 A part of an infinite array of unit cells with 30°-rotated split-rings relative to the initial state.

For the same reason, each element will have slight differences in the frequency responses. While utilizing the unit cell approach these simulated cases constitute the most regular form of the array. In actual utilization, the unit cells may have almost random states independently Figure 3.18. The approach should include the comparison of the frequency responses of unit cells with different rotations angles. Finally the operation frequency should be determined by comparing the frequency responses of unit cells in different states.

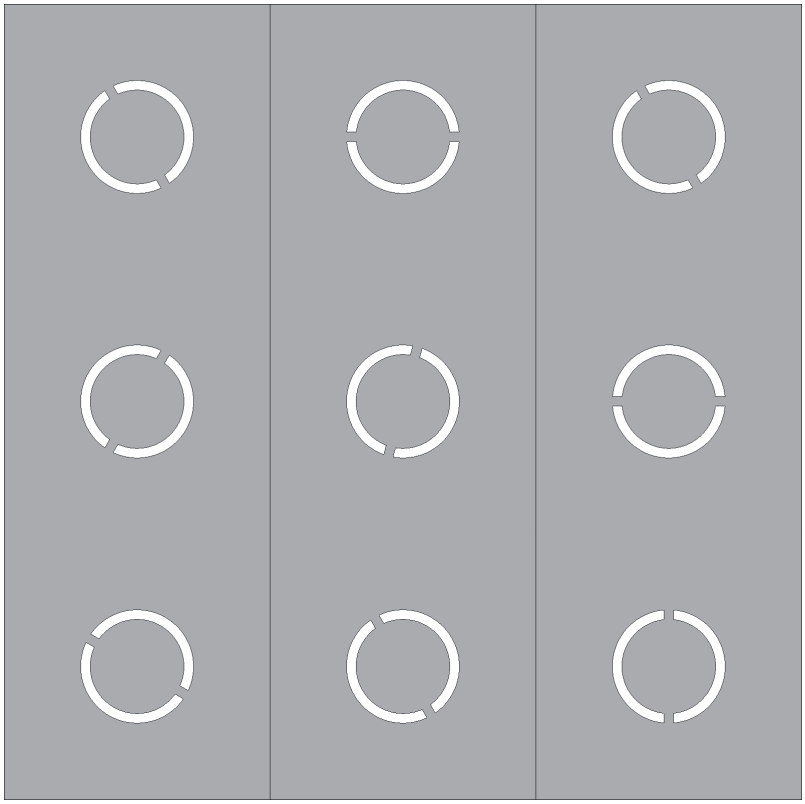

Figure 3.18 A part of an array of elements with random states.

Due to symmetry and the square shape of the unit cell, the angular states of the split-ring between 0° and 45° are enough to extract the necessary information. The result for angles 0°, 15°, 30°, 45° are shown for the reference design of the parametrical study.

As seen in Figure 3.19, as the rotation angle of the split-ring changes the frequency response is affected. This is apparently an unwanted situation, since the cross-pol. increases as the split-ring is rotated to control the phase. This is an important point the designer should avoid. The first thing to avoid this phenomenon is to increase the bandwidth of the element, so that the shifts in the frequency response due to rotation of the element would not result in higher cross-pol. levels. Given the bandwidth is optimized and kept intact; another parameter to prevent this phenomenon from happening is to change the unit cell size. For example in Figure 3.20, the same simulation results are shown for another unit cell size. As seen the minima of the

cross-pol. levels get closer to each other. For the previous case, the operation frequency for the best cross-pol. suppression constraint would be at 27.31 GHz / -11dB (Figure 3.19), for the second case it would be at 27.34 GHz / -20dB (Figure 3.20) which is a far better design. For the sake of better characteristics the dimensions of the unit cell would eventually be modified to 0.44mm.

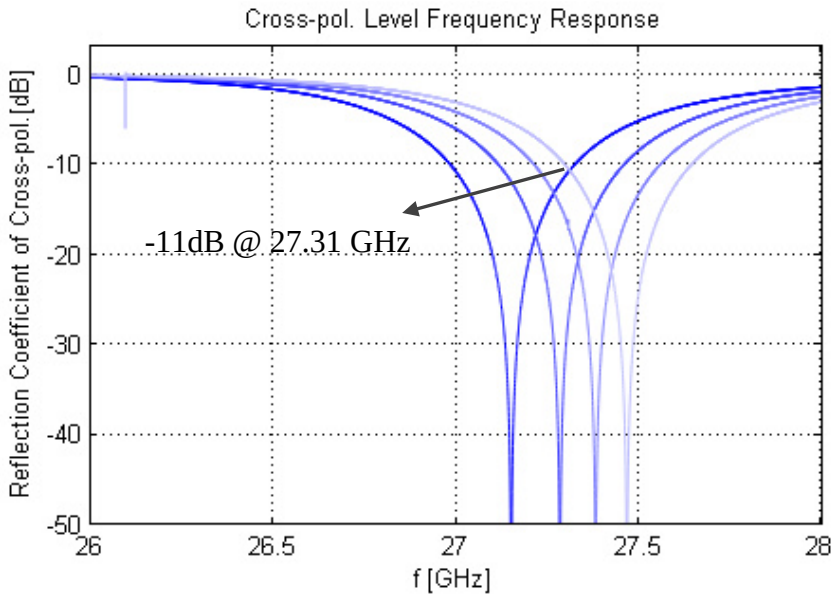

Figure 3.19 Frequency Response of the cross-pol. reflection, for various physical rotation angles of the split-ring. Unit cell dimension: 0.55mm.

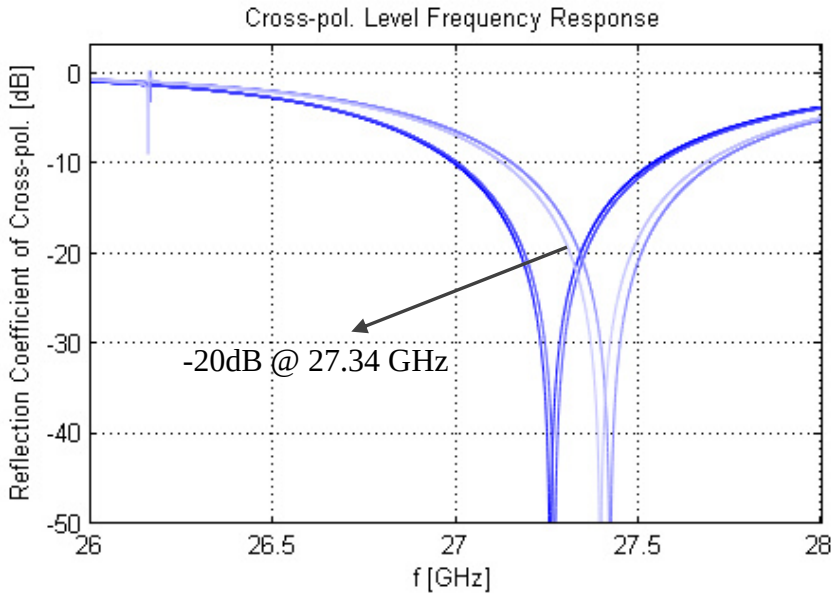

Figure 3.20 Frequency Response of the cross-pol. reflection, for various physical rotation angles of the split-ring. Unit cell dimension: 0.44mm.

The results of the simulations are given in the rest of this section to verify the application of the rotational phase shift principle with a single frequency split-ring element. The phase of the co-polarized wave plotted versus the physical rotation angle of split-ring is the phase design curve of this unit cell. Similarly the cross-pol. reflection coefficient by the rotation angle is demonstrated. Also these properties are investigated under oblique incidence.

In Figure 3.21, the phase of the reflected co-pol. component is plotted versus the rotation angle of the split-ring. The phase design curve has 360° coverage and almost a linear form. This is a simulated verification of the rotational phase shift principle applied to the split-ring reflectarray element via unit cell approach.

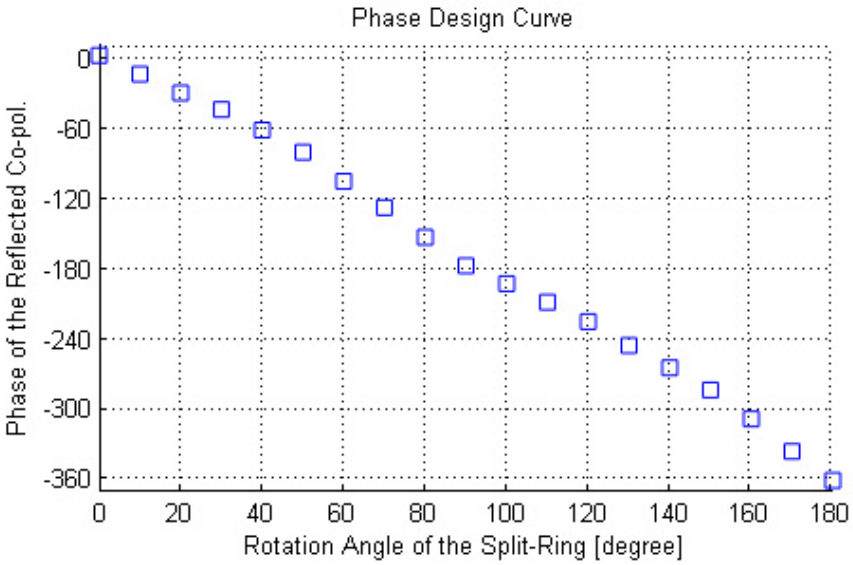

Figure 3.21 Phase design curve of the split-ring unit cell @ 27.34 GHz.

In Figure 3.22, magnitude of the reflection coefficient of e cross-pol. Component is plotted versus the rotation angle of the split-ring. The variation in the levels is due to the change in frequency response of reflection with varying rotation angle of the split-ring as previously mentioned. The suppression is preserved as low as -15dB, although the target was -20dB. This is because of the simulation technique employed during the frequency response simulations was interpolating sweep and phase-curve simulations was simulated with discrete sweeping. However this can also be tuned with further simulation trials with discrete sweeps. Since the aim was to prove the phase control technique, the tuning effort will be put forward in the final design of the dual band reflectarray element.

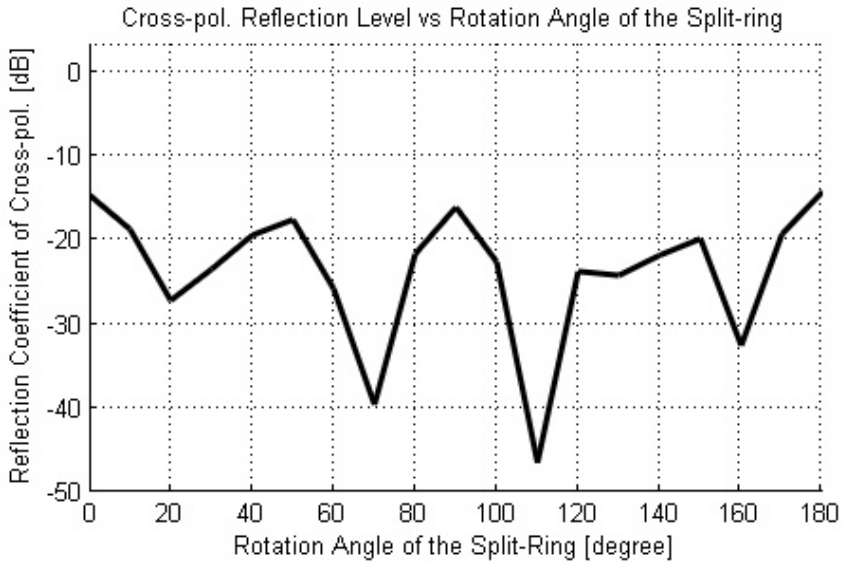

Figure 3.22 Magnitude curve of the split-ring unit cell @ 27.34 GHz.

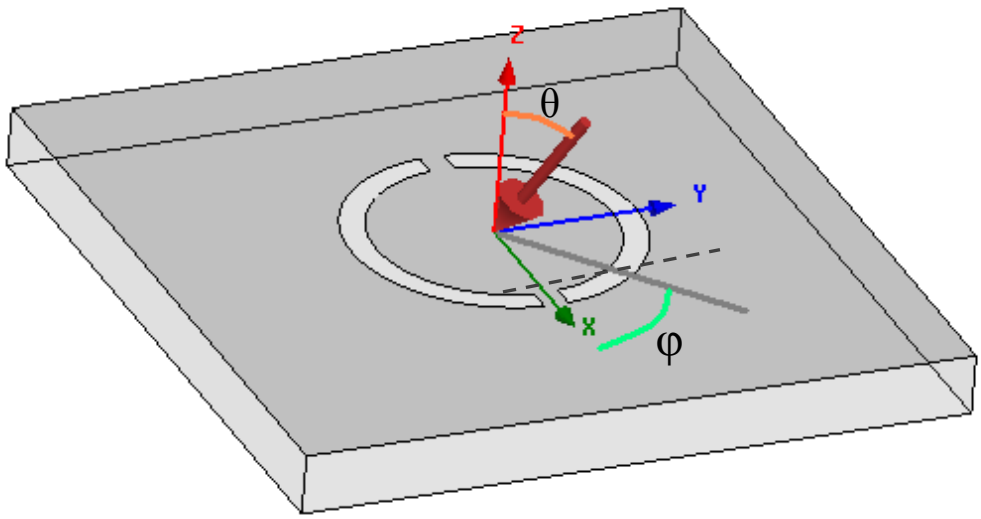

Figure 3.23 The oblique incidence angles with respect to spherical coordinates.

The oblique incidence cases to be simulated are quite narrow. Because of the symmetry of the unit cell, a simple case can be the set of φ=0° and θ={0°,10°,20°,30°,40°}. The simulations of oblique incidence are done and

compared.

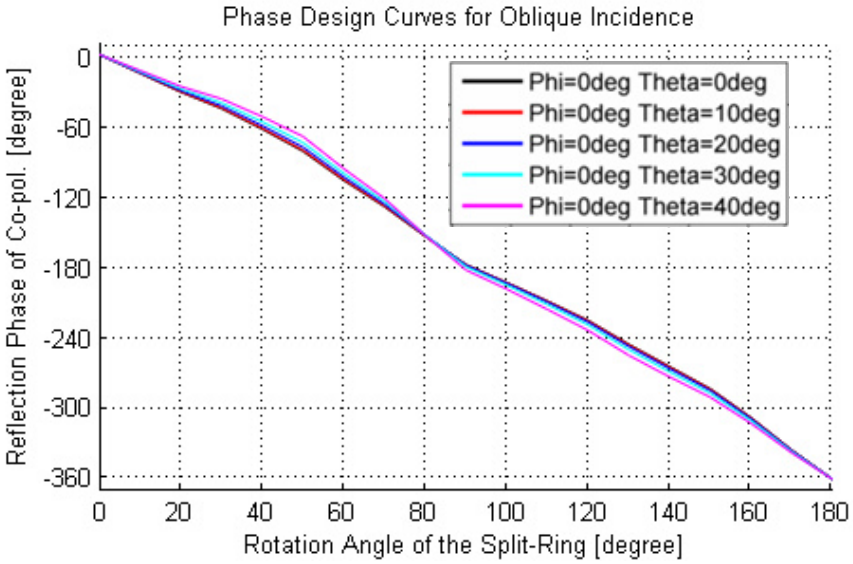

Figure 3.24 Phase design curve of the split-ring unit cell @ 27.34 GHz for various oblique incidence angles.

Figure 3.24 shows the phase design curves of the reflect array element under various oblique incident illumination. The phase curves are quite limited, although the slight deviations are observable as the angle of incidence increases. In Figure 3.25, it is apparent that the cross-pol. suppression is worsened with increasing incidence angle. This is an expected result. Moreover it can be integrated into the design of a reflectarray antenna composing of this element.

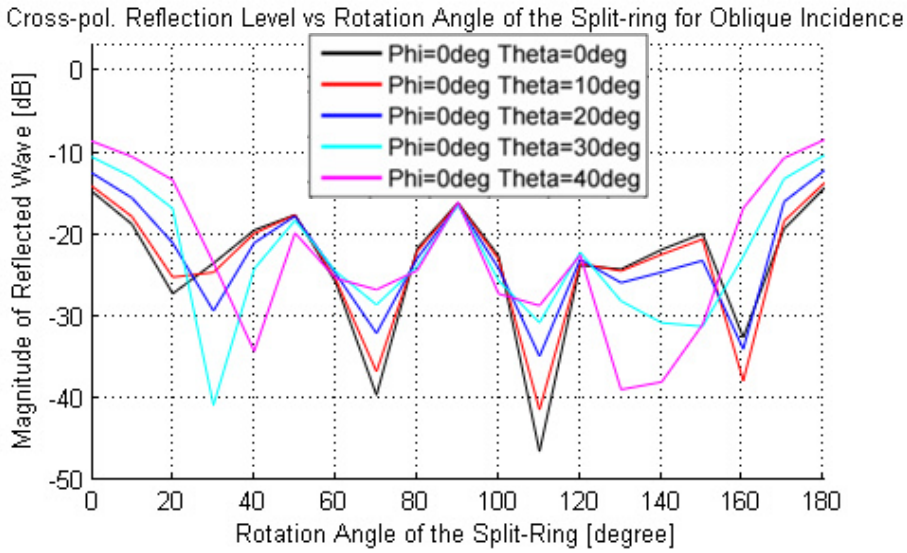

Figure 3.25 Magnitude curve of the split-ring unit cell @ 27.34 GHz for various oblique incidence angles.

3.5 Conclusion

The unit cell approach to characterize the reflectarray element with split-ring is explained and applied, yielding a single frequency split-ring element. The results of parametrical study are presented and discussed. The phase design curve based on rotation of split ring and the frequency response of the cross pol. component are obtained. This characterization procedure is utilized to design the dual band reflectarray element of split-rings in the following Chapter.

CHAPTER 4

DUAL BAND REFLECTARRAY ELEMENT AND REFLECTARRAY ANTENNA DESIGN

4.1 Introduction

The rotational phase shift principle is mathematically derived and simulations are completed to show that the split-ring element is suitable for phase control as a reflectarray element. The author's aim is to propose a simple topology for dual frequency operation employing the rotational phase shift principle. The dual frequency unit cell with split-rings is presented in this chapter. The possible configurations with split-ring are mentioned for dual frequency operation. The final choice of the reflectarray element is demonstrated. The reflectarray antenna formed by combining the dual band reflectarray element is designed, fabricated and measured. The comparison of measured patterns with simulated ones is discussed. The reflectarray element is integrated with RF MEMS switches, the result is put forward. After the element design, the dual frequency elements are combined to build a reflectarray antenna, the design principles and simulation results are given.

4.2 Dual Band Element Design

The goal is to achieve a dual band reflectarray element design using the aforementioned techniques and approaches to combine the split-rings in an appropriate form. This section is dedicated to the choice of the dual frequency configuration, determining the dimensions of the split-rings and characterization of

the final design.

4.2.1 Choice of the Dual Frequency Configuration

Among several split-ring structures to build up a reflectarray element operating at dual frequency, the set of choice is narrowed down by the fabrication methods and technology.

The fabrication technology in Middle East Technical University MEMS Center is to be utilized for the realization of the design. Thus the reconfigurability of the antenna will be provided by integrating RF MEMS switches. The capabilities of the RF MEMS process developed previously by the RF MEMS Group were demonstrated in [37], [14]. The demonstration of a switch similar to use in this design is given in [13]. The aim was to design a low profile and low volume antenna. Thus, single layer implementation of dual frequency rings is preferred.

Figure 4.1 Concentric configuration of two split-rings.

The operation frequency of the split-ring is directly related to the size of the rings. Using two split-rings in different sizes with possible configurations are studied to check if the configurations can satisfy the conditions to guarantee that the unit cell can operate in dual band and control the phase in the two bands independently. The characterizations of the elements are compared accordingly.

One possible configuration of the split-rings to obtain double frequency operation is concentric placement as in Figure 4.1. Before determining the dual frequency configuration, there are some constraints to keep in mind. The final design should be suitable for bias lines of the switches. The process flow to fabricate the element with surface micromachining is a well defined one whose most problems solved. Using the concentric configuration poses problems of reach for the bias lines of the switches on the inner ring. Then the process flow should be modified and optimized to build the necessary insulated transitions through the split-ring metallization. Furthermore, the bias lines that pass through the split-ring metallization can increase the microwave simulation efforts needed. Then another configuration is put forward and accepted as the dual frequency element after essential studies, the interleaved manner as in Figure 4.2. The latter configuration can overcome the problems of the concentric configuration.

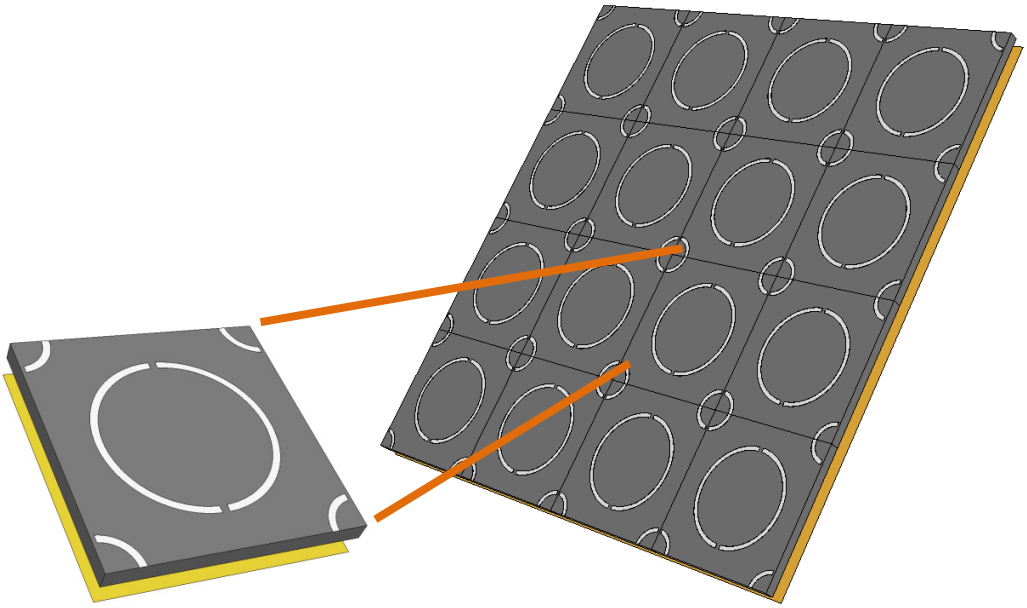

Figure 4.2 Interleaved configuration of two split-rings.

4.2.2 The Dual Frequency Reflectarray Element Design

The reflectarray element design with one split-ring is examined in the previous chapter. The similar procedure should be handled carefully to combine the two split-rings such that the phase control principle is still valid and applicable as well as the desired frequency response is achieved.

The dual-frequency configuration as a unit cell pertaining to an interleaved array of split-rings of two sizes is shown in Figure 4.3. Briefly, the larger ring operates at the lower frequency and the smaller ring operates at the higher frequency. The element's split-rings are first designed, and the element dimensions are optimized for a frequency response fairly independent of split ring position. And finally the operation in dual band is investigated and phase curve is verified. The element is further studied for its capabilities and then is to be integrated with RF MEMS switches.

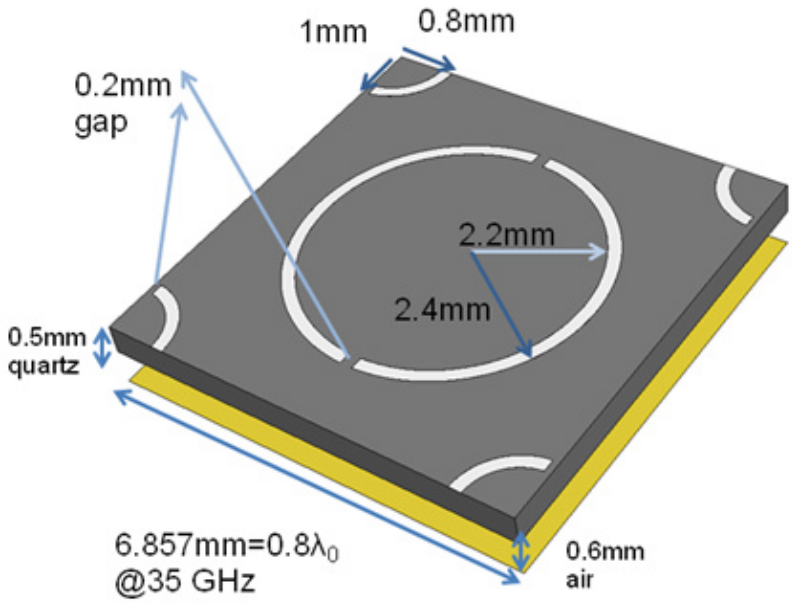

Figure 4.3 The tuned interleaved design of the dual frequency reflectarray element.

4.2.2.1 Optimizing the Frequency Response

As previously mentioned, the frequency response is prone to shifts with respect to the rotational states of the split-rings. That is why studying the frequency responses for various angular positions of the split-rings are necessary in order to achieve a rather unvarying frequency response. The unit cell dimension may be modified, all others being constant, to see if it is possible to reach an element design with an unvarying frequency response. Various angular positions of the two split-rings are chosen as a representative set, as in Figure 4.4. And these rings in many cells of different sizes are simulated to achieve the frequency response.

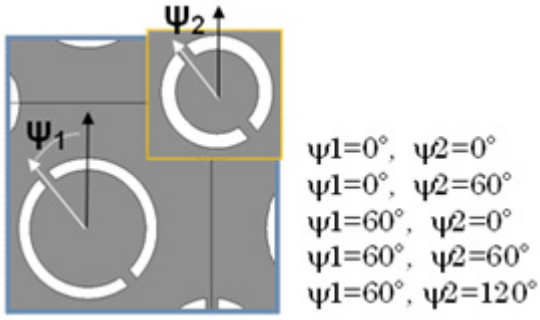

Figure 4.4 The set of angular position for the split-rings used to test if the frequency response is stable

The comparison of Figure 4.5, Figure 4.6, and Figure 4.7 clearly puts forward that the unit cell dimension should be set to 0.8λ @35 GHz in order to maintain a stable frequency response for various angular position of the two split-rings. The lower operating frequency can be determined as 24.4 GHz and the higher operating frequency as 35.5 GHz.

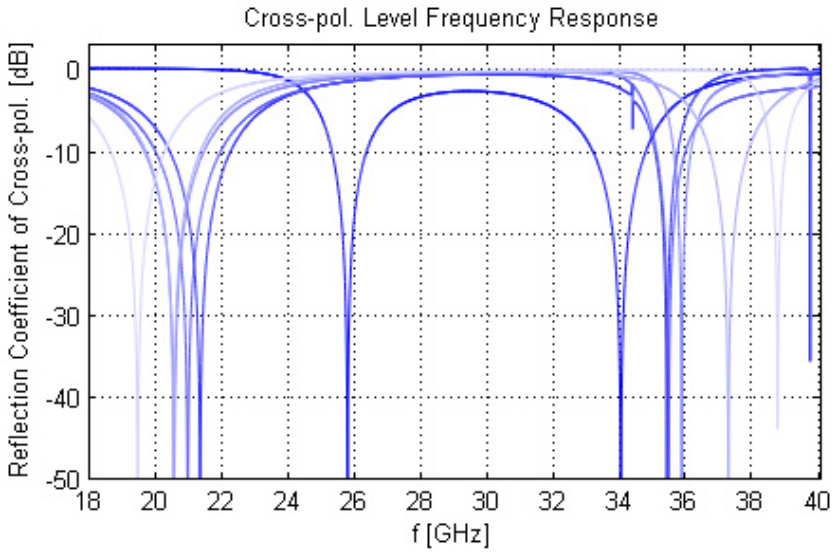

Figure 4.5 Frequency Response of the cross-pol. reflection, for various physical rotation angles of the split-ring. Unit cell dimension: 0.6λ @35 GHz.

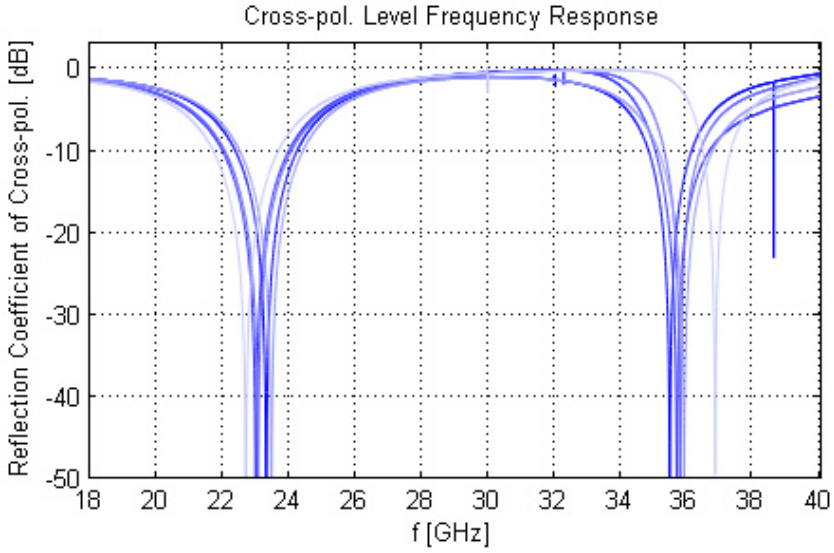

Figure 4.6 Frequency Response of the cross-pol. reflection, for various physical rotation angles of the split-rings. Unit cell dimension: 0.7λ @35 GHz.

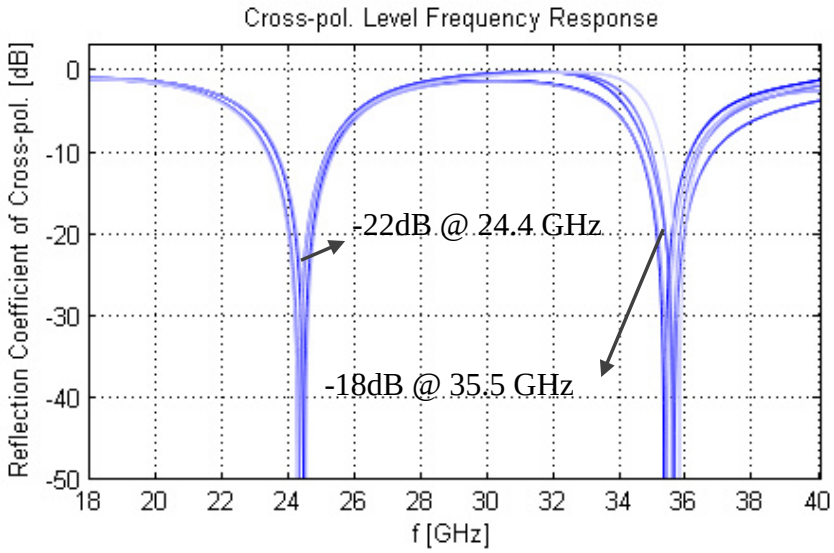

Figure 4.7 Frequency Response of the cross-pol. reflection, for various physical rotation angles of the split-rings. Unit cell dimension: 0.8λ @35 GHz.

4.2.2.2 The Combination of the Split-Rings in Two Sizes

To design the split-rings of different frequencies independently may be the starting point before combining them and achieving the dual frequency operation. It is obvious that the operation frequencies are prone to shifts related to the parasitic effects that they apply on each other. That is a reason to check their re-radiating currents at operation frequency after obtaining an unvarying frequency response. The mechanism that changes the operation frequencies of the split-rings when they are put together may also affect the phase control mechanism. It is thus worth examining.

In Figure 4.8, the frequency response of the larger ring alone is given, with the same air gap layer, substrate thickness, and unit cell dimensions as the final design given in Figure 4.3. The same simulation set-up is also used to simulate the smaller ring alone Figure 4.9. The design of the two split-ring elements does not mean that they will operate as expected after combining them in the interleaved array manner.

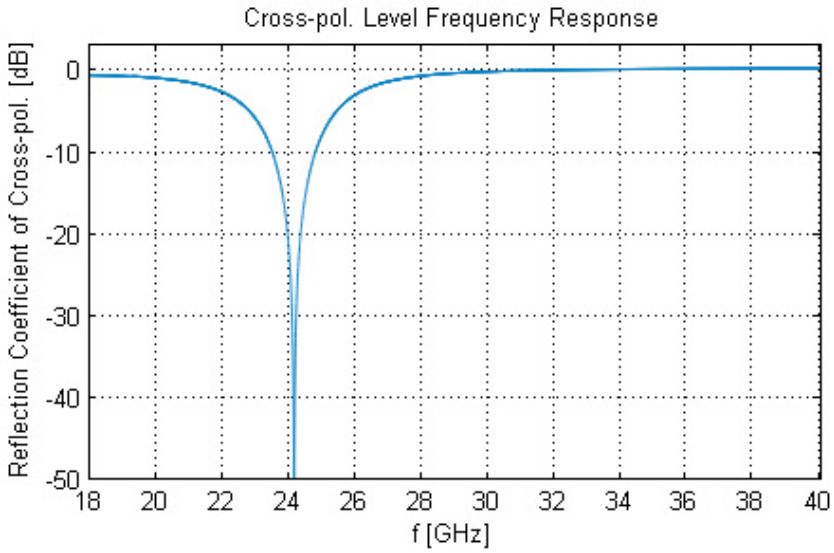

Figure 4.8 The reflection coefficient of cross-pol. vs. frequency for the larger ring alone.

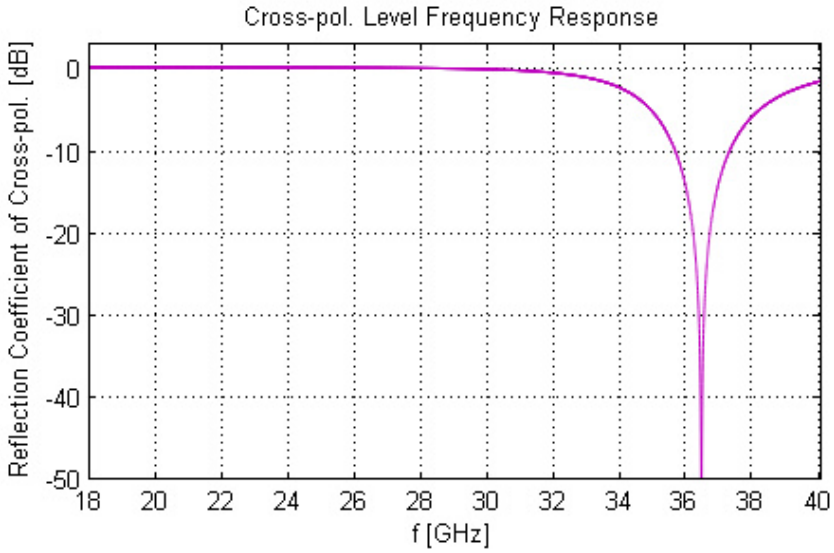

Figure 4.9 The reflection coefficient of cross-pol. vs. frequency for the smaller ring alone.

In Figure 4.10, it is seen that the both higher and lower operating frequencies are shifted. This is an expected result since the surrounding metallization can affect the frequency response and also yields to the interpretation that there is sure an interaction between the split-rings of two sizes. That is why the dual frequency element is further due to a question: Are they able to control the phase as expected and demonstrated in for single frequency?

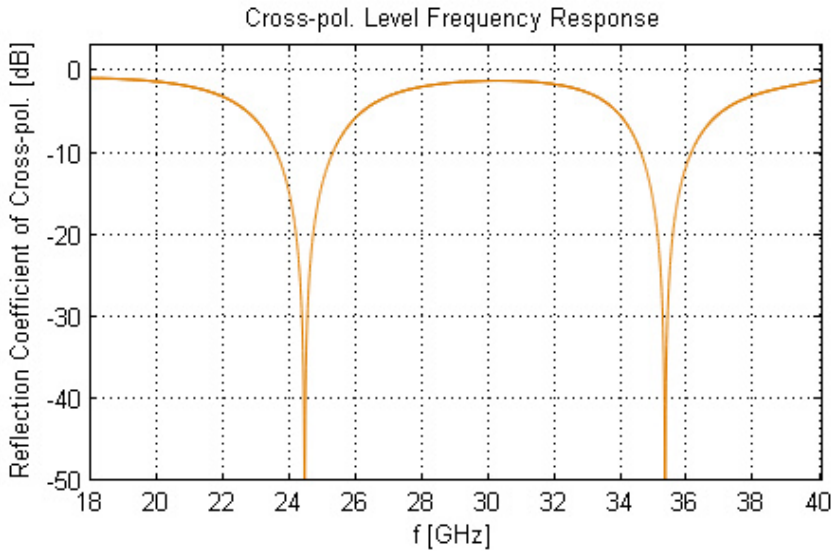

Figure 4.10 The reflection coefficient of cross-pol. vs. frequency when the two split-rings are put together.

There is also another aspect that may be helpful to check before passing to the simulations for the phase control capabilities of the array. The rotational phase control principle states that the phase of the reflected co-pol. component is linearly proportional to the rotation angle of the element. Then, combining this idea with the fact that the reflection is occurring by the currents on the metallization that re-radiate; the split-rings are required to control the phase at different frequencies independently. It is necessary that the currents should concentrate in the larger ring at the lower operation frequency and in the smaller ring for the higher operation

frequency, in order to guarantee that the application of the phase control principle.

In Figure 4.11 and Figure 4.12 the surface current density on split-rings are depicted respectively at lower and higher operating frequencies. The illustrations are put in a 10-to-1 magnitude ratio with logarithmic scaling. It is obvious that, the currents flow dominantly on the smaller split-ring for higher frequency, on the larger ring for the lower frequency. The fact that the reflected fields are formed via the surface currents, these rings are meant to dominate the reflection mechanism and the most of power is coupled to the currents on them at their specific frequencies dominantly. That is the reason why the rotational phase shift principle can be employed for the split-rings in two sizes to control the phase at different frequencies independently.

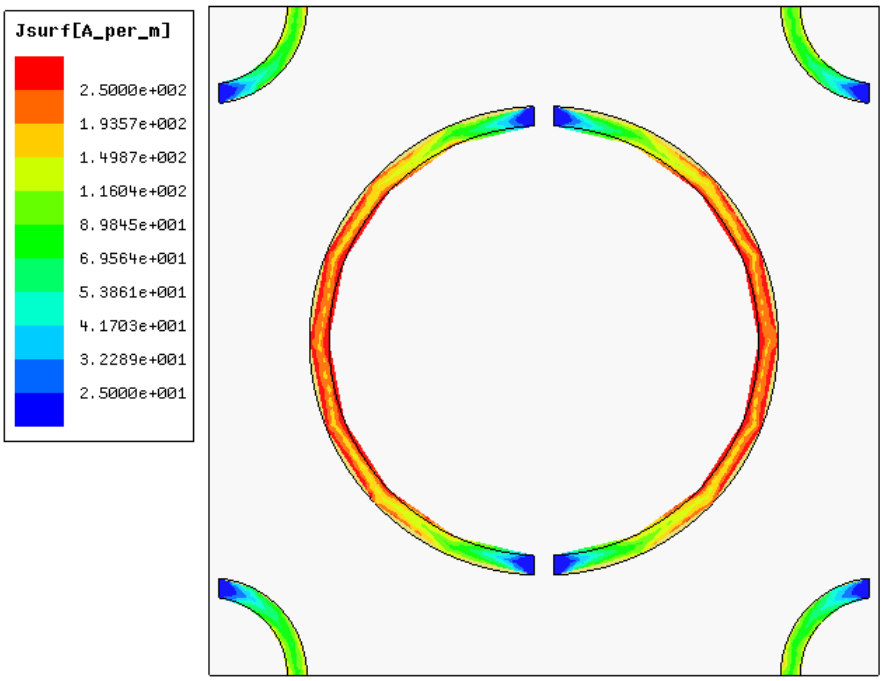

Figure 4.11 The surface current density on the dual frequency element metallization, at 27.4 GHz.

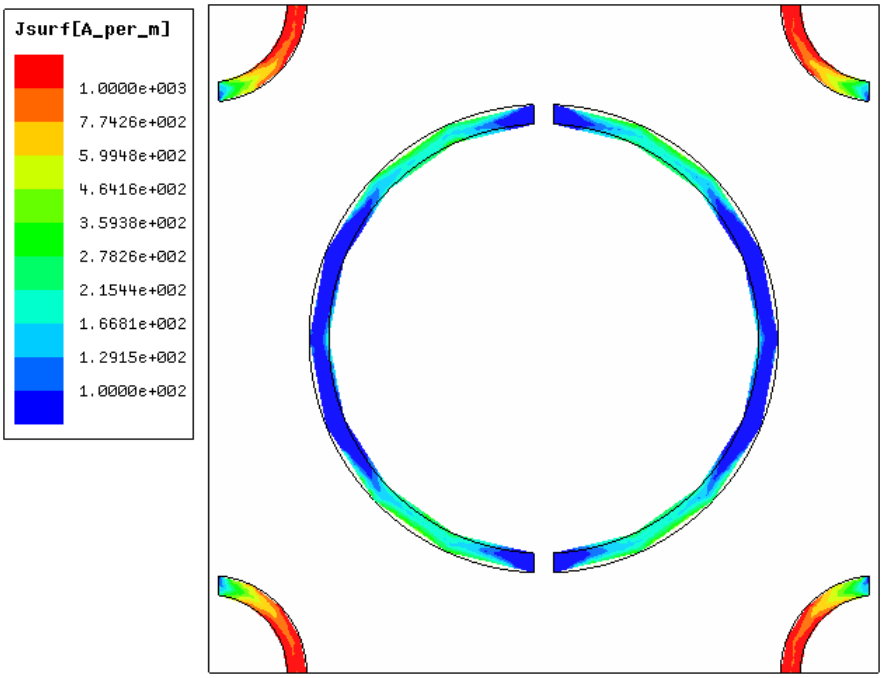

Figure 4.12 The surface current density on the dual frequency element metallization, at 35.3 GHz.

4.2.2.3 Characterization of the Dual Frequency Element

The element design steps are explained previously in this section. The results show that the phase control is realizable. The next step is to verify the phase design curve. This section includes the characterization of the final design and the specifications are shown to match the desired quality. The phase design curve and cross-pol. level plots are given to examine the performance.

In Figure 4.13, the phase design curve at lower band is given. The phase is linearly changing with respect to the rotation angle of the larger ring, this is the expected result. Moreover it can be seen in Figure 4.14 that the cross-pol. is suppressed for all states of the larger split-rings.

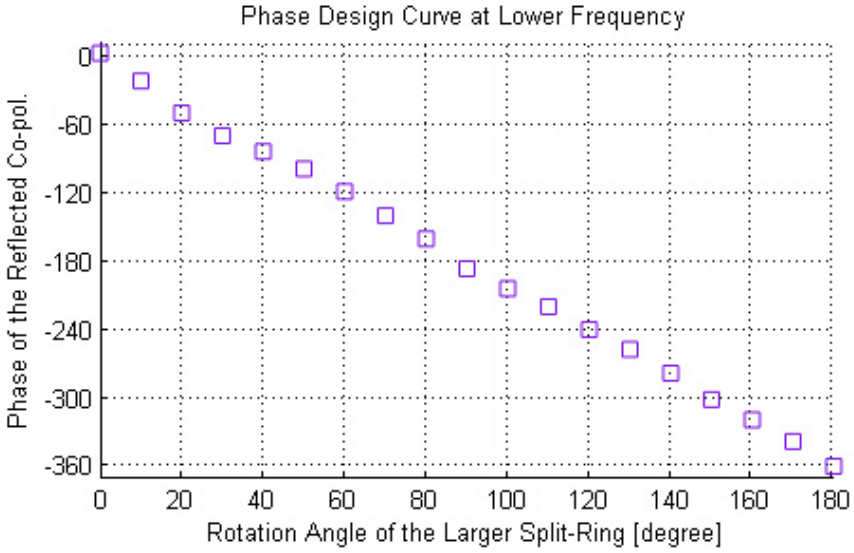

Figure 4.13 Phase Design Curve at 24.4 GHz.

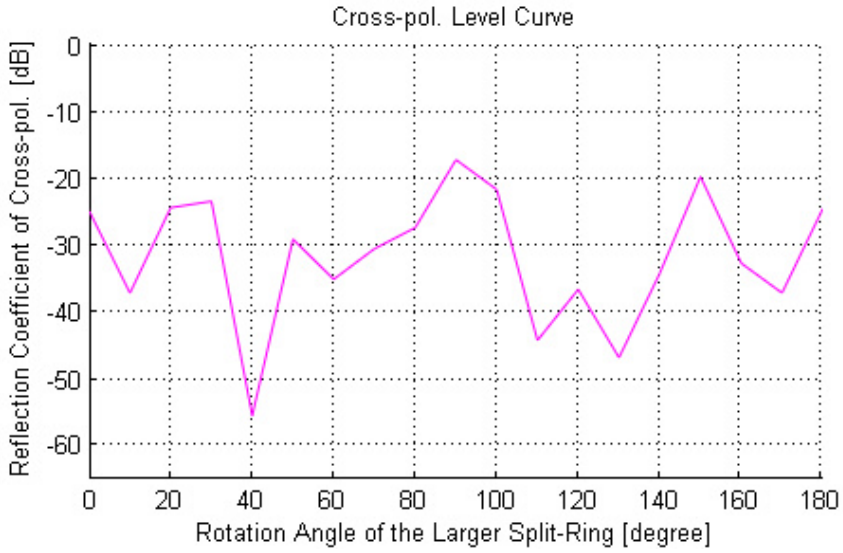

Figure 4.14 Magnitude of Reflection Coefficient of Cross-pol. vs ψ_{larger} at 24.4 GHz.

Then it should also be clear whether rotation of the larger split-ring affects the phase of the co-pol. wave at the higher band - it is required that it does not affect. To check

this, also the phase of the co-pol. wave and cross-pol. level at the higher frequency is plotted. In Figure 4.15, it is apparent that the phase is affected but the effect is very limited and acceptable. And Figure 4.16 shows that the cross-pol. suppression is not affected, either. Then the rotation of the larger split-ring behaves as desired, not disturbing the irrelevant band and controlling the phase at the lower band.

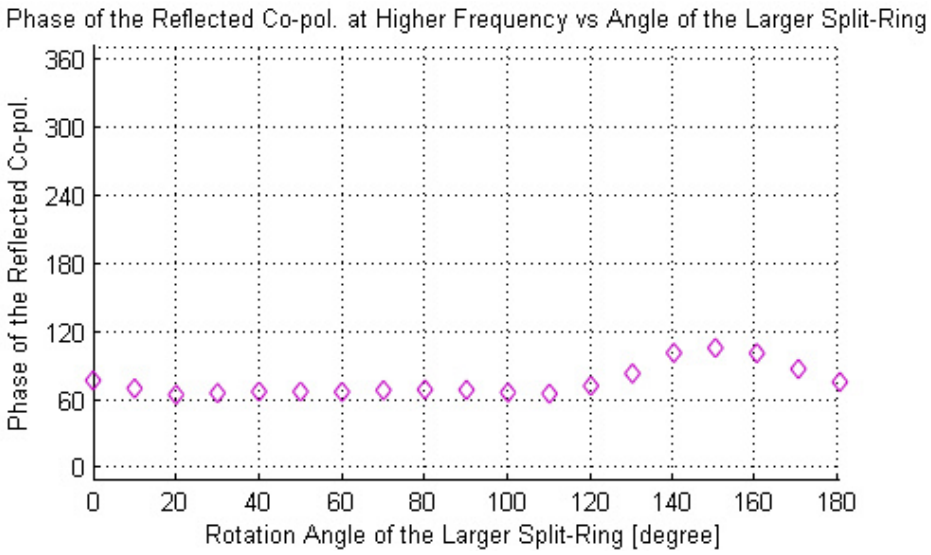

Figure 4.15 Phase of the Co-pol. vs ψ_{larger} at 35.5 GHz.

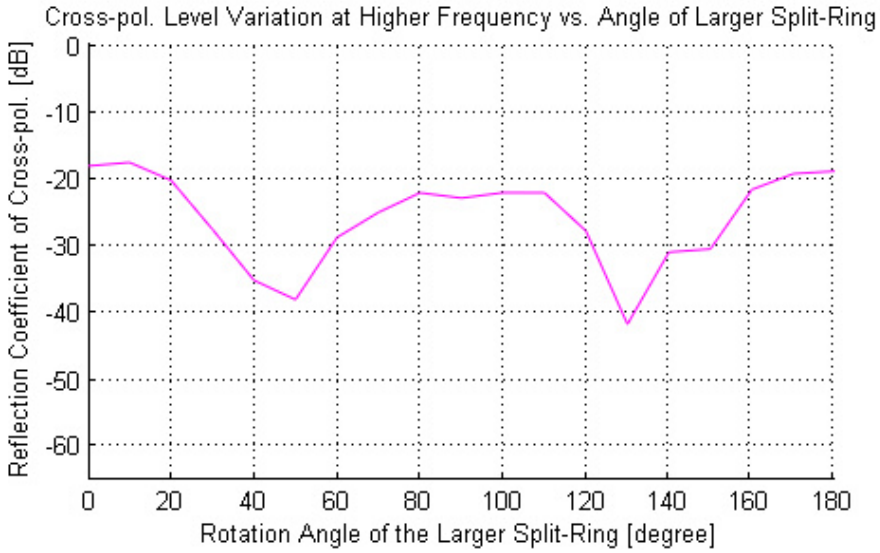

Figure 4.16 Reflection Coefficient of Cross-pol. vs. ψ_{larger} at 35.5 GHz.

Similarly Figure 4.17 and Figure 4.18 shows that the smaller ring controls the phase of the co-pol. component in the reflection linearly with the rotation angle while preserving the cross-pol. levels acceptably low. And in the lower band which it has no effect, it does not disturb the operation. The phase of the co-pol. and the cross-pol. suppression is affected at minimum, as seen in Figure 4.19 and Figure 4.20.

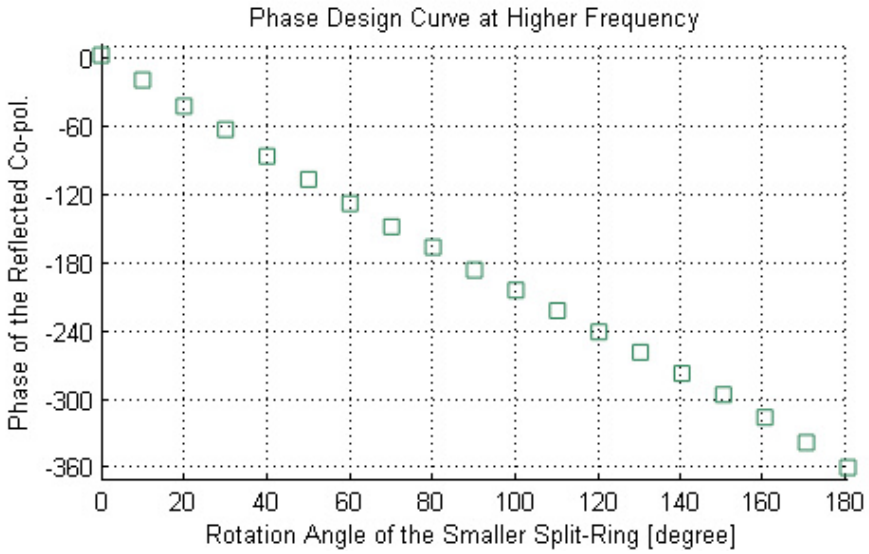

Figure 4.17 Phase Design Curve at 35.5 GHz.

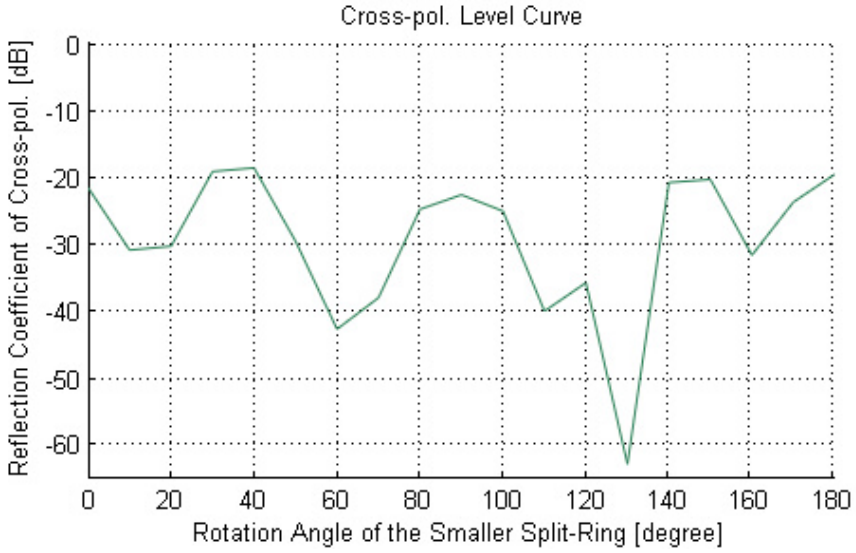

Figure 4.18 Magnitude of Reflection Coefficient of Cross-pol. vs $\psi_{smaller}$ at 35.5 GHz.

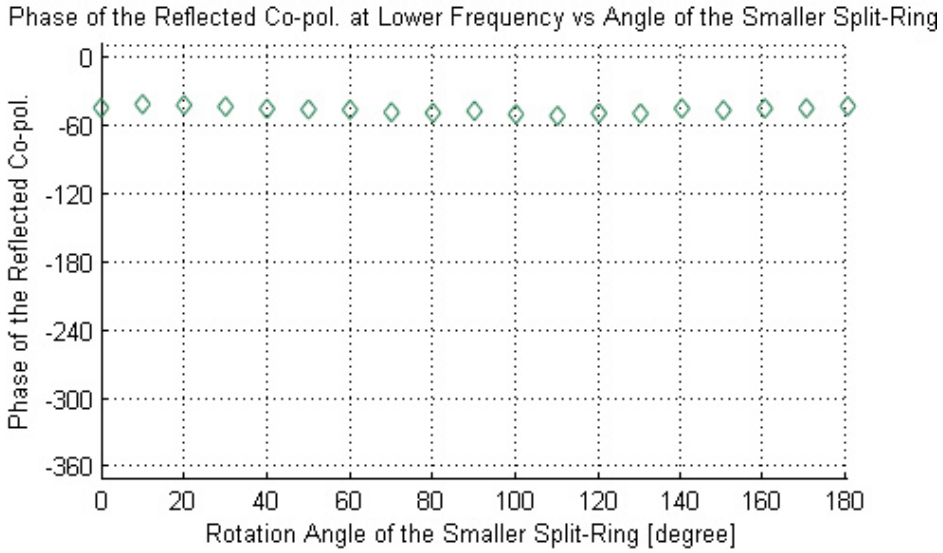

Figure 4.19 Phase of the Co-pol. vs $\psi_{smaller}$ at 24.4 GHz.

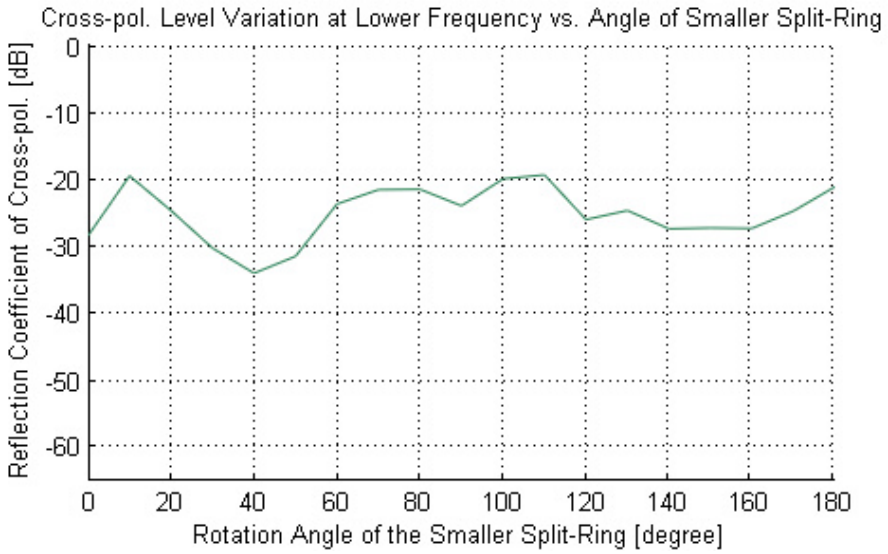

Figure 4.20 Magnitude of Reflection Coefficient of Cross-pol. vs $\psi_{smaller}$ at 24.4 GHz.

The phase curve and the cross-pol. suppression characteristics are all in desired quality. But the previous cases are simulated for the normal incidence. For a better understanding of the response of the reflectarray element, the oblique incidence should be checked. However the total number of cases to be simulated can increase

drastically, it would be sufficient and helpful to see what happens by giving the results for the lower frequency operation under oblique incidence. The case is only simulated at 24.4GHz, since oblique incident wave may lead to new propagating Floquet modes in higher frequency due to the unit cell size.

Regarding Figure 4.221 and Figure 4.22, variation in phase is limited to 40° which is very acceptable and the cross-pol. reflection level is limited to -10dB for up to θ=30°. The cross-pol. levels should be better than -20dB. But when the reflectarray design is examined, it is obvious that while the co-pol. is controlled to have a high directivity, the constant phase of the cross-pol. causes it to contribute into the specular reflection. That is the reason for element level thinking the -10dB cross-pol. reflection may be undesirable but the bigger picture seems to be more optimistic. In the frame of the reflectarray antenna, cross-pol. may not be as high.

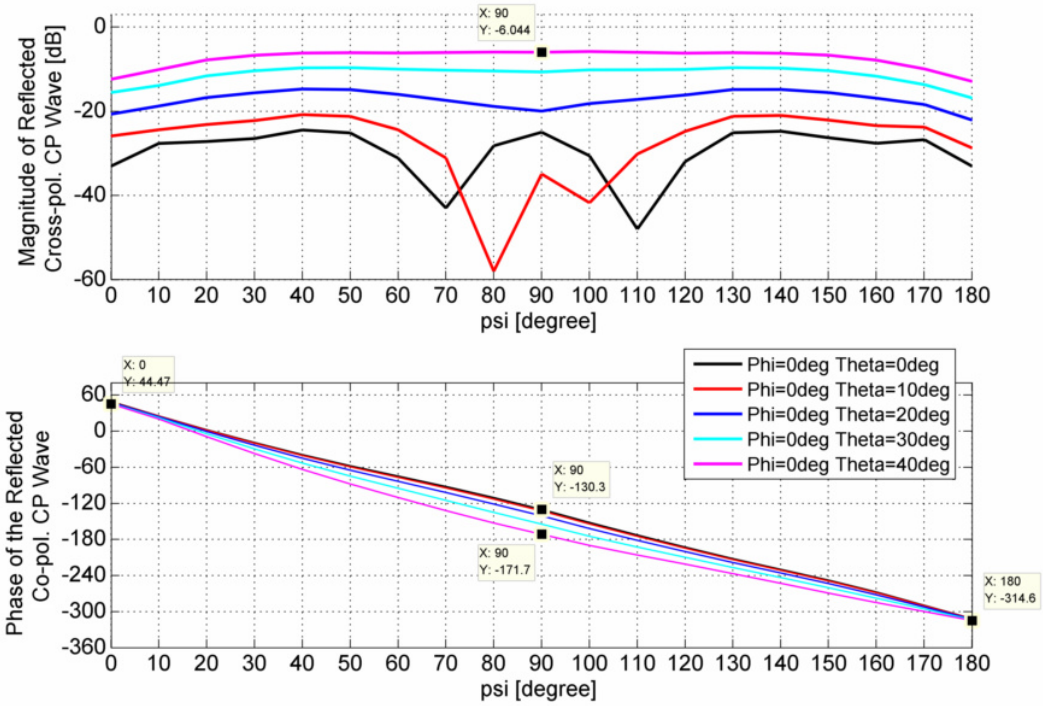

Figure 4.21 Magnitude of the reflected cross pol. and the phase design curve with respect to various oblique incidence angles, at 24.4GHz.

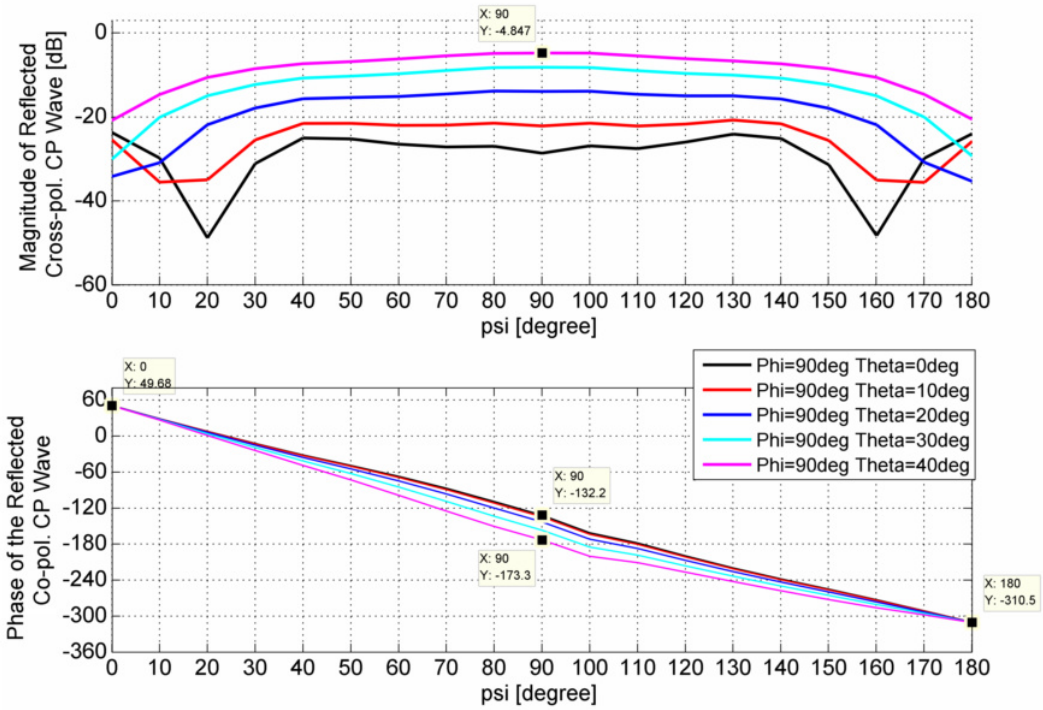

Figure 4.22 Magnitude of the reflected cross pol. and the Phase design with respect to various oblique incidence angles, for φ=90° plane at 24.4GHz.

To conclude this section, it can be stated that the designed dual band reflectarray element is matching the requirements.

4.2.3 Integration of the Element with RF MEMS Switches

The implementation of the rotational phase control principle with split-rings is done using the RF MEMS switches to change the orientation of the splits. By this way, reconfigurability is achieved. For the dual frequency element, the total number of switches is 12. 6 RF MEMS switches per ring are placed with 60° angular spacing about the center of the ring. These 6 switches on one ring are grouped into 3 pairs, where two switches lying on the same diameter constitute a pair. These 3 pairs of switches are biased accordingly to provide 60° rotation effect for the split-ring. Each state corresponds to 2 pairs of switches in on-state and 1 pair in off-state. In this

work, the state numbers are 3 for each frequency, corresponding to 120° phase resolution.

In fact, using a high number of MEMS switches is required to enjoy the reconfigurability with high resolution. However the problems of yield and bias line routing emerge, as the number of MEMS devices increase. Also the increase in phase resolution does not linearly contribute to the beam steering capabilities of an array. The designer should weigh the trade off. Thus a reasonable number of MEMS switches are decided by the designer.

Ohmic contact series switch, capacitive series and shunt switches are available for in house fabrication in METU MEMS Center. Since the design is based on the split-ring structures, the switch based design is also implemented on the previously investigated structure. The previously investigated structure constitutes a basis for the design with switches where the on and off switches correspond to short and open metallization. To achieve this goal capacitance ratio at a degree of 100 is necessary for RF short and open to be in accordance with the previous split-ring designs. This capacitance ratio is typically not achieved with capacitive MEMS switches in which the down state composes of two metal layers separated by a dielectric film, [38]. Thus the ohmic contact series MEMS switch shown in Figure 4.23, which constitutes a contacting metal path between two separated conductor lines in down state, is chosen. This topology is suitable to be modeled with open and short metallization on the split-ring. The design is based on the switch in [13] whose photograph is given in Figure 4.24 after fabrication steps given in [13]. The dimensions are modified with slight changes keeping the topology intact in order to fit into the gaps of the ring; the final dimensions are given in Figure 4.26. The view of the reflectarray element with RF MEMS switches is given in Figure 4.27. The fabrication layers whose final form is represented in Figure 4.25, a complete flow of process is found in [39].

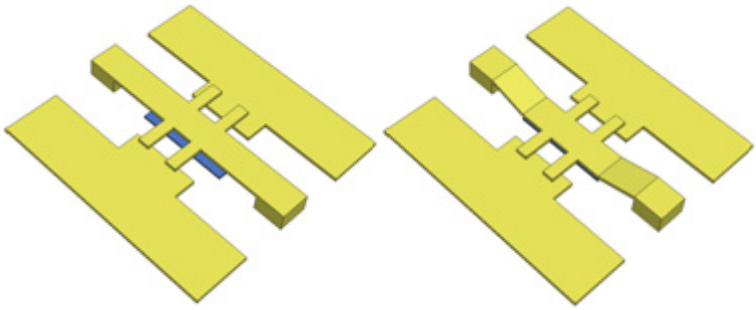

Figure 4.23 The overview of the designed RF MEMS switch.

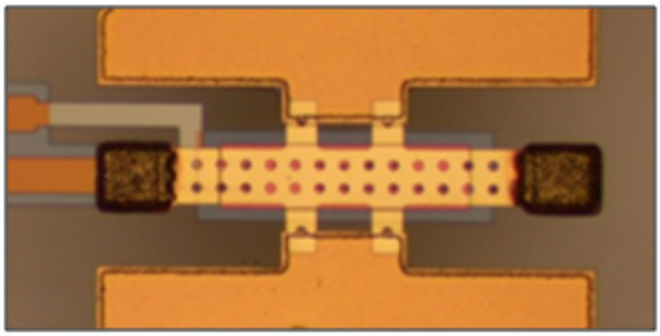

Figure 4.24 Ohmic contact series MEMS switch fabricated in METU.

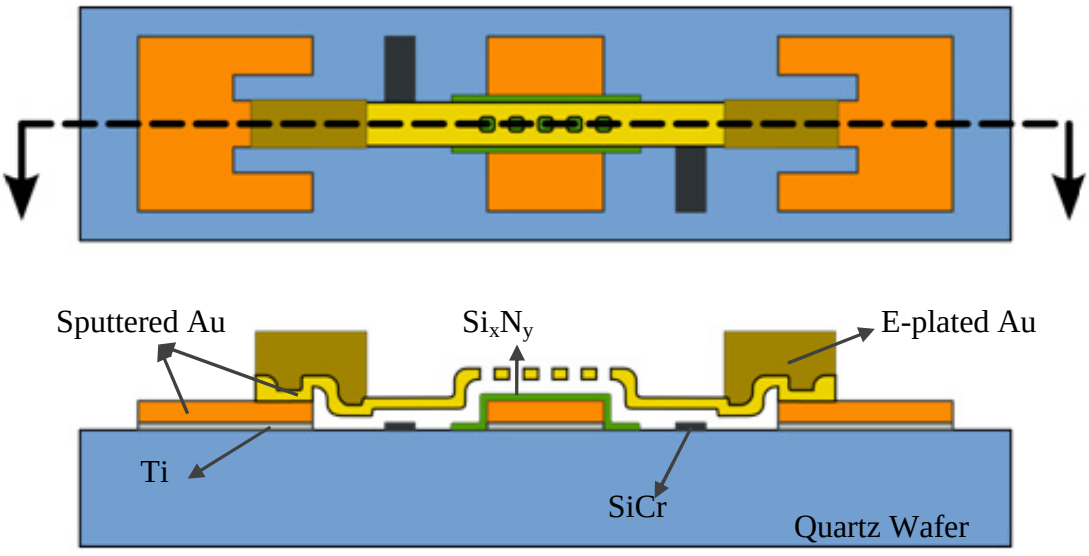

Figure 4.25 RF MEMS switch structure (Courtesy of Çağrı Çetintepe).

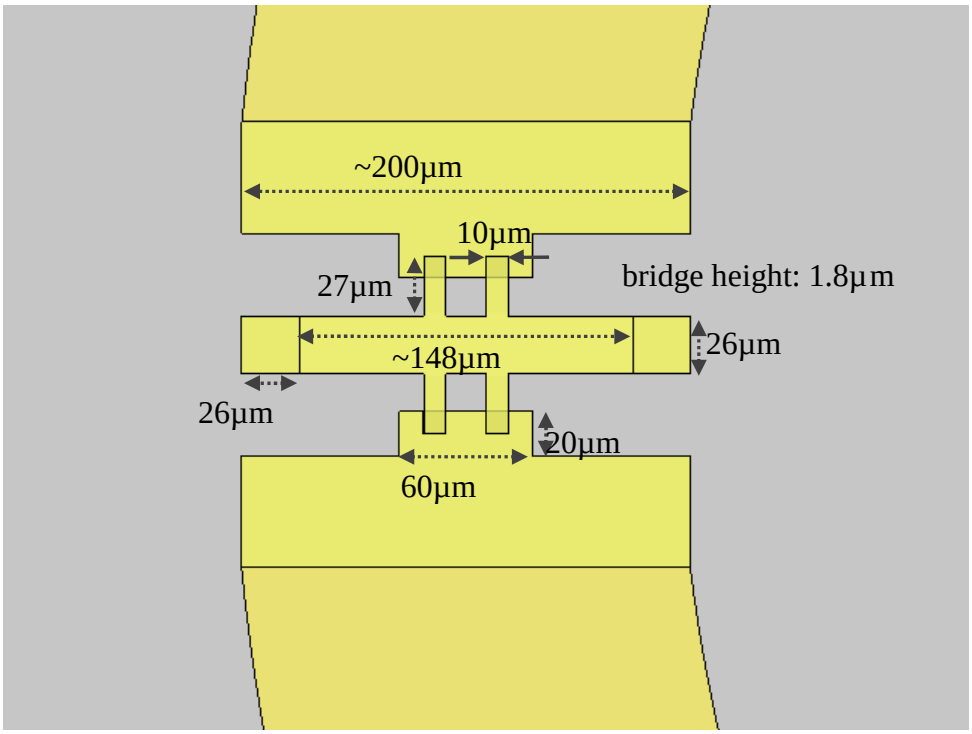

Figure 4.26 Dimensions of the ohmic contact series MEMS switch is illustrated.

Throughout the simulation of the reflectarray element with RF MEMS switches, the bias lines are not contributed into the topology. Furthermore, the 3D full wave simulation takes too much time and needs high memory space, when the accurate 3D MEMS switches are implemented in the simulation environment. Therefore the full 3D model of the reflectarray element, as seen in Figure 4.27, is only simulated once to yield the frequency response of the cross-pol. suppression. Then it is used for validation of modeling the switches.

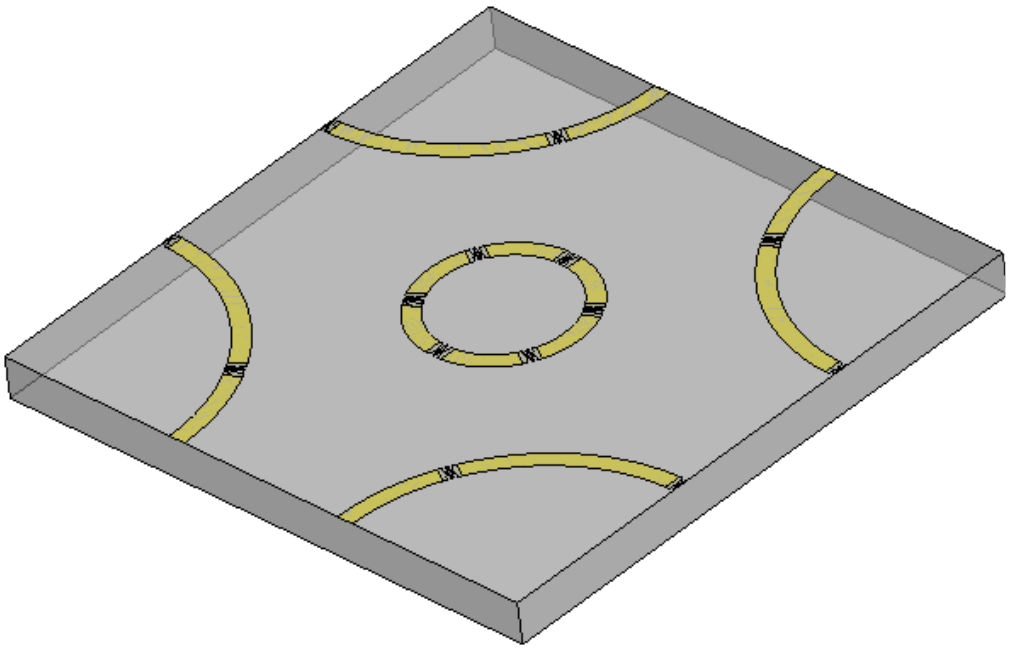

Figure 4.27 Overview of the reflectarray element with RF MEMS switches.

In Figure 4.28, it is seen that the integration of switches caused a shift in the frequency response. The radii of the rings in the element with RF MEMS switches are not tuned to the same operation frequencies not to waste time. These parameters can be tuned to operate in desired frequencies for a final design. Simply the dual band reflectarray element without the switches is a model of this final form where switches in on and off states are modeled simply by perfect shorts and opens respectively. To verify the phase controlling capability of the reflectarray element with 12 RF MEMS switches, the element has to be simulated with unit cell approach with numerous states and frequencies. However the fact that the 3D switch structures in the simulation environment causes drastically high numbers of meshes. The reason is that the edges of the switch topology are in high aspect ratio. To overcome this increased time of computation and memory usage, the switch is modeled using impedance boundary implemented in HFSS.

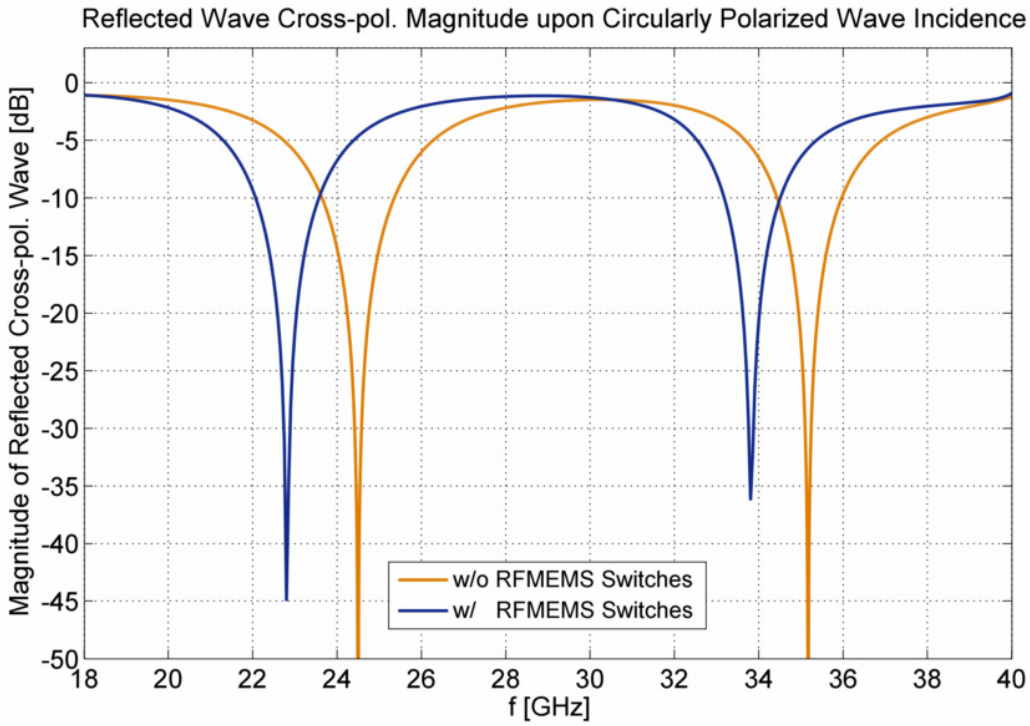

Figure 4.28 Frequency response of the reflectarray element compared before and after the integration of RF MEMS switches.

The aim of impedance boundary modeling of the RF MEMS switch is to verify that the dual band reflectarray element integrated with RF MEMS switches is capable of controlling phase as desired. Thus the high simulation time need for a successful simulation of the high-aspect-ratio switches is avoided, while numerous cases are simulated. Impedance boundaries are also supported by Ansoft HFSS. The impedance boundaries are implemented with 2D surfaces having resistance, inductance and capacitance in parallel. The R, L, C are given with respect to the lumped model together with the current direction. Then any lumped RLC circuit can be formed with necessary compositions of these surfaces in series and parallel.

The models are capable of successfully governing the series ohmic MEMS switch. Down state of the switch can be modeled with an inductor and a resistor in series and a shunt capacitor; and up state of the switch can be modeled with a series capacitor

and a shunt one [40]. The values of the components in the circuit model are optimized by the microwave circuit simulator software AWR using the simulations of the switch in a two port configuration. Thus the necessary lumped R, L, C values are obtained for both on and off states of the switch.

The lumped impedance values to be applied to the impedance boundaries in the simulation environment are to be investigated separately. The reason is that these impedance boundaries are imposed on the electric and magnetic fields by the simulation software. But these boundaries are present in the geometry. In addition to their imposed lumped relations, they intrinsically have inductive and capacitive effects due to their shape and interaction with the physical environment. This is the reason why the optimized lumped circuit parameters cannot be applied directly for the impedance boundaries. The designer should relate the impedance boundary parameters imposed with its corresponding circuit parameters. In this design the imposed values and their circuit parameters are related by curve fitting. Then the desired circuit model of the switch is realized with impedance boundary implementation. Thus the same characteristics for the accurate 3D switch model and impedance boundary model are found.

The aforementioned relation is applied for the shunt capacitors. The simulation results and previous studies [41] show that the shunt capacitor between the switch topology (which is coplanar with the signal trace) and the ground plane is already present in the simulation environment. There is no need to implement it with impedance boundaries.

In Figure 4.29 and Figure 4.30, the implementation of the RLC lumped impedance boundary for the on and off states of the RF MEMS ohmic contact switch. The RLC boundaries are implemented symmetrically to be consistent physically.

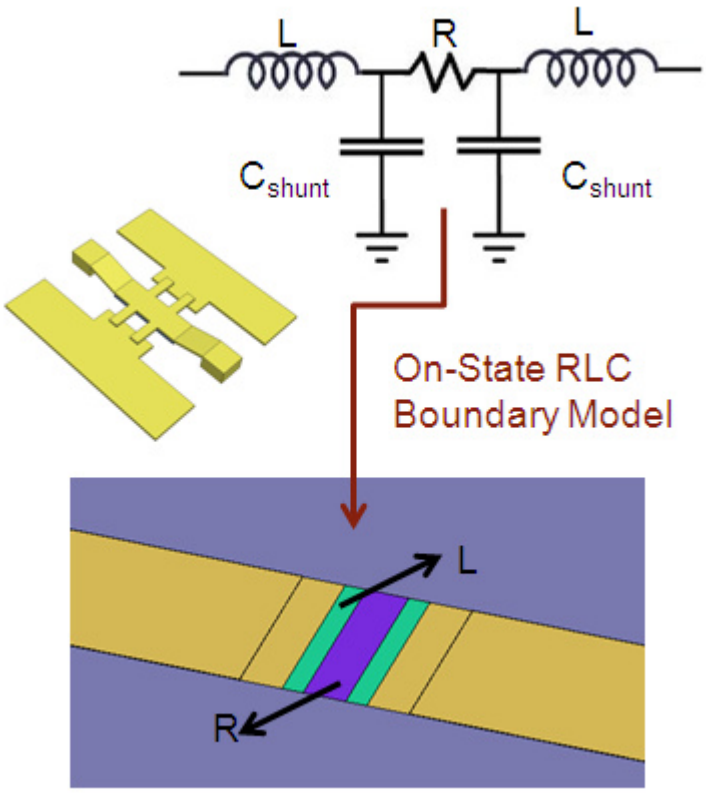

Figure 4.29 Impedance boundary modeling of the switch in on-state (bridge is down).

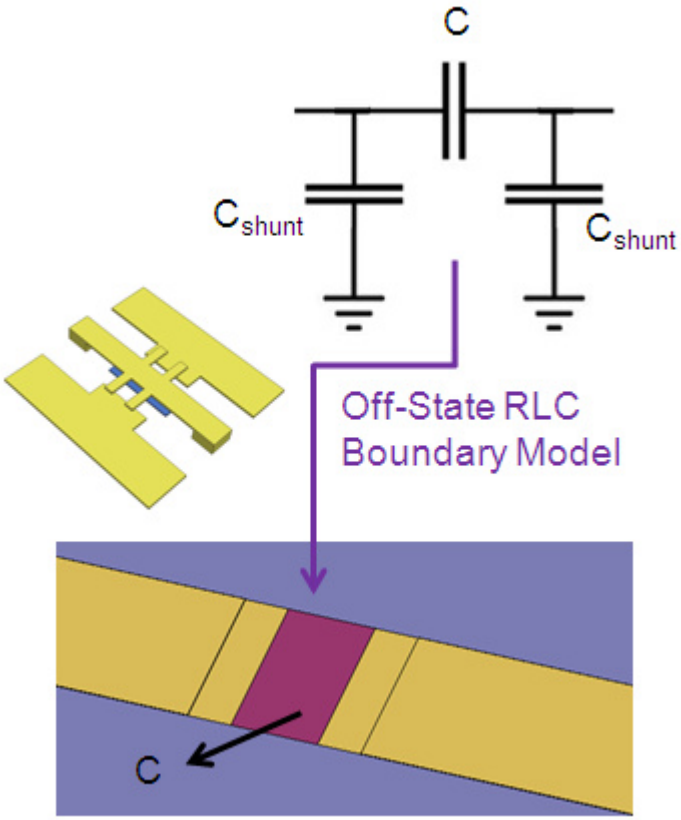

Figure 4.30 Impedance boundary modeling of the switch in off-state (bridge is up).

In Figure 4.31, the frequency responses of the dual frequency reflectarray element with switches as 3D drawing, and with the RLC model of the switch are compared. The graph shows a perfect agreement, proving that the RLC boundary model is successful in modeling the switches. Moreover the impedance boundary modeling method reduced the computation time to 10 minutes, from 8 hours. The simulations are carried out using a 2.5GHz Core2 Quad© processor, 8GB RAM computer with the highest number of mesh available and identical settings.

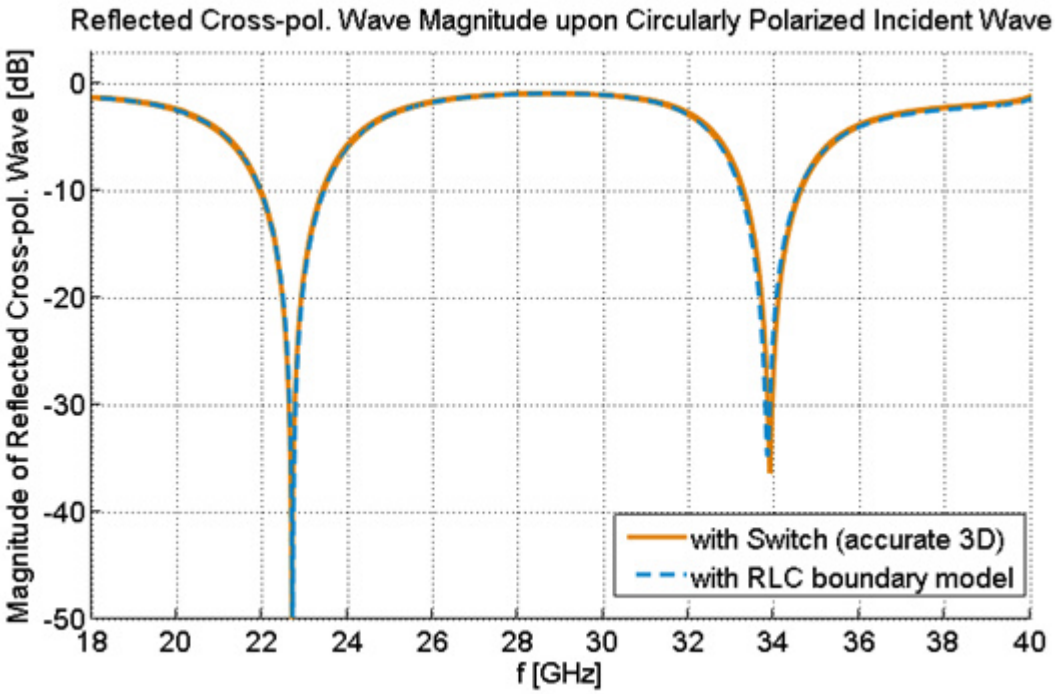

Figure 4.31 Comparison of the unit cell simulation results with 3D switch and its RLC model.

By the help of impedance boundary modeling, there is a sharp decrease in simulation time while preserving the accuracy. This makes the simulation of the reflectarray element integrated with MEMS switches for various cases available. The results of the simulations with modeled switches to verify the phase controlling capability are shown in Figure 4.32 and Figure 4.33. The cross-polarization levels are suppressed perfectly, and the phase design curve is linear.

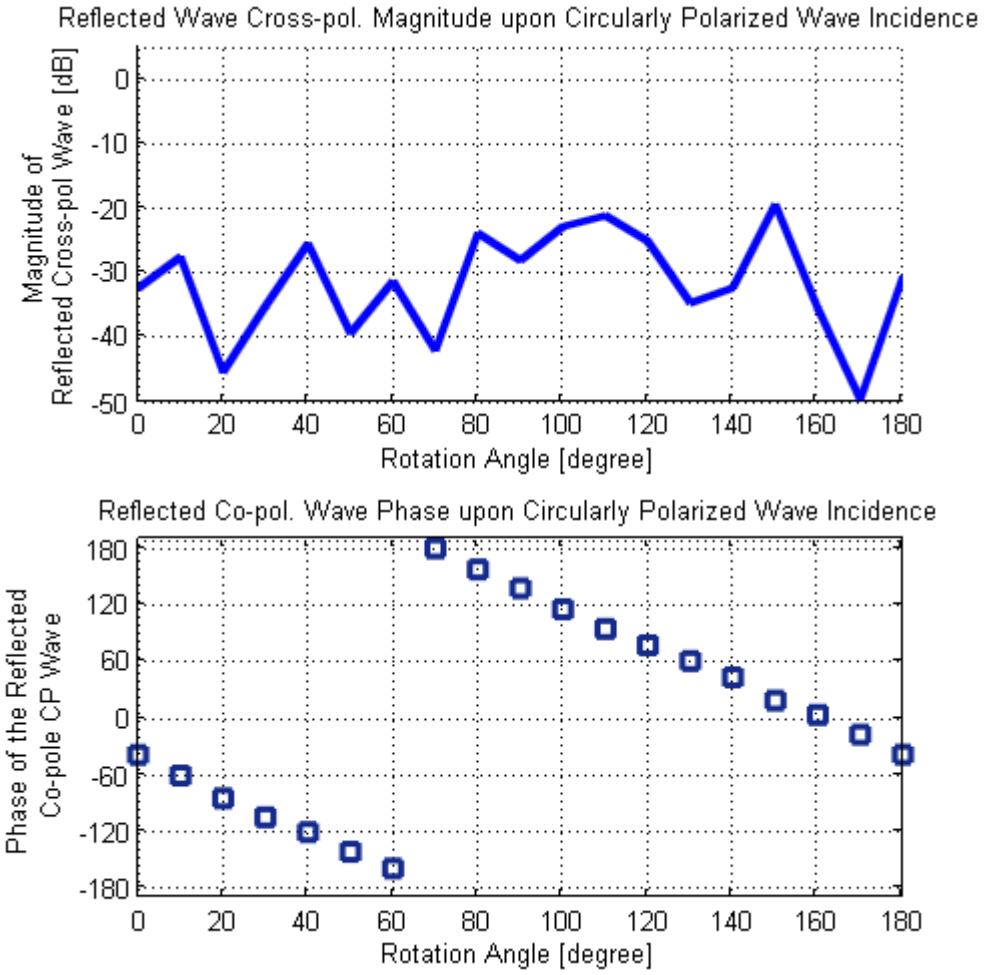

Figure 4.32 Magnitude of the reflected cross-pol. and the phase design curve at 22.65 GHz, for the element with impedance-boundary-modeled switches.

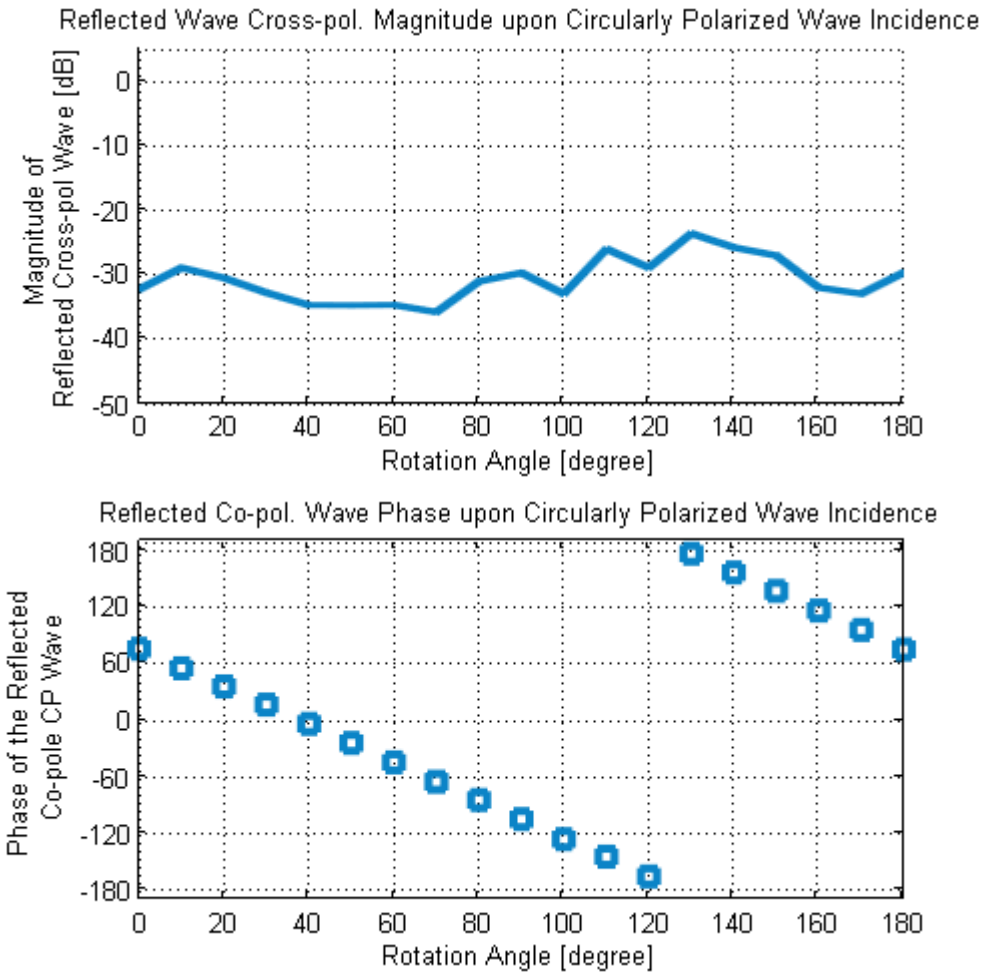

Figure 4.33 Magnitude of the reflected cross-pol. and the phase design curve at 34 GHz, for the element with impedance-boundary-modeled switches.

Although no bias lines were contributed to the simulations, it is helpful to mention bias line routing. If state of any ring is required to be set independently for electronic beam forming, via holes are the main solutions. However the technology is required and process can get harder. The bias lines from each pair of switches can thus be transferred to a printed circuit board. This is the most general solution, and the latter is left to the controlling circuitry. In this method, there has to be at least 3 bias feeds per ring as seen in Figure 4.34-(a), summing up to a high number of bias points. Moreover for verification aims of the antenna, the designer might opt out the independent operation in dual bands, and may narrow the capabilities to a switched

beam antenna. In this case as seen in Figure 4.34-(b), the routing is possible on the micromachined surface of the antenna. Then the antenna to be fabricated in this manner would switch the beam to 3 angles, however independent controlling of the beam direction in dual bands would not be possible. All these proposals are made with the assumption of maximum 2 levels crossing on top of each other. Process complexity may increase the possible routing schemes. And all these bias lines must be included in simulations to make sure the routing does not disturb required characteristic.

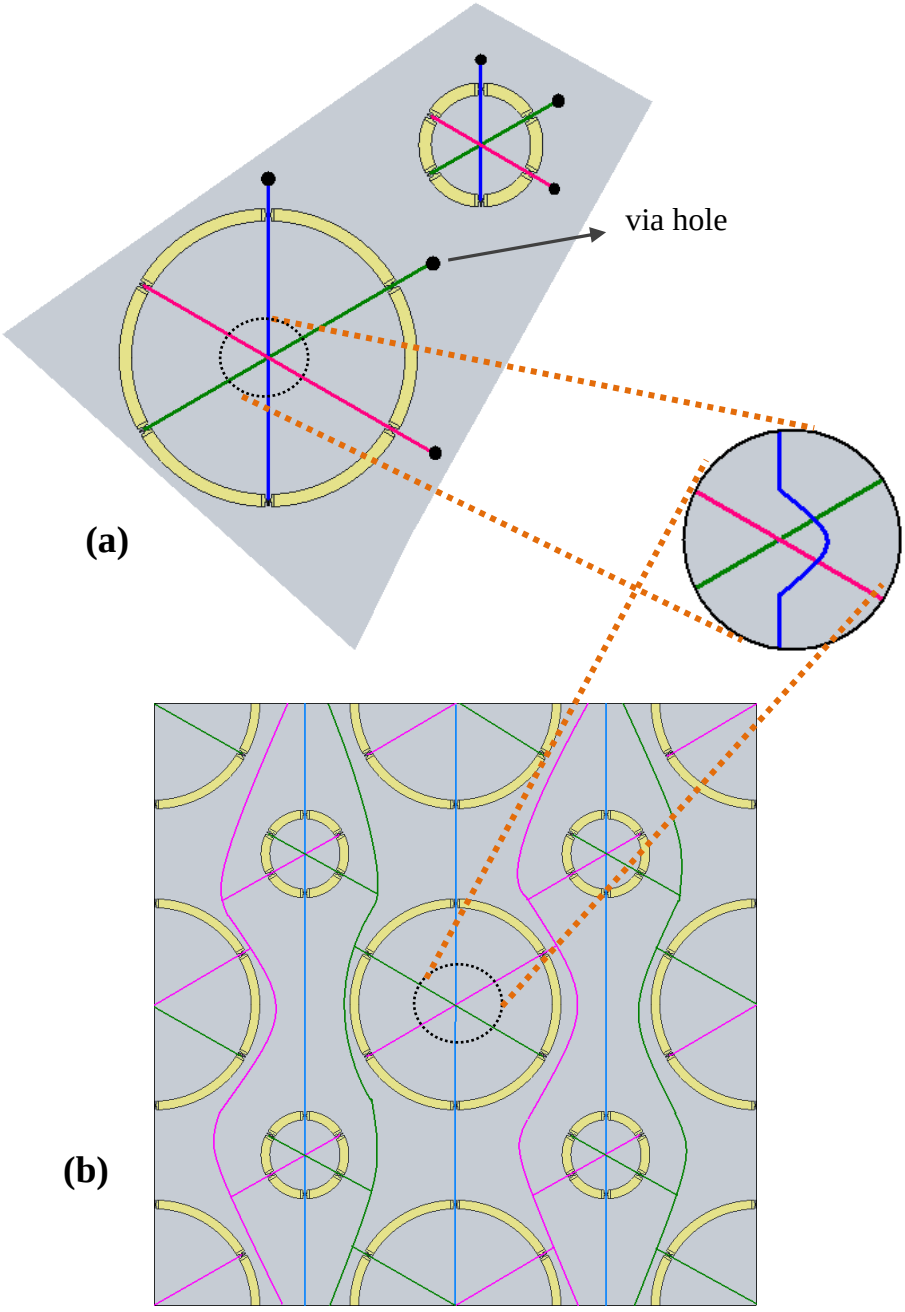

Figure 4.34 Two proposed biasing schemes.

4.3 Reflectarray Antenna Prototype

The full reflectarray antenna composing of the elements with the MEMS switches is the goal of the design. Beforehand designing and fabricating the full reflectarray antenna, it is essential to verify the concept in a prototype design. The prototype design is aimed to be simulated in HFSS and then fabricated, measured and compared to the simulations. Due to the long time requirements and high memory costs, to validate the design the reflectarray element integrated with RF MEMS, in a reflectarray antenna is not preferred. Also in the simulations of the reflectarray antenna, the aspect ratio of the metallization on the antenna surface is of high importance, for the meshing, thus the time increases drastically depending on the mesh detail. This is the reason that the prototype design of the reflectarray antenna utilizes the reflectarray element in Section 4.2.2. This element's fabrication is a simple base metal process available in METU MEMS Center. The on and off MEMS switches are modeled as perfect short and open.

The two RHCP horns at Ka and K bands available in METU mm-Wave Laboratories are taken as the illumination horns. The feed horn antennas are placed at their far-field distances with a 30° deviation from the normal of the wafer (antenna). The designed antenna is offset-fed; the elements are printed onto a 4-in. quartz wafer. The reflectarray elements have 3 states for each frequency, with phase resolution of 120°. These elements are combined in a manner that 3 states have progressive phase difference of 120° and -120° for steered beam and 0° for the broad-side.

The prototype is not reconfigurable; instead two antennas for the 0° and 120° progressive phase difference in y-direction (Figure 4.35) are fabricated with base-metal surface micromachining. The beam is steered on the YZ-plane. The reflect array antenna is composed of 109 and 124 elements respectively in Ka and K bands.

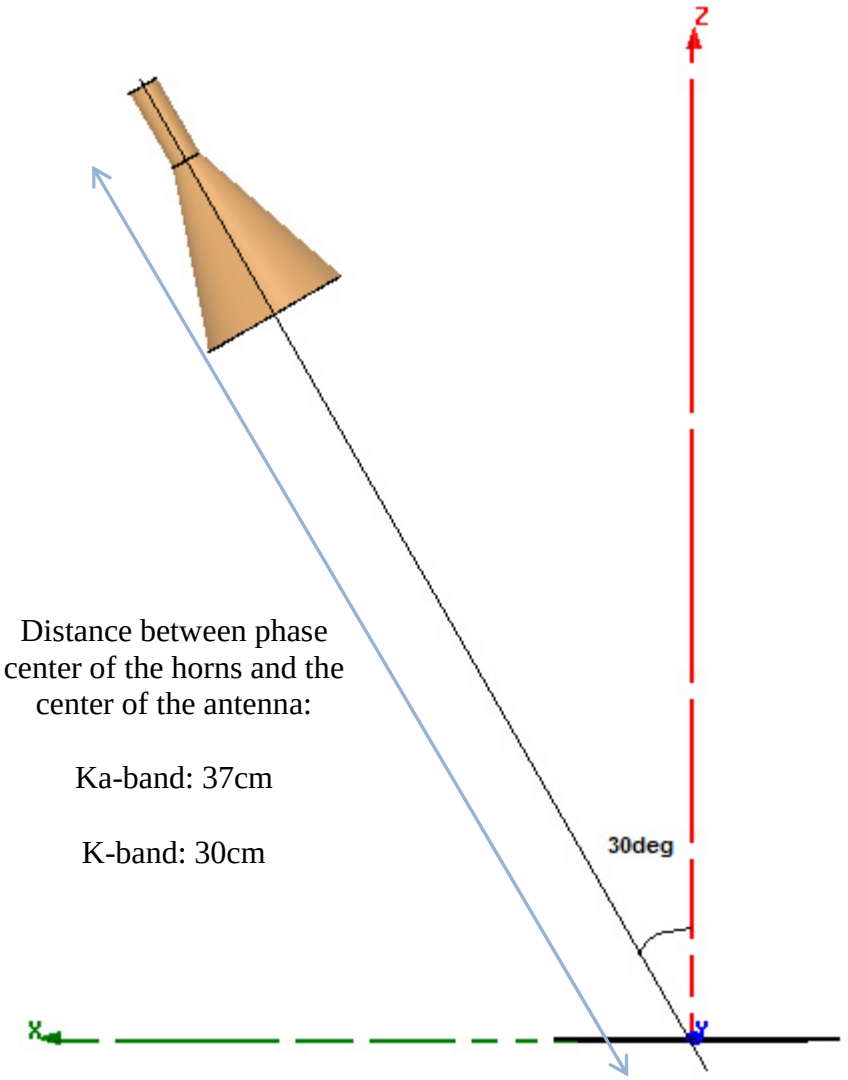

Figure 4.35 Horn placement.

4.3.1 Phase Compensation over the Reflectarray Antenna

The illumination phases due to the path differences between the illumination horn's phase center and the reflectarray elements, creates a phase distribution over the reflectarray surface. This phase is computed using the point source approach, and the split-rings in the broad-side state are put with an off-set angle to compensate the illumination phase and constitute a uniform phase distribution all over the reflectarray antenna. In the steered state, the elements are rotated to sustain 120°

progressive phase difference.

The phase of the incident field in front of elements is given as

$$\Phi_{incidence} = (x_{horn} - x_{elem.})^2 + (y_{horn} - y_{elem.})^2 + (z_{horn} - z_{elem.})^2 / \lambda_0 \qquad (4.1)$$

This phase can be compensated by rotation of split-rings in proper angles, knowing that the phase of an RHCP wave is linearly dependent on 2*ψ (ψ: rotation angle of the split-ring). By this method the phase difference between all the elements on the antenna are set to 0. The broad-side antenna prototype creates an equiphase plane upon reflection, perpendicular to the antenna normal.

4.3.2 Illumination Horn Placement

The horn antennas at K (24.4GHz) and Ka (35.5 GHz) bands are put with 30° oblique incidence respectively at 37cm and 30cm to maintain the far field condition and prevent the horns from obscuring the beam-steering plane (YZ) in Figure 4.35.

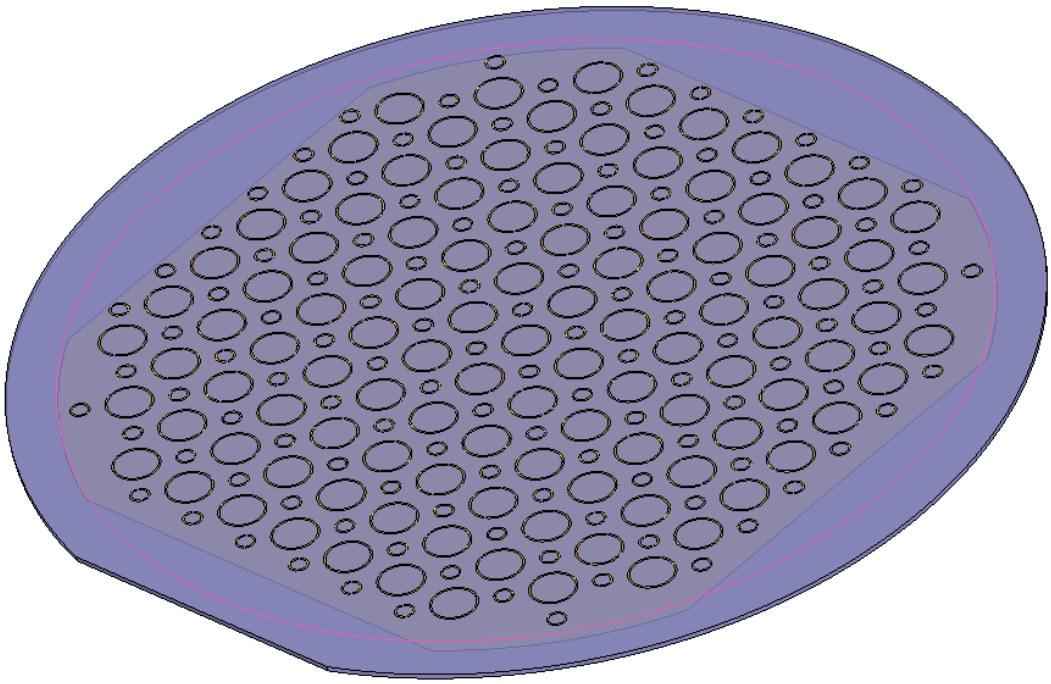

Figure 4.36 Overall view of the simulated reflectarray antenna.

4.3.3 Simulation Results of The Reflectarray Antenna

The antenna prepared for simulation and fabrication can be observed in Figure 4.36. The reflectarray is simulated with given horn distance and offset angle. Two designs have been employed to simulate and fabricate the broad-side and steered beam states with 120° progressive phase shift at 24.4 GHz and 35.5 GHz.

The simulations are done by building the horns and the reflectarray antenna in HFSS 3D modeler. The horns are simulated independently and far field link property in HFSS is utilized to simulate their illumination on the reflectarray antenna. This method forms the far field wave in a simulation set-up then applies it as incident field into another simulation. The simulations lasted more than 5 hr for a 4-inch reflectarray antenna in a 8GB RAM and 2.4GHz Core2 computer, but the high mesh number was reached before meeting the error energy below 10^{-3}.

Note that the element was 0.8λ spaced in higher frequency and 0.6λ spaced in lower frequency. The higher frequency is prone to high grating lobe levels. Anyway, the magnitude tapering naturally acquired from the horns and the frequency response degradation due to oblique incidence is thought to overcome the problem.

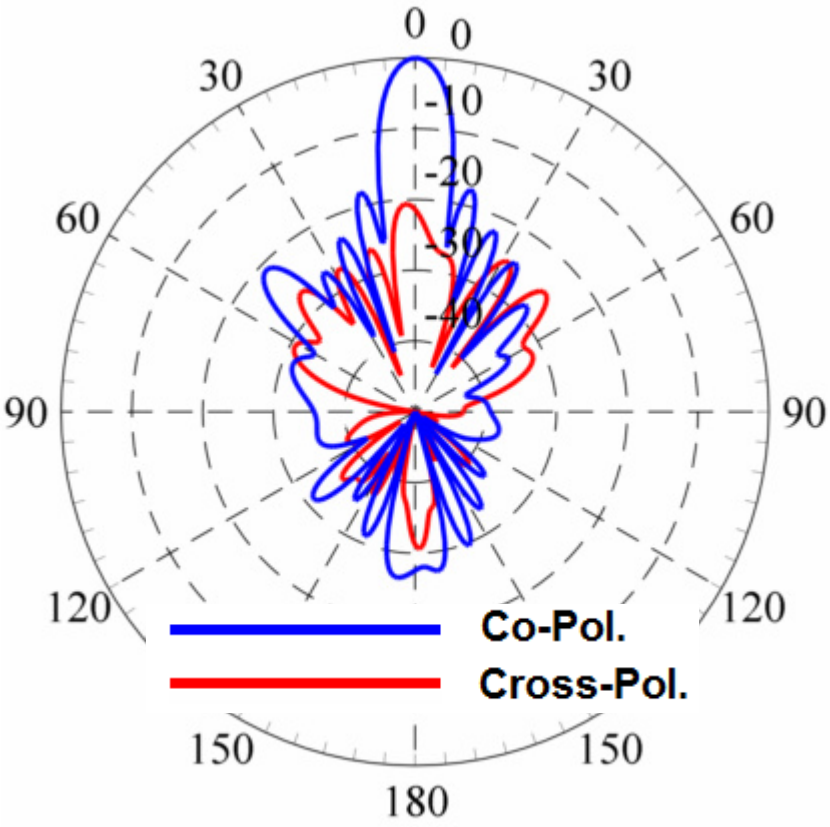

Figure 4.37 The radiation pattern at 24.4GHz, broad-side state.

The radiation patterns of the simulated reflectarray antenna in broad-side configuration at 24.4 GHz are given in Figure 4.37. It is observed that the phase compensation is accurate, the cross-pol. is suppressed as good as 20dB. Side-lobes are in -20dB and back-lobe levels are in -30dB.

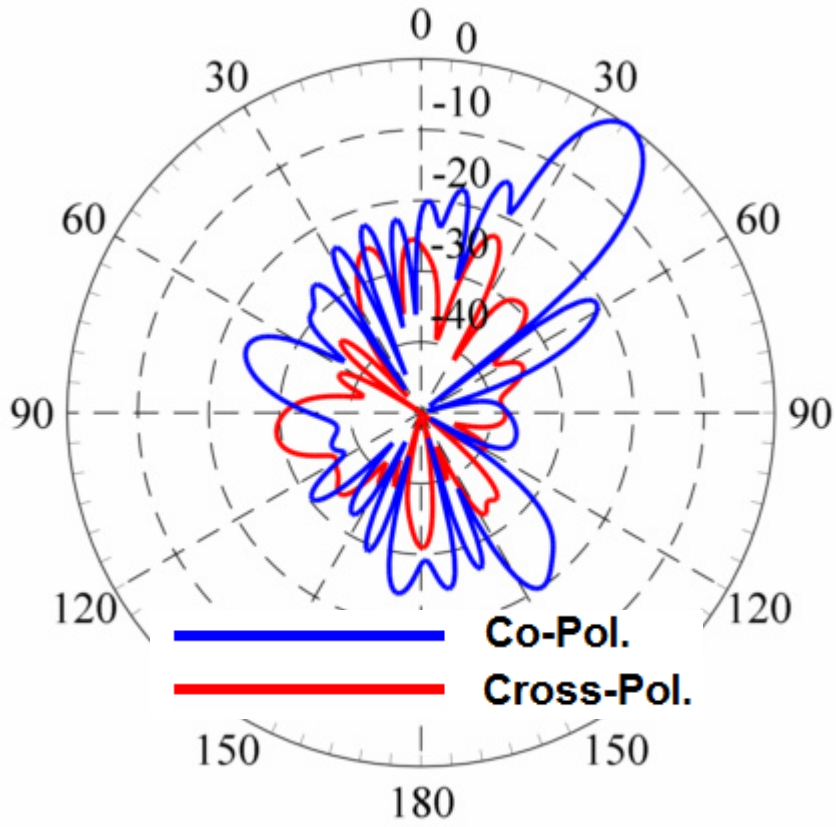

Figure 4.38 The radiation pattern at 24.4GHz frequency, steered-beam state.

The radiation patterns of the simulated reflectarray antenna in steered-beam configuration at 24.4 GHz are given in Figure 4.38. It is seen that the main beam is steered to 35° as expected. The cross-pol. is suppressed as good as 20dB. Side-lobe level is again preserved to be -20dB and back-lobe radiation is negligible.

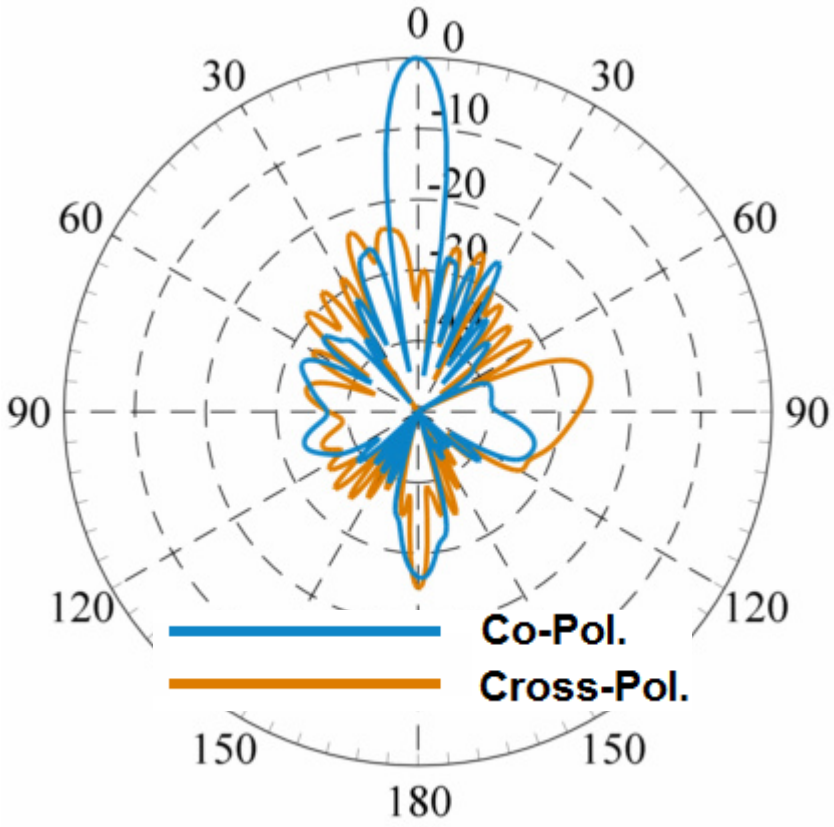

Figure 4.39 The radiation pattern at 35.5 GHz, broad-side state.

The radiation patterns of the simulated reflectarray antenna in broad-side configuration at 35.5 GHz are given in Figure 4.39. It is observed that the phase compensation is accurate thus the main beam points the broadside direction, the cross-pol. is suppressed as good as 20dB. Side-lobe level and back-lobe radiation are in the level of -20dB.

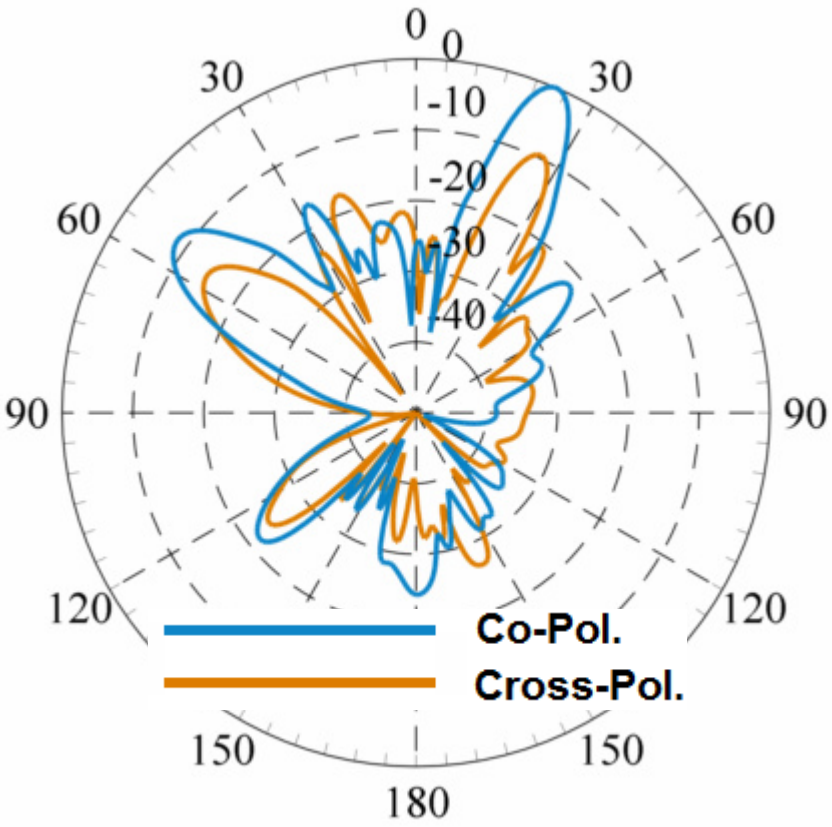

Figure 4.40 The radiation pattern at 35.5 GHz, steered-beam state.

The radiation patterns of the simulated reflectarray antenna in steered-beam configuration at 35.5 GHz are presented in Figure 4.40. It is observed that the main beam is steered to 24°. The cross-pol. is suppressed in levels of 10dB, which is not sufficient. The grating lobe emerged around 58 degrees at -10dB level. The performance of the antenna at higher frequency is not as desired.

4.3.4 Measurement Setup and Radiation Patterns

The radiation patterns of the antenna have been measured in the anechoic chamber of Department of Electrical and Electronics Engineering in METU. The measurement setup is composed of a linear rectangular horn antenna in the transmitting side, and

the designed reflectarray antenna at the receiving end, as seen in Figure 4.41.

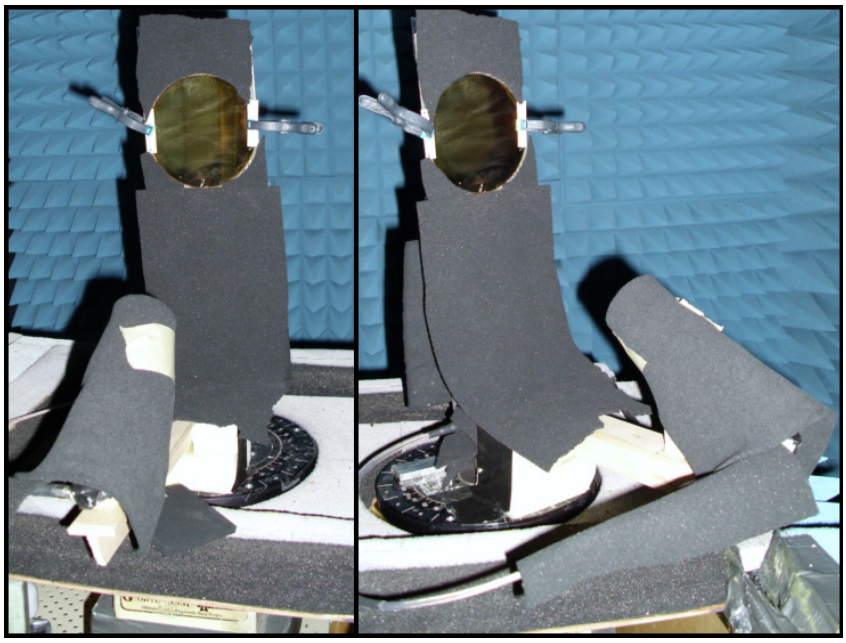

Figure 4.41 Reflectarray antenna and the illumination horn in the anechoic chamber.

It is evident that measurement of co- and cross-polarized components is not possible with this setup. What is measured using this setup can be well understood with the reciprocity theorem. The simulations were done for reflectarray antennas under circularly polarized wave, and the reception was both computed in co- and cross-polarized components. The reciprocity theorem implied that, if the illumination antenna of the reflectarray was linearly polarized and the antenna on the transmitting side of the setup was circularly polarized; the results would be intact. The equivalent case is the case that the cross- and co-polarized components in the simulation results are summed up to give the linear component. In another saying, the results found in the measurement setup include the cross-polarized component along with the desired co-polarized component. The simulation results are mathematically elaborated to be compared to the measurement results, according to the measurement setup. Only measurements of the fabricated switched beam prototype are available.

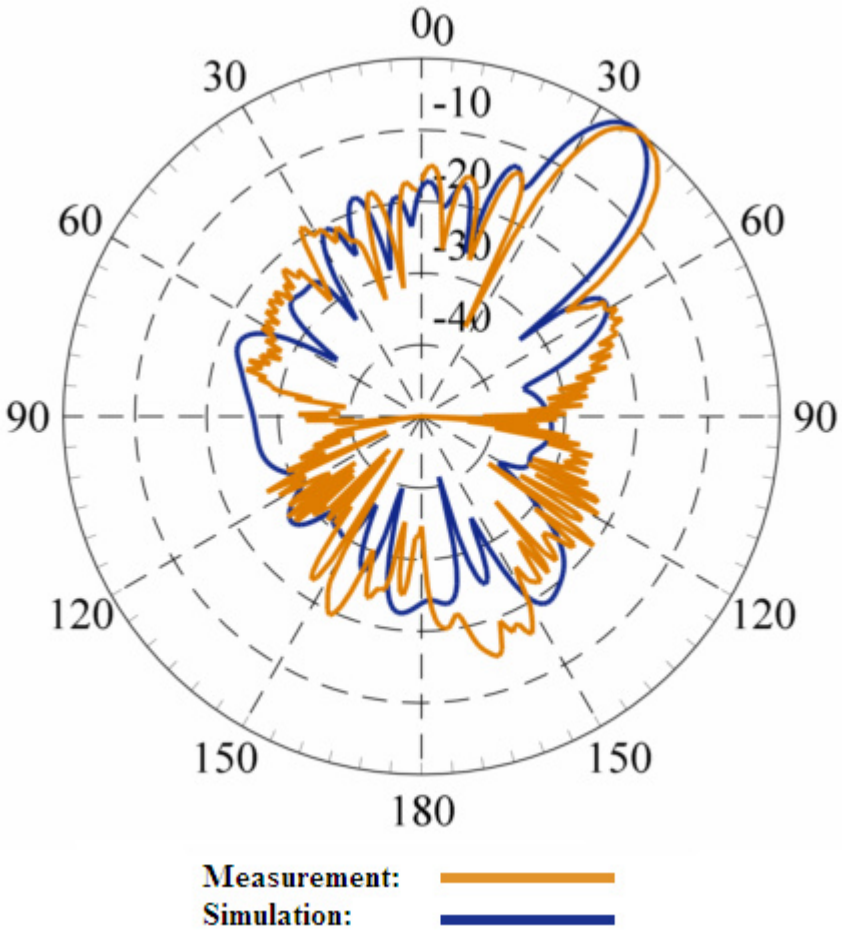

Figure 4.42 Comparison of simulation and measurements of normalized radiation pattern at 24.4 GHz.

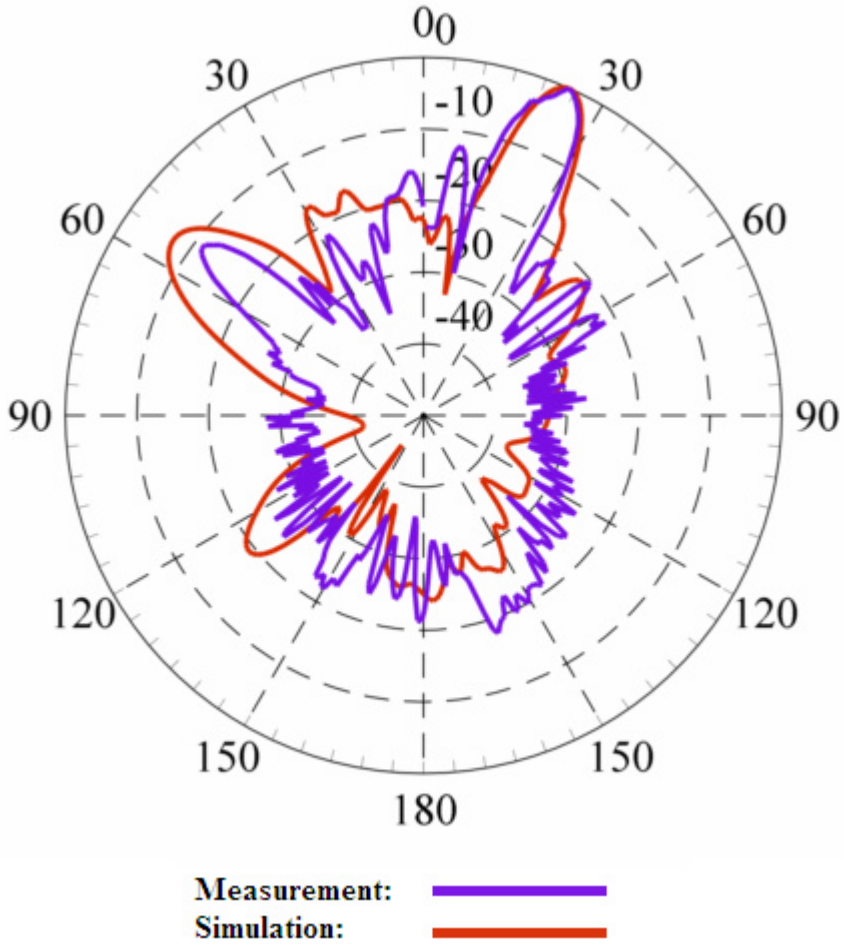

Figure 4.43 Comparison of simulation and measurements of normalized radiation pattern at 35.5 GHz.

The simulation and measurement results are consistent for the radiation patterns of the switched beam prototype. Figure 4.42 and Figure 4.43 show that the beam directions are in good agreement. One should keep in mind that the measurement setup is prone to errors in 1°-2° range. The simulation and measurement results prove the antenna design principles.

4.4 Conclusion

In this section, the dual band reflectarray element is designed and characterized in

various aspects. It is integrated with RF MEMS switches. Finally a reflectarray antenna prototype composing of the designed elements is simulated, the radiation patterns are given. The measurement results of the fabricated prototype are compared with those of the simulations.

CHAPTER 5

CONCLUSIONS AND FUTURE WORK

5.1 Conclusions

In this thesis, a circularly polarized reconfigurable reflectarray antenna capable of dual frequency operation is presented. The reflectarray antenna element was chosen to be split-rings on 0.5mm-thick quartz (ε_R=3.78) substrate over 0.6mm-thick air layer by a ground plane. The split-rings of two sizes were employed for independent operation in dual frequency. The rotational phase shift mechanism was used as the phase control technique which states that the reflection phase of a circularly polarized wave can be controlled by rotating the reflective element. When a circularly polarized wave is incident on a reflective element, the phase of the reflected wave with the same sense of circular polarization is linearly dependent on the physical angular position with a slope of 2. The realization of this principle to design a reconfigurable element was done with RF MEMS series ohmic contact switches. 6 switches were placed on a ring with 60° spacing. These were grouped into 3 pairs where a pair is composed of two switches on the same diameter. The split-ring is such realized with 3 pairs of switches when at each state only one pair is off. This corresponds to a 120° phase resolution between states in both bands. Such two rings with different sizes, on which there are 6 switches, are placed with an interleaved planar array design. These elements are used to design a reflectarray antenna on a 4in. quartz wafer. The conceptual design of the reflectarray was tested by a prototype antenna. The prototype antenna was design by modeling the RF MEMS switches in on and off states with short and open metallization. This antenna had 109 split-rings operating in Ka band and 124 split-rings operating in K band.

Each ring on the antenna is rotated by an initial offset angle to compensate for the phase difference emerging from different path lengths between the antenna plane and the feed horn. Thus the designed antenna in its 0-state directs the beam in the normal direction for both operation frequencies. And for the switched beam states, there is a ±120° progressive phase difference between elements. It is capable of beam switching to ±35° in Ka band, ±24° in K band.

The starting point was to mathematically derive the expression for the rotational phase shift principle. This derivation provided the in-depth interpretation of the principle that cross-polarization should be suppressed upon incidence for high gained and the incident field should be a perfect circularly polarized wave. Then a single frequency reflectarray antenna element composed of a split-ring was designed using unit cell approach. The rotational phase shift mechanism was thus proven with this element. The experience acquired from the single frequency element was transferred to the dual frequency composition. The split-rings in two different sizes were put together in an interleaved array configuration. The dual frequency element was tuned to suppress cross-polarized wave in Ka and K bands. Then in these bands it was shown that each ring could control the phase in its corresponding frequency independently. The RF MEMS switches were integrated into the design for reconfigurability. The simulation of the element with 12 RF MEMS switches was time consuming, for better and faster results the RF MEMS switches are modeled using impedance boundary conditions. Dual frequency element with RF MEMS switches is shown to control the reflection phase linearly over 360° phase range. The reflectarray prototype is simulated in HFSS, the results are presented. The radiation pattern measurements of fabricated prototype are shown to be in good agreement with the simulation results.

The designed element shows that the split-ring structure is a good option to be employed for dual band operation with circularly polarized waves. In addition the phase control mechanism by rotating the split-rings can be realized with RF MEMS technology. The simulations and the measurement results shows that the design

elements can be brought together in a straight forward manner to build a reflectarray antenna, and the antenna works as expected.

5.2 Future Work

The effort put forward in order to realize the novel dual band reconfigurable reflectarray antenna aimed in this thesis showed that the topology is capable of providing the desired quality. In the guidance of the analysis experience of this thesis and the results of the reflectarray prototype, the future works can be listed as follows:

- A monolithic fabrication with RF MEMS switches should be accomplished to present a novel and fully functioning reflectarray antenna.
- A larger antenna can provide narrower beam and lower spill-over and side lobes with a natural tapering.
- To increase the phase resolution, the number of states should be increased. This means more RF MEMS on the antenna. The yield and bias line routing solutions may be developed to achieve this.
- For an element-wise enhancement, the cross-pol. suppression bandwidth should be increased for better performance. This can increase the gain with reduced cross-pol. reflection contributing to the specular reflection.
- Different reflectarray cell configurations of split-rings can be tested to decrease the coupling and achieve a smaller element size to avoid the grating lobes.
- Different switch types may be implemented in the gaps of the split-rings to compare the performance of various reconfigurability choices.

As a result, the experience gained during the design, fabrication and measurement is a valuable contribution to the reconfigurable antenna, dual band antennas and the reflectarray antenna areas. The abilities of similar structures in reflectarray antennas can be studied further. Today's technology which drives the future of humanity towards the wireless communication systems makes it important to achieve

reconfigurable low profile antennas with low cost. This study and the results shown therein can be adopted to build high-end antennas as well as to define the necessary future tools to improve the reflectarray antenna design.

REFERENCES

[1] H. Phelan, "Spiraphase reflectarray for multitarget radar," *Microwave Journal,* vol. 20, p. 67, 1977.

[2] D. Berry, *et al.*, "The reflectarray antenna," *Antennas and Propagation, IEEE Transactions on,* vol. 11, pp. 645-651, 1963.

[3] C. Malagisi, "Microstrip disc element reflect array," in *Electronics and Aerospace Systems Convention*, 1978, pp. 186-192.

[4] D. M. Pozar and T. A. Metzler, "Analysis of a reflectarray antenna using microstrip patches of variable size," *Electronics Letters,* vol. 29, pp. 657-658, 1993.

[5] M. E. Bialkowski and K. H. Sayidmarie, "Investigations Into Phase Characteristics of a Single-Layer Reflectarray Employing Patch or Ring Elements of Variable Size," *Antennas and Propagation, IEEE Transactions on,* vol. 56, pp. 3366-3372, 2008.

[6] A. Kelkar, "FLAPS: conformal phased reflecting surfaces," in *Radar Conference, 1991., Proceedings of the 1991 IEEE National*, 1991, pp. 58-62.

[7] J. A. Encinar, "Design of two-layer printed reflectarrays using patches of variable size," *Antennas and Propagation, IEEE Transactions on,* vol. 49, pp. 1403-1410, 2001.

[8] J. A. Encinar and J. A. Zornoza, "Broadband design of three-layer printed reflectarrays," *Antennas and Propagation, IEEE Transactions on,* vol. 51, pp. 1662-1664, 2003.

[9] T. Metzler and D. Schaubert, "Scattering from a stub loaded microstrip antenna," in *Antennas and Propagation Society International Symposium, 1989. AP-S. Digest,* 1989, pp. 446-449 vol.1.

[10] A. W. Robinson, *et al.*, "An X-band passive reflect-array using dual-feed aperture-coupled patch antennas," in *Microwave Conference, 1999 Asia Pacific*, 1999, pp. 906-909 vol.3.

[11] E. Carrasco, *et al.*, "Aperture-coupled reflectarray element with wide range of phase delay," *Electronics Letters,* vol. 42, pp. 667-668, 2006.

[12] M. E. Bialkowski, *et al.*, "Design, development, and testing of X-band amplifying reflectarrays," *Antennas and Propagation, IEEE Transactions on,* vol. 50, pp. 1065-1076, 2002.

[13] O. Bayraktar, *et al.*, "Beam switching reflectarray with MEMS controls," in *Antennas and Propagation (EuCAP), 2010 Proceedings of the Fourth European Conference on*, 2010, pp. 1-4.

[14] O. Bayraktar, *et al.*, "Beam Switching Reflectarray using RF MEMS Technology," in *Antennas and Propagation, 2007. EuCAP 2007. The Second European Conference on*, 2007, pp. 1-6.

[15] O. Bayraktar, "Beam Switching Reflectarray with RF MEMS Technology," MS., Institute of Natural Sciences, Middle East Technical University, Ankara, 2007.

[16] J. Huang and R. J. Pogorzelski, "Microstrip reflectarray with elements having variable rotation angles," in *Antennas and Propagation Society International Symposium, 1997. IEEE., 1997 Digest*, 1997, pp. 1280-1283 vol.2.

[17] B. Subbarao, *et al.*, "Element suitability for circularly polarised phase agile reflectarray applications," *Microwaves, Antennas and Propagation, IEE Proceedings -*, vol. 151, pp. 287-292, 2004.

[18] H. Chulmin and C. Kai, "Ka-band reflectarray using ring elements," *Electronics Letters*, vol. 39, pp. 491-493, 2003.

[19] C. Han, *et al.*, "A C/Ka dual frequency dual Layer circularly polarized reflectarray antenna with microstrip ring elements," *Antennas and Propagation, IEEE Transactions on*, vol. 52, pp. 2871-2876, 2004.

[20] A. E. Martynyuk, *et al.*, "Spiraphase-type reflectarrays based on loaded ring slot resonators," *Antennas and Propagation, IEEE Transactions on*, vol. 52, pp. 142-153, 2004.

[21] B. Strassner, *et al.*, "Circularly polarized reflectarray with microstrip ring elements having variable rotation angles," *Antennas and Propagation, IEEE Transactions on*, vol. 52, pp. 1122-1125, 2004.

[22] D. F. Sievenpiper, *et al.*, "Two-dimensional beam steering using an electrically tunable impedance surface," *Antennas and Propagation, IEEE Transactions on*, vol. 51, pp. 2713-2722, 2003.

[23] J. Perruisseau-Carrier, "Dual-Polarized and Polarization-Flexible Reflective Cells With Dynamic Phase Control," *Antennas and Propagation, IEEE Transactions on*, vol. 58, pp. 1494-1502, 2010.

[24] R. Romanofsky, *et al.*, "A K-band linear phased array antenna based on $Ba_{0.60}Sr_{0.40}TiO_3$ thin film phase shifters," in *Microwave Symposium Digest., 2000 IEEE MTT-S International*, 2000, pp. 1351-1354 vol.3.

[25] A. Moessinger, *et al.*, "Electronically reconfigurable reflectarrays with nematic liquid crystals," *Electronics Letters*, vol. 42, pp. 899-900, 2006.

[26] R. R. Romanofsky, "Advances in Scanning Reflectarray Antennas Based on Ferroelectric Thin-Film Phase Shifters for Deep-Space Communications," *Proceedings of the IEEE*, vol. 95, pp. 1968-1975, 2007.

[27] R. Marin, *et al.*, "Realization of 35 GHz Steerable Reflectarray using Highly Anisotropic Liquid Crystal," in *Antennas and Propagation Society International Symposium 2006, IEEE*, 2006, pp. 4307-4310.

[28] A. Moessinger, *et al.*, "Investigations on 77 GHz tunable reflectarray unit cells with liquid crystal," in *Antennas and Propagation, 2006. EuCAP 2006. First European Conference on*, 2006, pp. 1-4.

[29] J. Perruisseau-Carrier and A. K. Skrivervik, "Monolithic MEMS-Based Reflectarray Cell Digitally Reconfigurable Over a 360° Phase Range," *Antennas and Wireless Propagation Letters, IEEE*, vol. 7, pp. 138-141, 2008.

[30] J. P. Gianvittorio and Y. Rahmat-Samii, "Reconfigurable patch antennas for steerable reflectarray applications," *Antennas and Propagation, IEEE Transactions on*, vol. 54, pp. 1388-1392, 2006.

[31] H. Rajagopalan, *et al.*, "RF MEMS Actuated Reconfigurable Reflectarray Patch-Slot Element," *Antennas and Propagation, IEEE Transactions on*, vol. 56, pp. 3689-3699, 2008.

[32] S. V. Hum, *et al.*, "Integrated mems reflectarray elements," in *Antennas and Propagation, 2006. EuCAP 2006. First European Conference on*, 2006, pp. 1-6.

[33] H. Legay, *et al.*, "A steerable reflectarray antenna with MEMS controls," in *Phased Array Systems and Technology, 2003. IEEE International Symposium on*, 2003, pp. 494-499.

[34] R. Sorrentino, "Reconfigurable reflectarrays based on RF MEMS technology," in *Microwaves, Radar and Remote Sensing Symposium, 2008. MRRS 2008*, 2008, pp. 16-21.

[35] J. Huang, "Bandwidth study of microstrip reflectarray and a novel phased reflectarray concept," in *Antennas and Propagation Society International Symposium, 1995. AP-S. Digest*, 1995, pp. 582-585 vol.1.

[36] WANG, *et al.*, *Generalised moment methods in electromagnetics* vol. 137. Stevenage, ROYAUME-UNI: Institution of Electrical Engineers, 1990.

[37] K. Topalli, *et al.*, "A Monolithic Phased Array Using 3-bit Distributed RF MEMS Phase Shifters," *Microwave Theory and Techniques, IEEE Transactions on*, vol. 56, pp. 270-277, 2008.

[38] G. M. Rebeiz and J. B. Muldavin, "RF MEMS switches and switch circuits," *Microwave Magazine, IEEE*, vol. 2, pp. 59-71, 2001.

[39] C. Cetintepe, "Development of MEMS Technology Based Microwave and Millimeter-Wave Components," MSc, Electrical - Electronics Eng., Middle East Technical University (METU), Ankara, 2010.

[40] H. Sedaghat-Pisheh, *et al.*, "A Novel Stress-Gradient-Robust Metal-Contact Switch," in *Micro Electro Mechanical Systems, 2009. MEMS 2009. IEEE 22nd International Conference on*, 2009, pp. 27-30.

[41] J. Perruisseau-Carrier, *et al.*, "Contributions to the Modeling and Design of Reconfigurable Reflecting Cells Embedding Discrete Control Elements," *Microwave Theory and Techniques, IEEE Transactions on,* vol. 58, pp. 1621-1628, 2010.